

On the mathematical properties of multi-loop scattering amplitudes through the loop-tree duality

Thesis submitted in fulfillment of the requirements of the “Programa de Doctorat en Física” in Facultat de Física, Universitat de València.

Author:

Jose de Jesus Aguilera Verdugo

Directors:

Germán V. Rodrigo García

German F. R. Sborlini

Roger José Hernández Pinto

UNIVERSITAT DE VALÈNCIA



3126 Programa Oficial de Doctorado en Física

Instituto de Física Corpuscular, Departamento de Física Teórica
Universitat de València – Consejo Superior de Investigaciones Científicas

Declaration of authorship

I, Jose de Jesus Aguilera Verdugo, hereby certify that this thesis, titled *On the mathematical properties of multi-loop scattering amplitudes through the loop-tree duality*, has been composed by myself. All the work contained herein is my own except where explicitly stated otherwise, and all main sources of help have been properly referenced and acknowledged.

The work presented in this thesis is based on original results previously published by myself, in collaboration with Germán Rodrigo, German F. R. Sborlini, Roger José Hernández-Pinto, William J. Torres Bobadilla, Judith Plenter, N. Selomit Ramírez-Uribe, Andrés E. Rentería-Olivo and Szymon Tracz. Chapters 4, 6 and 5, in particular, are based on the following publications:

Articles

- [1] Jesús Aguilera-Verdugo, F. Driencourt-Mangin, R. Hernández-Pinto, J. Plenter, R. M. Prisco, S. Ramírez-Uribe, A. E. Rentería-Olivo, G. Rodrigo, G. F. R. Sborlini, W. J. Torres Bobadilla and F. Tramontano, *A Stroll through the Loop-Tree Duality, Symmetry* **13** (2021) 6, 1029, [[2104.14621](#)].
- [2] J. Jesús Aguilera-Verdugo, R. J. Hernández-Pinto, G. Rodrigo, G. F. R. Sborlini and W. J. Torres Bobadilla, *Mathematical properties of nested residues and their application to multi-loop scattering amplitudes, JHEP* **02** (2021) 112, [[2010.12971](#)].
- [3] J. J. Aguilera-Verdugo, R. J. Hernandez-Pinto, G. Rodrigo, G. F. R. Sborlini and W. J. Torres Bobadilla, *Causal representation of multi-loop Feynman integrands within the loop-tree duality, JHEP* **01** (2021) 069, [[2006.11217](#)].
- [4] J. J. Aguilera-Verdugo, F. Driencourt-Mangin, R. J. Hernández-Pinto, J. Plenter, S. Ramirez-Uribe, A. E. Renteria Olivo, G. Rodrigo, G. F. R. Sborlini, W. J. Torres Bobadilla and S. Tracz, *Open Loop Amplitudes and Causality to All Orders and Powers from the Loop-Tree Duality, Phys. Rev. Lett.* **124** (2020) 21, 211602, [[2001.03564](#)].
- [5] J. J. Aguilera-Verdugo, F. Driencourt-Mangin, J. Plenter, S. Ramírez-Uribe, G. Rodrigo, G. F. R. Sborlini, W. J. Torres Bobadilla and S. Tracz, *Causality, unitarity thresholds, anomalous thresholds and infrared singularities from the loop-tree duality at higher orders, JHEP* **12** (2019) 163, [[1904.08389](#)].

Proceedings

- [6] J. J. Aguilera-Verdugo, F. Driencourt-Mangin, J. Plenter, S. Ramírez-Uribe, G. Rodrigo, G. F. R. Sborlini, W. J. Torres Bobadilla and S. Tracz, *Unsubtractions at NNLO, CERN Yellow Reports: Monographs* **3** (2020) 169-176.

A talk about the topic was also given at the following conference:

- PARTICLEFACE 2020, *Working Group Meeting and Management Committee Meeting*, Krakow (Poland), February 2020

A mis padres que me han dado todo su apoyo con
el desarrollo de este trabajo.

Contents

1	Introduction	19
1.1	Outline	20
2	The success of Quantum Field Theories: The Standard Model	23
2.1	Klein-Gordon Lagrangian	23
2.2	Dirac Lagrangian	24
2.3	Quantum Electrodynamics	25
2.4	Non-Abelian gauge theories	27
2.5	QFT at work: The Standard Model	30
2.5.1	Breaking symmetries and mass generation in the SM	30
2.6	Computation of physical observables	36
2.6.1	Scattering matrix and cross sections	36
2.6.2	Perturbation theory and Feynman diagrams	37
3	Singularities in QFT	43
3.1	The origin of divergences	43
3.2	Dimensional regularisation	45
3.3	Cancellation of UV and IR divergences	49
3.4	Threshold singularities and the optical theorem	49
4	The Loop-Tree Duality at higher perturbative orders	53
4.1	Loop-Tree Duality in a nutshell	53
4.1.1	The Loop-Tree Duality at one loop	54
4.1.2	The Loop-Tree Duality at two loops	57
4.1.3	Topological classification of multi-loop Feynman diagrams	60
5	Mathematical properties of nested residues within the Loop-Tree Duality	73
5.1	Iterated and nested residues	73
5.2	Higher-order poles	81
6	Causal representation of multi-loop amplitudes within the loop-tree duality	85
6.1	Finite fields and analytic reconstruction	86
6.2	Causal representation of multi-loop integrals by analytic reconstruction	87
6.2.1	The two-loop sunrise diagram	88
6.2.2	Maximal Loop Topology	89
6.2.3	NMLT vacuum integral	89
6.2.4	N ² MLT vacuum integral	91
6.2.5	NMLT and N ² MLT topologies with external momenta	92
6.3	Topologies with higher powers of the propagators	94
6.4	Numerical evaluation of N ^{k-1} MLT	96

6.4.1	Two-dimensional integrals	96
6.4.2	Three- and four-dimensional integrals	96
6.5	Geometrical interpretation of the causal thresholds	100
7	Summary and outlook	101
A	Feynman rules	103
B	Code for the computation of the nested residues	105
C	Cancellation of displaced poles	109
D	Proof by induction of the multi-loop $MLT(L)$ representation	111

Abstract

The astonishing development of high-energy physics experiments such as CERN's Large Hadron Collider has yielded high quality data. The interest in understanding these data has given rise to the necessity of increasing the precision in theoretical physics calculations. In this thesis, an unconventional computational method for perturbative Quantum Field Theories called Loop-Tree Duality is developed from its mathematical foundations. We present a classification of Feynman diagrams regarding their topology rather than the number of loops, where all topological classes can have arbitrary L loops and they are different in their topology or, equivalently, on the dependence of its internal momenta on the loop momenta, and we develop the mathematical framework of the computational algorithm needed for the calculations of scattering amplitudes in an arbitrary order within perturbation theory. This formalism, based on Cauchy residue theorem, transforms an integral over an Ld -dimensional Minkowskian space into another one over an $L(d-1)$ -dimensional space. Through this method, we find the causal structure of the simplest topological class, and we obtain factorization formulae for higher topological classes, where an arbitrary topological class can be studied by means of lower topological classes. Given the causal structure of the simplest topological class and the factorization formulae, the causal structure of higher topological classes are expected to be obtained iteratively through the Loop-Tree Duality formalism.

This document presents an effort to understand high-precision computations from its mathematical foundations based on the Loop-Tree Duality formalism. The structure of this work is the following. In Chapter 1, a brief introduction is given in which we present some of the historical advances that have been developed in the search for a better description of the fundamental interactions of nature. Likewise, an outline of what will be seen in the thesis work is given. In Chapter 2 we present the mathematical framework needed to understand the physics of Standard Model. Besides, the computation of physical observables through Quantum Field Theories is shown and the perturbation theory will be related to Feynman diagrams. Hence, the divergences arising in a natural fashion from the theory are presented in Chapter 3. In addition, a description of the divergences and their physical meanings are introduced. Mathematical tools called regularization schemes are briefly presented in this chapter, focused on Dimensional Regularization. In Chapter 4, the Loop-Tree Duality formalism will be stated. In addition, an explanation on the meromorphic structure of the Feynman integrands shall be given in order to get a better understanding of the physical and non-physical divergences. There, a short-hand notation is presented together with the efficient computational tools of Loop-Tree Duality framework. A well suited classification of Feynman diagrams is given. Through Chapter 5, the mathematical aspects of Feynman integrands are analysed in order to give a solid theoretical foundation to the Loop-Tree Duality at an arbitrary L -loop order. Moreover, we exploit the analytical properties of Feynman integrands to understand the cancellation of non-causal divergences for every n -th order poles. In Chapter 6, an analytical reconstruction of the results obtained in the previous chapters is presented using an approach based on numerical results. Some interesting consequences on causal and non-causal structures of the integrands are mentioned. In Chapter 7, a brief summary of the work is exhibited together with possible future research lines.

The study of theoretical physics in the high-energy regime has been developing in an astonishing manner over the last half century. This development has pushed the progress on high-precision computations to impressive results. Within these calculations, those

studied by means of perturbative theory have increased considerably in complexity with each extra order of approximation.

Loop-Tree Duality (LTD) has proved its efficiency as a framework for high-precision computations through the last years, a new classification of Feynman diagrams which is independent on the number of loops but on the topology of the diagram, has been introduced. Using this classification, LTD has shown an amazing power to tackle scattering amplitudes for an arbitrary number of loops, leading to factorization formulae relating an arbitrary topological class to classes with lower topological complexity and, in turn, these factorization formulae lead to the causal structure of the scattering amplitude, showing an explicit agreement between analytical and numerical results. The application of the LTD formalism leads to a natural connection between integration over a d -dimensional Minkowski space and integration over a $(d - 1)$ -dimensional Euclidian space. A great amount of the work presented in this thesis has been developed in order to give solid mathematical foundations to the LTD formalism.

The first part of this work consisted in the establishment of the general ideas on the computational tools of LTD formalism to all perturbative orders in agreement with Cauchy's residue theorem. With these general ideas, the computational tools for the LTD formalism are presented, and some intuitive ideas are established. As a motivation, the 1-loop scalar diagram is presented and the LTD is developed for this case. It is highlighted that the complexity of the integrand obtained from the application of Cauchy's residue theorem abruptly increases with the number of external particles. Even more, for the simple case of 2 external particles, the simplification of the integrand to the causal representation is obtained, showing how the non-physical divergences cancel between each other. As a second example, the scalar 2-loop diagram is presented and some interesting features that were not presented in the 1-loop case appear. This includes the presence of displaced poles, and the cancellation of their contributions is sketched. It became impressive to notice that the scalar sunrise diagram and the scalar 1-loop 2-point diagram have the same functional structure of their causal representation.

After the study of the 1- and 2-loop scalar diagrams were completed, the next step was to present the full topological classification of Feynman diagrams. As the computations in this thesis were thought for an arbitrary number L of loops, a new notation is given in order to have not an overwhelming reading. With this notation, an algorithm to identify the contributions to the iterated application of Cauchy's residue theorem is given, identifying positive- and negative-imaginary-part poles, as well as the displaced poles. An explicit explanation of the way the indices are evolving with each iteration of Cauchy's residue theorem is given, and the application of LTD formalism, together with this notation, is given to the general $\text{MLT}(L)$ diagram. The diagrammatic representation of the result of this computation in terms of the spanning trees of the underlying multi-graph of the MLT diagram is presented, and its causal representation is obtained after an algebraic simplification. We then interpret this causal representation of the scalar MLT topological family as a single propagator. Afterwards, the definition of the NMLT topological family is given, and the LTD formalism is applied in order to obtain the factorization formula of these diagrams. Then, the interpretation of this formula in terms of the spanning trees of the underlying graph is presented. This interpretation gave us some insight on what to expect for their causal representation. The same procedure is given for the $\text{N}^2\text{MLT}(L)$ diagram.

Once the computational tools of the LTD formalism were presented, together with a

few of its applications (the MLT, NMLT and N²MLT topological families), we have deepened on their mathematical foundations. The iterated residue is defined as the algorithm used in the LTD formalism, and after the proof of the cancellation of displaced poles for single poles is given, and the general case with higher-order poles is delayed to the Appendices, an analogue algorithm blind to the displaced poles called nested residues is defined. A geometrical interpretation of this cancellation is given and a direct proof of the cancellation of non-physical divergences in the MLT(L) diagram is presented. Furthermore, we give a formal proof of the uniqueness of the causal structure of the MLT topological family independently on the order which the integrations are performed. Then we define the auxiliary propagator, which is the keystone of the topological classification of the Feynman diagrams, as it enable us to reduce the number of loops in each topological family. We finished the work with the study of higher order poles. We performed this study in detail in order to give a proof of the sufficiency of the simple poles case and how it is possible to obtain the causal structure of a diagram with higher-order poles once the one for a diagram with only simple poles is obtained.

We went on with the analytical reconstruction of the causal representations for the NMLT and N²MLT topological families, identifying the entangled causal thresholds and associated the entanglement with a compatibility on the momentum flow of each causal threshold. We verified our results with numerical implementations, showing the smoothness of the causal structure compared with the function obtained directly from the iterated application of Cauchy's residue theorem. The non-physical divergences were naturally identified as the numerical fluctuations of these computations. Numerical integration of the NMLT(3) and N²MLT(3) in 2, 3 and 4 dimensions is presented, showing a complete agreement with the analytic results, scanning the mass of a propagator. Also, a geometrical interpretation of the entangled causal thresholds is given.

Finally, a brief summary of this work is presented together with the conclusions, giving way to its Appendices.

Resumen

El asombroso desarrollo de los experimentos de física de altas energías, como el Gran Colisionador de Hadrones del CERN, ha permitido obtener datos de gran calidad. El interés por comprender estos datos ha dado lugar a la necesidad de aumentar la precisión de las predicciones teóricas correspondientes. En esta tesis se desarrolla desde sus fundamentos matemáticos un método enfocado en cálculos de alta precisión denominado Loop-Tree Duality (dualidad lazo-árbol). Presentamos una clasificación de los diagramas de Feynman con respecto a su topología más que en el número de loops, en donde todas las clases topológicas pueden tener un número arbitrario L de loops y que se distinguen en su topología o, equivalentemente, en la dependencia que tienen los momentos de las partículas virtuales con los momentos libres, y desarrollamos el marco matemático del algoritmo necesario para el cálculo de las amplitudes de scattering para un orden arbitrario en teoría perturbativa. Este algoritmo se basa en el teorema del residuo de Cauchy, transformando una integral sobre un espacio de Minkowski Ld -dimensional en otra sobre un espacio $L(d-1)$ -dimensional. Con el uso de este método, encontramos la estructura causal de las familias topológicas más simples, así como fórmulas de factorización para clases topológicas de orden superior. Dadas las estructuras causales y las fórmulas de factorización, se espera obtener las estructuras causales de las clases topológicas de orden superior de forma iterativa por medio del formalismo Loop-Tree Duality.

En el Capítulo 1 de este trabajo se presenta una breve introducción histórica de los desarrollos teóricos que se han dado para entender los constituyentes fundamentales de la materia de los que tenemos evidencia hasta el momento, comenzando con el descubrimiento del electrón en 1897 por Joseph John Thomson, continuando con el avance del conocimiento hacia la mecánica cuántica, pasando por los trabajos de Max Plank sobre la catástrofe ultravioleta, de Albert Einstein sobre la relatividad especial y el efecto fotoeléctrico, de Ernest Rutherford y su descubrimiento del núcleo atómico, de Louis de Broglie sobre la dualidad onda-partícula, de Erwin Schrödinger y su ecuación que modela a las ondas de de Broglie, de Oskar Klein y Walter Gordon sobre la versión relativista de la ecuación de Schrödinger para partículas con espín entero, de Paul Dirac con su versión relativista de la ecuación de Schrödinger para partículas con espín semientero, entre otros.

En el Capítulo 2 se presenta el marco teórico necesario para comprender la parte de la teoría de la física de partículas que será necesaria para el desarrollo de este trabajo de tesis, mismo que lleva por nombre *Teoría Cuántica de Campos*. Se comienza con una pequeña descripción del Modelo Estándar de las partículas fundamentales y se hace mención que el desarrollo que se seguirá es el asociado con la invarianza ante grupos de simetría, misma que es una forma elegante de introducir los campos de norma. La primera Sección de este Capítulo continúa con el estudio de la densidad Lagrangiana de Klein-Gordon, estableciendo la ecuación de Klein-Gordon para una partícula libre, y se establece la densidad Lagrangiana para una partícula que obedece a la ecuación de Klein-Gordon ya sea neutra o cargada, presentando a su vez el propagador de Feynman para una partícula escalar, misma que precisa la definición del producto temporalmente ordenado de los campos de Klein-Gordon. Así mismo, se da una interpretación de este propagador. En la segunda Sección se prosigue con el estudio de la densidad Lagrangiana de Dirac, presentando la ecuación de Dirac y mostrando dicho Lagrangiano para una partícula que se describe por medio de esta ecuación. En este caso, se presenta la solución de la ecuación de Dirac para una partícula libre, que queda representado por una pareja ordenada de espinores. Se continúa con la definición del producto temporalmente ordenado de campos espinoriales

y se presenta el propagador de Feynman para éstos. Se hace énfasis en que los resultados obtenidos de esta forma son aplicables a partículas libres, y que las interacciones se habían estudiado por medio del conocido como *acoplamiento mínimo*, que se puede interpretar como un desplazamiento de las derivadas parciales aplicadas al campo espinorial.

Más adelante en el Capítulo 2, Sección 2.3, se estudia la Electrodinámica Cuántica como una teoría cuántica de campos con densidad Lagrangiana invariante ante transformaciones del grupo unitario de dimensión 1. Se observa que al aplicarse una transformación de dicho grupo, aparecen de manera natural los campos vectoriales que se asociarán con el campo del fotón. Se encuentra la expresión para la derivada covariante y se muestra que, en efecto, una transformación unitaria aplicada al campo del fotón nos lleva naturalmente al acoplamiento mínimo. Se explica, además, que la invarianza de norma en la Electrodinámica Cuántica implica que el fotón no tiene masa. También se explica que el tensor electromagnético está dado como el conmutador de derivadas covariantes. Esta Sección continúa con el estudio de la quiralidad de los espinores de Dirac. Esto se realiza mediante el estudio de la representación de Weyl de los espinores de Dirac, se definen los proyectores quirales y se muestra la forma en la que estos espinores están acoplados por términos de masa, de manera tal que, si los espinores son no masivos, entonces sus componentes de quiralidad izquierda y derecha se desacoplan.

En la Sección 2.4 se hace un estudio similar al realizado en la Sección 2.3, pero con teorías no Abelianas de norma, esto es, con teorías cuyas densidades Lagrangianas son invariantes ante transformaciones de los grupos especiales unitarios. En este caso se presentan los generadores de los grupos no Abelianos y se les asigna su álgebra de Lie. Se siguen las mismas ideas que en el caso del electromagnetismo llegando a que, en el caso de las teorías no Abelianas, se tienen presentes términos de interacción entre los bosones de norma. Para encontrar la evolución de dichos bosones, se sigue el desarrollo realizado por Faddeev y Popov, que lleva a la presencia de términos en la densidad Lagrangiana que modelan objetos similares a partículas pero que no tienen una representación física llamadas *ghosts*, con los cuales se concluye la Sección con la densidad Lagrangiana de la Cromodinámica Cuántica, expresando la densidad Lagrangiana de esta teoría.

En la Sección 2.5 se presenta el mecanismo de Higgs, uno de los mecanismos en los que, de manera espontánea, se rompe la simetría de una teoría, se presenta al bosón de Higgs, y se obtiene su masa como resultado de su interacción consigo mismo. De la misma forma, se presenta el enfoque de Glashow-Weinberg-Salam sobre la descripción de la teoría electrodébil, mismo que asume un rompimiento espontáneo de la simetría en la Electrodinámica Cuántica. En la Sección 2.6 se presentan los cálculos para algunos observables físicos. Se presenta la *matriz S* y las secciones eficaces. A su vez, se da una breve introducción a la aplicación de la teoría perturbativa en los cálculos de la teoría de los campos y a los diagramas de Feynman, en conjunto con su clasificación de acuerdo con las características topológicas de los mismos. Se continúa el Capítulo con una breve descripción de algunas consecuencias de la ecuación de Callan-Symanzik, de la que se obtiene lo que se conoce como el *corrimiento de los acoplamientos* (o *running couplings* en inglés). Esto tiene como consecuencia que las interacciones varíen su intensidad con la energía con la que las partículas interactuantes se encuentran. Más aún, se explica que en el caso de las teorías no Abelianas, como en el caso de la Cromodinámica Cuántica, se presentan los fenómenos conocidos como *confinamiento* y *libertad asintótica*.

En el Capítulo 3 comienza la problematización de este trabajo, mostrando cómo la teoría estudiada en el Capítulo 2 puede llevar a infinitos en un espacio de 4 dimensiones,

conocido como el mundo de Minkowski. En la Sección 3.1 se presenta la clasificación usual de las divergencias, ya sean divergencias *ultravioleta* (UV), que se muestran en los cálculos al sumar las contribuciones de partículas a las que se les permite tener una energía arbitrariamente alta (durante el estudio de este tipo de divergencias se presenta el concepto de *grado superficial de divergencia*, que nos da una idea de la presencia de las divergencias UV a nivel del integrando o del diagrama de Feynman), o divergencias *infrarrojas* (IR), que son aquellas que ocurren a bajas energías, y que a su vez se dividen en divergencias de tipo *soft*, que son aquellas que aparecen cuando se permite la emisión de partículas de baja energía, y en divergencias de tipo *colineal*, que se presentan cuando se irradia una partícula en dirección paralela a la partícula radiante. También se hace mención de las divergencias de *threshold*, mismas que, a diferencia de las anteriores, tienen un significado físico y son integrables. En la Sección 3.2 se muestra un método conocido como *regularización dimensional*, usado comúnmente para el cálculo de observables físicos y se muestran algunos ejemplos de su uso. En estos mismos ejemplos se observa la forma en la que se logran aislar las divergencias en términos que dependen de un parámetro asociado a la dimensión del espacio donde se integra. En la Sección 3.3 se presenta una breve reseña del algoritmo conocido como *renormalización*, con el que se trabajan las divergencias ultravioleta. En la Sección 3.4 se presenta el teorema óptico y se muestra la forma en la que las divergencias de *threshold* son integrables, llevando a cantidades finitas si se suman todas sus contribuciones. A su vez, se presentan las *reglas de corte de Cutkosky*, que forman un algoritmo para sumar dichas contribuciones. Se hace, también, una distinción geométrica de las divergencias causales y las divergencias no causales, que nos será de utilidad. Así pues, el objetivo general de este trabajo de tesis es el análisis de las cancelaciones de las divergencias no causales que se presentan en las Teorías Cuánticas de los Campos, teniendo como objetivos específicos encontrar un algoritmo de aplicación de la Loop-Tree Duality que generalice los trabajos realizados sobre esta metodología, encontrar una clasificación complementaria de los diagramas de Feynman que se ajuste mejor a la caracterización de las cancelaciones de las divergencias no causales, obtener fórmulas de factorización que permitan relacionar las diferentes clases de la clasificación encontrada en el objetivo específico anterior, y por último, encontrar las expresiones causales obtenidas después de la cancelación de las divergencias no causales mediante el análisis estricto de los integrandos que se obtienen al aplicar la metodología de la Loop-Tree Duality.

La Loop-Tree Duality es un marco matemático que se utiliza en el estudio de las amplitudes de dispersión. En el Capítulo 4 se presenta el marco metodológico que se utiliza en el resto del presente trabajo de tesis. Siendo uno de los objetivos específicos el encontrar un algoritmo de aplicación de la Loop-Tree Duality de manera generalizada, en este Capítulo comienza la presentación de los resultados. Así, en la Sección 4.1 se estudia la Loop-Tree Duality desde sus cimientos matemáticos, que constan básicamente del teorema de residuos de Cauchy; sin embargo, por convención, las integraciones sobre el eje real en el plano complejo se realizan con ayuda de un contorno de integración que siempre se cierre rodeando el semiplano inferior, imponiendo la condición de tener un número de winding siempre igual a la unidad negativa. La Sección continúa con el estudio de la Loop-Tree Duality a un loop. Con este propósito, se considera una notación que no vuelva pesada la lectura de este trabajo. Debido a que la Loop-Tree Duality lleva consigo una integración en el plano complejo sobre un contorno que encierra el semiplano inferior, es necesario tener en cuenta que sólo contribuyen los polos del integrando que tengan parte imaginaria negativa, de tal manera que si se integra la componente de energía, se estarían seleccionando las partículas cuya energía tiene parte real positiva. Luego, la integración se lleva a cabo para integrandos con polos simples y se deja expresado el resultado para un diagrama con un número arbitrario de partículas internas. Se hace una interpretación del

resultado en términos de la teoría de grafos, de tal suerte que la aplicación de la Loop-Tree Duality a 1 loop se puede entender como el estudio de un diagrama con 1 ciclo mediante el estudio de sus árboles generadores. Se continúa la Sección con una explicación sobre la suficiencia del caso de polos simples, incluso para el caso de tener integrandos con polos de orden superior, ya que éstos últimos se pueden entender como derivadas con respecto a un parámetro de los integrandos con polos simples. Luego, para terminar el estudio de la Loop-Tree Duality a 1 loop se estudia de manera explícita el diagrama conocido como *diagrama de burbuja*, que es un caso especial de diagramas de Feynman con 1 loop. Al hacer el estudio específico se observa cómo se llega a una expresión en la que la ausencia de divergencias no causales es evidente.

La Sección continúa con el estudio de la Loop-Tree Duality para diagramas de Feynman con 2 loops. Se comienza este estudio con una extensión en la notación usada anteriormente, que permita el uso para más de 1 loop, y se hace énfasis que se puede utilizar lo obtenido para 1 loop si se integra loop por loop del diagrama de 2 loops. Para concretar ideas, se utiliza el diagrama conocido como *diagrama sunrise*, y se realizan las integrales en las componentes de energía de los loops siguiendo de cerca los polos con parte imaginaria negativa, lo cual lleva al concepto de *polos desplazados*, que son aquellos que tienen una energía cuya parte imaginaria no tiene un signo constante, sino que depende de la configuración del 3-momento del loop. Se hace el cálculo directo para hacer notar que las contribuciones a la integral de los polos desplazados se cancelan dos a dos. Después del estudio minucioso de los polos con parte imaginaria negativa, se llega a una expresión para el diagrama sunrise en la que evidentemente las divergencias no causales están ausentes. Más aún, el integrando de la representación causal para el diagrama de burbuja y el integrando de la misma representación para el diagrama sunrise tienen la misma forma, por lo que estos resultados nos dan una idea de la clasificación de los diagramas de Feynman que buscamos para el siguiente objetivo específico.

Esta Sección continúa con la clasificación topológica de los diagramas de Feynman. Esta clasificación es la que se buscaba en los objetivos específicos. Para poder realizar un estudio a fondo y detallado de esta clasificación, es necesario extender aún más la notación, por lo que se prosigue con esta extensión, de tal forma que se definen funciones cuyos argumentos son índices y que obedecen a la convención de barras, definida en esta Sección. Así, la notación es extendida de tal forma que los argumentos pueden contener subíndices, barras, y puede ser usada para representar el cálculo de las integrales en la componente de energía por medio del uso del teorema de residuos de Cauchy. Continuando con esta notación de índices, se muestra que, debido a la idempotencia de la convención de barras, es posible desarrollar aritmética con estos índices, y se desarrolla paso a paso el cálculo de la integral en las componentes de energía de los loops en el diagrama escalar sunrise utilizando esta notación, mostrando que los propagadores de Feynman tienen dos de tres tipos de polos: polos con parte imaginaria negativa, polos con parte imaginaria positiva, o polos desplazados. Se encuentra una forma sencilla de encontrar los polos con parte imaginaria positiva, y a su vez se pueden encontrar los polos desplazados, de tal suerte que los polos cuyas contribuciones no se cancelan en una primera instancia (como en el caso de los otros dos tipos de polo), que son los polos con parte imaginaria negativa, se encuentran de manera sencilla y por simple inspección. Siguiendo con la explicación del manejo de la notación de índices, se muestra que el desarrollo del cálculo de residuos mediante el aprovechamiento de esta notación se vuelve sencillo, pues el resultado se puede obtener siguiendo la posición de los índices y su configuración de barras. Una vez terminada la explicación del uso de esta notación, se prosigue a definir la *complejidad topológica* de un diagrama de Feynman, definida como el antecesor del número de vértices del multigrafo

subyacente de dicho diagrama de Feynman.

Definida la complejidad topológica de un diagrama de Feynman, encontramos la clasificación que se estaba buscando. Esta clasificación comienza con la clase topológica llamada *Maximal-Loop-Topology* (MLT), definida como la clase de diagramas de Feynman que tienen complejidad topológica igual a 1. A partir de la presentación de esta clase topológica, se muestra el resultado del cálculo que la Loop-Tree Duality nos arroja, llegando a una expresión que representa la contribución de todos los subdiagramas de tipo árbol que se obtienen de un diagrama de dicha clase topológica, misma que lleva a la representación causal. Se hace notar que esta representación causal coincide con la obtenida para el diagrama de burbuja y para el diagrama sunrise, siendo éstos los diagramas más simples de esta clase topológica. Se prosigue con la siguiente clase topológica, llamada *Next-to-Maximal-Loop-Topology* (NMLT), definida como la clase de diagramas de Feynman con complejidad topológica igual a 2. Al aplicar la Loop-Tree Duality a esta clase topológica se obtiene una expresión matemática que se puede expresar en términos de convoluciones. Esta expresión es la fórmula de factorización que se buscaba en los objetivos específicos, ya que nos permite expresar el integrando de un diagrama NMLT en términos de convoluciones de diagramas MLT. Se continúa con este estudio dando una interpretación geométrica de esta fórmula de factorización. Esta fórmula lleva consigo una función, llamada *propagador auxiliar*, que se obtiene como resultado de tener un conjunto de líneas internas ya sea todas on-shell o todas off-shell. Se continúa el estudio de las clases topológicas con la clase *Next-to-Next-To-Maximal-Loop-Topology* (N^2 MLT), definida como la clase de diagramas de Feynman con complejidad topológica igual a 3. De nueva cuenta, se aplica la Loop-Tree Duality y se obtiene una expresión que puede ser escrita en términos de convoluciones, definidas en el mismo texto, y que tienen una representación diagramática que se describe a continuación. Esta expresión muestra que el integrando de un diagrama N^2 MLT puede ser escrito como convoluciones de diagramas MLT o NMLT, siendo así esta expresión la fórmula de factorización buscada para esta clase topológica. Para finalizar este Capítulo se hace notar que, utilizando esta metodología, se puede obtener una fórmula de factorización para cualquier complejidad topológica k , esto es, para cualquier clase topológica N^{k-1} MLT (donde la clase MLT implica que la complejidad topológica k es 1).

En el Capítulo 5 se estudian las propiedades matemáticas del algoritmo que se ha seguido en el Capítulo 4, comenzando por la definición formal del funtor llamado *residuos iterados*. Con esta definición evitamos cualquier ambigüedad en los cálculos. Inmediatamente después se muestra que para cálculos de residuos iterados para productos de propagadores, las contribuciones de los polos desplazados se cancelan. Esto se expresa posteriormente para el caso general de una función con polos de orden superior. Se continúa con una interpretación geométrica de lo que ocurre con los residuos iterados, de tal forma que al calcular el primer residuo iterado, se obtienen dos términos cuyas estructuras de polos están relacionadas, de tal forma que al calcular el siguiente residuo iterado, la contribución de un polo desplazado en uno de los términos cancela la contribución del mismo polo en el otro término. Se procede definiendo un algoritmo similar a los residuos iterados, llamado *residuos anidados*, que realiza los cálculos de los residuos iterados únicamente para los polos con parte imaginaria negativa, debido a que los demás polos, ya sean con parte imaginaria positiva o polos desplazados, no contribuyen a los residuos iterados. Se hace notar que la expresión obtenida inmediatamente después de aplicar los residuos anidados depende explícitamente del orden en el que se calculan los residuos, o equivalentemente, del orden en que se realizan las integraciones de las componentes de energía de los loops. No obstante, para un diagrama MLT, se hace el cálculo de forma

explícita para encontrar su representación causal, mostrando que las cancelaciones de las divergencias no causales se dan al separar los residuos obtenidos en fracciones parciales, y se muestra que, independientemente del orden de integración, la representación causal es la misma. A continuación se muestra que si se realiza un cálculo análogo para una subcolección de términos, se obtiene una expresión que tiene la estructura de un propagador, a esta expresión es a la que se le define como *propagador auxiliar*. Se muestra que este propagador auxiliar da una idea de que las clases topológicas tienen un diagrama con el mínimo número posible de loops. Esto se explica a continuación, utilizando el propagador auxiliar para representar todos los propagadores que conectan dos vértices adyacentes. Al finalizar la Sección 5.1 se hace notar que esta simplificación es válida para diagramas escalares, y que al aparecer un numerador polinomial, de manera general no es posible reducir una inserción MLT a un único propagador. En la Sección 5.2 se realiza un análisis del álgebra que siguen los residuos iterados y cómo se relaciona con la aplicación de la Loop-Tree Duality para polos de orden superior. Así, se muestra que una derivación con respecto al cuadrado del polo aumenta el orden del polo, y se encuentra una función que manda un integrando de Feynman escalar arbitrario al integrando asociado con polos simples, así como la función que manda el resultado de tomar los residuos anidados de esta función con polos simples al resultado de tomar los residuos anidados de la función original con polos de orden superior. De esta manera se muestra la suficiencia de estudiar solamente integrandos con polos simples. Se da como ejemplo el caso del diagrama escalar sunrise con un polo doble.

En el Capítulo 6 se estudia la reconstrucción analítica de las representaciones causales de las clases topológicas NMLT y N^2 MLT. En la Sección 6.1 se da una breve explicación del algoritmo a seguir para esta reconstrucción basado en los campos finitos (entendiendo la palabra *campos* como la estructura algebraica) y en congruencias. En la Sección 6.2 se muestra el resultado de aplicar este algoritmo al diagrama escalar sunrise a modo de verificación, obteniendo la misma estructura causal que en el Capítulo 5. Además, se contrasta el resultado de los residuos anidados con la representación causal, mostrando que esta última es más estable debido a que los residuos anidados aún contienen las divergencias no causales. Se continúa con las estructuras causales obtenidas para la clase topológica MLT, así como para los diagramas de vacío de las clases topológicas NMLT y N^2 MLT. Se define lo que conocemos como los *thresholds causales entrelazados*, que diagramáticamente son aquellas cuyos flujos de momento quedan alineados, y se hace notar que las contribuciones a la representación causal de estas clases topológicas sólo pueden contener thresholds causales entrelazados. La Sección concluye con las representaciones causales para las clases topológicas NMLT y N^2 MLT con partículas externas. En la Sección 6.3 se hace énfasis en los resultados obtenidos para polos de orden superior y en la Sección 6.4 se muestran los resultados de las evaluaciones numéricas para las clases topológicas MLT, NMLT y N^2 MLT con 3 y 4 loops. Estas evaluaciones numéricas se realizaron para integrales en 2, 3 y 4 dimensiones, con coordenadas esféricas, mostrando gran similitud con los resultados analíticos obtenidos en la Sección 6.2. En la Sección 6.5 se hace notar que los thresholds causales entrelazados que aparecen en las representaciones causales de las clases topológicas cumplen tres propiedades: 1) en un mismo término, todas las energías on-shell de las partículas del diagrama aparecen, 2) los threshold causales, al representarse como cortes del diagrama, no se intersectan y 3) los flujos de momento de las líneas internas del diagrama asociados a diferentes thresholds causales son compatibles. Al finalizar el Capítulo, se hace mención que esto último puede interpretarse como una conexión entre el análisis complejo y la teoría de grafos.

En el Capítulo 7 se da un resumen de este trabajo de tesis. Como conclusiones tenemos

que en el estudio de la Teoría Cuántica de Campos donde aplique la teoría perturbativa, la aplicación de la Loop-Tree Duality nos asegura que las divergencias no causales se cancelan, obteniendo resultados que únicamente contienen divergencias causales.

Finalmente, presentamos un breve resumen de este trabajo con conclusiones, dando paso a sus Apéndices.

Acknowledgements

Without any doubt, the present thesis is by far the most difficult task I have ever undertaken. These three years were filled with hard work and efforts that I was not aware I could do. Throughout these years, I have been amazed at how far I have come. I look back and I still cannot believe the strides I have made in this, my academic preparation. But I have not been able to achieve these accomplishments alone. I owe these achievements to everyone who has been supporting me step by step. Words would be lacking to thank them as they deserve, but I do feel the necessity to thank them accordingly.

I would like to start with my thesis director, Germán Rodrigo. He has been always there whenever I have a question. With his experience and insight, he has given me incredible advice to develop my ideas whenever we talk. With his guidance and help, I have reached amazing progress.

I also want to thank one of my thesis co-director, German Sborlini, who is also my friend. His amazing way of explaining thought subtleties in particle physics were of great importance through these years. Several long talks about advanced topics in high-energy physics and mathematics were immensely valuable on the development of ideas that ended up in publications. Also, his friendship pushed me to start a healthier life, which is, to my understanding, one of the most valuable lessons he gave me.

My teacher, my co-director, my friend, Roger Hernández, who has always pushed me to work harder and also has given me amazing academic and life advice. Even when we are in different continents, he has always had a time for a talk whenever I was not in my better moments.

Definitely, I would like to thank Generalitat Valenciana, Universitat de València and CSIC for the financial support throughout these three years of my Ph.D., as well as giving me the opportunity to travel to many different places in Europe, with different cultures, where I have met a lot of other Ph.D. students and researchers with whom I had amazing talks. Studying in this country has been an amazing experience, where the importance of the development, promotion and spread of science is appreciated these days.

Quiero agradecer particularmente a Gabriela por ser mi inspiración siempre y especialmente, durante estos estudios de doctorado, que me da la motivación por superarme cada instante y me ha dado ánimos de seguir adelante a pesar de sentir en algunos momentos que no podía más.

Así mismo, deseo darle las gracias a mis padres que me han dado todo su apoyo a pesar de estar tan lejos. Mi padre que me transmitió su pasión por la física y las matemáticas y que me ayudó desde que yo tenía 12 años con las dudas que me salían en estas materias. Mi madre que siempre me ha apoyado incondicionalmente, ante todo tipo de problemas que he tenido en la vida, y que siempre me ha dado su comprensión. Mi hermana que,

siendo yo el menor de la familia, siempre me ha visto como el pequeño de la casa y que me ha cuidado emocionalmente y dado consejo cuando lo he necesitado. Mi hermano, que siempre ha estado para darme una mano desde que yo era un niño.

A su vez, Paloma tiene todos mis agradecimientos por su completa paciencia y comprensión ante estos tiempos tan complicados, que me ha dado todo su apoyo a la distancia y que me ha inspirado y dado fortaleza para avanzar y tener los ánimos para completar este trabajo.

Last but not least, I want to express my gratitude to all my friends and companions who have accompanied me throughout these years. Andrés, Selomit, Judith, Masha, Eleftheria, Luiz, Vanessa, Aida, María, Víctor, Adolfo... and everyone else in or outside IFIC with whom I have had amazing times going to different places, for going to the gym or climbing together, for playing music and watching (not really good) movies.

Foreword

Interesting times we are living in this moment. It was a coincidence that the SARS-CoV-2 pandemic started at the middle of my Ph.D. studies. These times have been rough, but tough moments bring out the best of us. Actually, the pandemic has unveiled the necessity of science in order to tackle important problems. Together with COVID-19 pandemic, several interesting experimental results in particle physics have been obtained. Also, the astonishing data obtained from colliders such as the Large Hadron Collider (LHC), a 27 km circular collider beneath the France-Switzerland border at the European Organization for Nuclear Research (CERN), where the Higgs boson was discovered, and the proposed 100 km facility expected to reach 100 TeV in proton-proton collisions, called Future Circular Collider (FCC) at CERN, demand better theoretical predictions and high-precision computations.

I have to confess that, by the time I started writing this thesis, I wanted this work to follow an strict logical approach, following every inference rule and giving each argument as solid as possible, but at the middle of the process I read what it was written, and decided to follow a more didactic structure. I do hope I reached that goal. Also, if the present thesis helps at least one future student with their understanding of the analytical properties of the scattering amplitudes, the probability amplitude of the scattering process described, then I would feel that all the efforts printed in here were worth it.

The present thesis is the summary of my little contribution to physics, more specifically, to the field of theoretical particle physics at high-energy colliders, and I hope the reader could enjoy the reading as much as I enjoyed while understanding the properties of scattering amplitudes.

Chapter 1

Introduction

What are we made of? This question has been present in humanity since millennia. The attempts to answer this enigma have led the world from the four elements of pre-Socratic philosophers to what we know today as the Standard Model (SM). This change has taken place in different steps: the discovery of the electron, the ultraviolet catastrophe, the photoelectric effect, the discovery of the nucleus of the atom and the study of quantum mechanics, among others. All these steps had a great impact on the community, as they changed the way of understanding Nature in a surprising way. The discovery of the electron by Joseph John Thomson in 1897 [7] was the foundational stone in the process of understanding the fundamental components of matter.

The ultraviolet catastrophe understood by the work developed by Max Plank in 1900 [8] leading to the interpretation of the discretization of electromagnetic wave energy, suggested the existence of particles of light that were called “quanta”, nowadays called photons. Later, the understanding of the discrete Nature of light through the photoelectric effect, following the work done by Albert Einstein in 1905 [9], explained this phenomenon by means of the quanta, recovering at the same time the corpuscular theory of light, which was pioneered by Isaac Newton by 1672. At the same time, A. Einstein also proposed the special theory of relativity [10], which describes mechanics under the fundamental principle that the speed of light is constant in every inertial reference frame. Then, the discovery of the nucleus of the atom by Ernest Rutherford in 1911 [11] led to the question of why the electron did not radiate, losing energy and decaying to the nucleus. This question showed an enormous lack of understanding of Nature at atomic level. A scientific revolution was necessary to achieve a better understanding of the physics of the electron inside the atom.

The description of photons as electromagnetic waves led Louis de Broglie [12] to assume the existence of a periodic phenomenon attributable to each energy parcel in 1924. The idea of De Broglie waves pushed Erwin Schrödinger to study these waves, heading to the well known Schrödinger equation in 1926 [13], together with a new interpretation of Nature, moving from the determinism of classical physics to the probabilistic interpretation of quantum mechanics. Moreover, the union of quantum mechanics with special relativity gave rise to Oskar Klein [14] and Walter Gordon’s equation in 1926, and Paul Dirac [15] equation in 1928, both understood as equations of motion of a single particle. This point of view of Dirac equation generated unphysical results, such as negative energy states for a solely particle. Nevertheless, the reinterpretation of Dirac equation as a quantum field equation managed to solve the undesirable results, predicting the existence of anti-particles. By 1927, Pascual Jordan [16] worked on the statistics of a many-body system. This work is now known as second quantization. By 1928, P. Jordan and Wolfgang Pauli showed that quantum fields could be built in such a way that the commutators of the

fields were Lorentz invariant commutators, in agreement with special relativity. The same year, P. Jordan and Eugene Wigner [17] showed that the quantization of the Dirac field should be expanded with anti-commutation relations instead of commutation relations in order to be in fully agreement with Pauli exclusion principle.

Through 1946 to 1949, a deeper understanding on quantum fields was developed. Julian Schwinger [18–23] and Shin’ichiro Tomonaga [24–27] worked on a relativistic covariant scheme known as the interaction representation. Within this representation, the study of the Hamiltonian values could be tracked in order to study the dynamics of a phenomenon. Also, Richard Feynman [28] worked on a diagrammatic representation of the S -matrix contributions with a set of rules that worked in both directions: given an S -matrix contribution it can be drawn a corresponding diagram and, given a diagram it can be written the contribution to the S -matrix. These rules are naturally called the *Feynman rules*. Quantum Electrodynamics (QED), as an Abelian gauge theory relying on the symmetry group $U(1)$ with one massless gauge field, became the prototype of a quantum field theory. By 1959, Sheldon Glashow, Abdus Salam and John Clive Ward [29] proposed the $SU(2) \otimes U(1)$ group structure together with a symmetry breaking mechanism in order to understand the weak interactions and merging them with the electromagnetic theory.

On the other hand, through the 1950’s a huge amount of hadrons were discovered. In 1954, Chen Ning Yang and Robert Mills [30] carefully studied the symmetries and the invariances that should be satisfied by any field theory. This theory, called the Yang-Mills theory, was the first non-Abelian gauge theory, and it attempted to explain the strong interactions. By 1964, Murray Gell-Mann [31] and George Zweig [32, 33] proposed the existence of the quarks as the constituent particles of hadrons. This proposition was interesting, as in the case of some hadrons there should be three of these quarks, which would have been forbidden by Pauli exclusion principle, unless there exists a new quantum number. Two theoretical works, one by Oscar Wallace Greenberg [34] in 1964 and the other by Moo Young Han and Yoichiro Nambu [35] in 1965, independently proposed the $SU(3)$ symmetry group to explain strong interactions, leading to an octet vector gauge boson now called *gluon*. The conserved charge due to this symmetry was called *color* in 1973 by M. Gell-Mann, Harald Fritzsch and Heinrich Leutwyler [36], following the Yang-Mills theory, and allowing the gluon to radiate. The theory of strong interactions was then called Quantum Chromodynamics (QCD). This same year, 1973, David Gross, Frank Wilczek [37] and, independently, David Politzer [38], discovered the phenomenon known as *asymptotic freedom*, in which interactions become asymptotically weaker with the energy scale. With the asymptotic freedom it was, then, allowed to use perturbation theory within QCD at the high-energy regime.

This has been the path to consolidate theoretically the SM of particle physics. On the following years, the theory has been tested in different reactions to the highest precision ever achieved of experimental results at high-energy colliders such as the CERN’s Large Hadron Collider (LHC) and low energy measurements such as the muon anomalous magnetic moment, are pushing towards more precise calculation to disentangle possible New Physics scenarios from the SM predictions.

1.1 Outline

This document presents an effort to understand high-precision computations from its mathematical foundations based on the Loop-Tree Duality formalism. The structure of this work is the following. In Chapter 2 we present the mathematical framework needed

to understand the physics of Standard Model. Besides, the computation of physical observables through Quantum Field Theories is shown and the perturbation theory will be related to Feynman diagrams. Hence, the divergences arising in a natural fashion from the theory are presented in Chapter 3. In addition, a description of the divergences and their physical meanings are introduced. Mathematical tools called regularization schemes are briefly presented in this chapter, focused on Dimensional Regularization. In Chapter 4, the Loop-Tree Duality formalism will be stated. In addition, an explanation on the meromorphic structure of the Feynman integrands shall be given in order to get a better understanding of the physical and non-physical divergences. There, a short-hand notation is presented together with the efficient computational tools of Loop-Tree Duality framework. A well suited classification of Feynman diagrams is given. Through Chapter 5, the mathematical aspects of Feynman integrands are analysed in order to give a solid theoretical foundation to the Loop-Tree Duality at an arbitrary L -loop order. Moreover, we exploit the analytical properties of Feynman integrands to understand the cancellation of non-causal divergences for every n -th order poles. In Chapter 6, an analytical reconstruction of the results obtained in the previous chapters is presented using an approach based on numerical results. Some interesting consequences on causal and non-causal structures of the integrands are mentioned. In Chapter 7, a brief summary of the work is exhibited together with possible future research lines.

Chapter 2

The success of Quantum Field Theories: The Standard Model

The study of elementary particles has been developed in an elegant manner. The understanding of this side of physics has reached astonishing agreement between theoretical predictions and experimental results, such as the anomalous magnetic dipole moment of the electron, known as the most accurately verified prediction (with an agreement of one part in 10^{13}). A good starting point for the study of particle physics is their classification due to their quantum numbers. One of the more common classifications is according to their spin: particles with spin $\frac{1}{2}$ are known as fermions (subdivided in leptons and quarks) and particles with spin 0 and 1 are known as bosons, Higgs boson and photons, gluons, W^\pm and Z^0 bosons respectively. The dominant interactions among them are the electromagnetic, the weak and the strong forces. The study of these interactions is encoded within a model called *Standard Model* (SM), and has led to the discovery of the Higgs boson in 2012, among other particles. As gravitational interactions are not included in this model, the underlying Lie group is the Poincaré group. Hence, Minkowski metric is mandatory².

Through the XX century, the description of sub-atomic particles was studied through quantum mechanics which, with aid of Schrödinger equation, described electrons in an atomic structure. However, this study could not reach the Nature of spin. This property of elementary particles was described with Dirac equation for spin $\frac{1}{2}$ particles and with Klein-Gordon equation for particles with spin 0 and 1. These equations attempted to study the relativistic effects in the high-energy regime of free particles. Nowadays, this description of elementary particles is given in terms of the mathematical framework of *Quantum Field Theories* (QFTs), and the interactions appear naturally imposing local invariance under gauge group action of the Lagrangian describing the particles. Although this is a non-trivial approach, it is an elegant route to introduce gauge fields.

2.1 Klein-Gordon Lagrangian

Klein-Gordon equation describes integer spin particles such as the Higgs boson and the photon, in general called bosons as they satisfy Bose-Einstein statistics. The relation between statistics and spin is not trivial, but both are related to the commutation relations between field functions. This equation, for a free particle with mass m , can be written as

$$(\partial_\mu \partial^\mu + m^2)\phi = 0. \quad (2.1)$$

²Here we use the usual signature in particle physics of $g^{\mu\nu}$ given by $g^{\mu\nu} = \text{diag}(+1, -1, \dots, -1)$, which has been used in order to have $p^2 = m^2 \geq 0$.

Eq. (2.1) can be derived using Euler-Lagrange field equations from the classical Lagrangian density known as the *Klein-Gordon Lagrangian*, which can be given for a real (neutral) field ϕ as

$$\mathcal{L}_{KG} = \frac{1}{2}\partial_\mu\phi\partial^\mu\phi - \frac{1}{2}m^2\phi^2, \quad (2.2)$$

or for a complex (charged) field ϕ as

$$\mathcal{L}_{KG} = \partial_\mu\phi^*\partial^\mu\phi - m^2\phi^*\phi. \quad (2.3)$$

The quantization of Klein-Gordon field can be developed as a harmonic oscillator or with the aid of Feynman path integrals, both yielding to the *propagator* of a scalar field given as the Green function of Klein-Gordon equation, Eq. (2.1). This is,

$$G_F(x-y) = \langle 0|T\phi(x)\phi(y)|0\rangle = \int \frac{d^4k}{(2\pi)^4} \frac{i e^{-ik\cdot x}}{k^2 - m^2 + i0} = \int \frac{d^4k}{(2\pi)^k} \tilde{G}_F(k) e^{-ik\cdot x}, \quad (2.4)$$

where $i0$ is *Feynman prescription* which allows the selection of positive or negative frequency solutions of Klein-Gordon equation, the function \tilde{G}_F is the Fourier transformation of the function G_F , and the operator T is called *time ordered product*, which is defined for bosons as

$$T\phi(x)\phi(y) = \begin{cases} \phi(x)\phi(y), & x^0 > y^0, \\ \phi(y)\phi(x), & y^0 > x^0. \end{cases} \quad (2.5)$$

Feynman propagator $G_F(x-y)$ is understood as the probability amplitude for a particle to propagate in space-time. Equivalently, \tilde{G}_F is understood as the probability amplitude for a particle to propagate with a given 4-momentum.

2.2 Dirac Lagrangian

Just as Klein-Gordon equation describes bosons, Dirac equation describes half-integer spin particles, such as electrons, quarks and neutrinos. In general, half-integer spin particles are called fermions as they satisfy Fermi-Dirac statistics. A non-interacting fermion with mass m is described by Dirac equation, namely,

$$(i\gamma^\mu\partial_\mu - m)\psi = 0, \quad (2.6)$$

or, with Feynman slash notation $\not{A} \equiv \gamma_\mu A^\mu$,

$$(i\not{\partial} - m)\psi = 0, \quad (2.7)$$

where γ^μ represent the Dirac matrices, satisfying the anticommutation relation $\{\gamma^\mu, \gamma^\nu\} = 2g^{\mu\nu}$. Eq. (2.6) can be also obtained, through Euler-Lagrange field equations, from the Lagrangian density (merely Lagrangian in the following)

$$\mathcal{L}_{Dirac} = \bar{\psi}(i\not{\partial} - m)\psi, \quad (2.8)$$

where $\bar{\psi} \equiv \psi^\dagger\gamma^0$.

The solutions of Dirac equation, Eq. (2.6), for $p_0 > 0$ can be found by using the expansion $\psi(x) = u(p)e^{-ip\cdot x}$. After inserted into Eq. (2.6) we obtain

$$u^s(p) = \begin{pmatrix} \sqrt{p\cdot\sigma}\xi^s \\ \sqrt{p\cdot\bar{\sigma}}\xi^s \end{pmatrix}, \quad s = 1, 2, \quad (2.9)$$

where $\sigma^\mu = (1, \boldsymbol{\sigma})$ and $\bar{\sigma}^\mu = (1, -\boldsymbol{\sigma})$ are Pauli matrices and ξ^s form a basis for the two-component spinor space. Analogously, the solutions of Dirac equation for $p_0 < 0$ are obtained using the expansion $\psi(x) = v(p)e^{ip \cdot x}$, from which

$$v^s(p) = \begin{pmatrix} \sqrt{p \cdot \sigma} \eta^s \\ -\sqrt{p \cdot \bar{\sigma}} \eta^s \end{pmatrix}, \quad s = 1, 2. \quad (2.10)$$

Defining the time ordered product T by

$$\langle 0 | T \psi(x) \bar{\psi}(y) | 0 \rangle = \begin{cases} \langle 0 | \psi(x) \bar{\psi}(y) | 0 \rangle, & x^0 > y^0 \\ -\langle 0 | \bar{\psi}(y) \psi(x) | 0 \rangle, & x^0 < y^0 \end{cases}, \quad (2.11)$$

it is possible to compute the function correlating the states $\psi(x)$ with $\psi(y)$, whose expectation value, related with the propagator of a fermion field, ends up being the Green function of Eq. (2.6). This is,

$$S_F(x - y) = \langle 0 | T \psi(x) \bar{\psi}(y) | 0 \rangle = \int \frac{d^4 k}{(2\pi)^4} \frac{i(\not{k} + m)e^{-ik \cdot x}}{k^2 - m^2 + i0} = \int \frac{d^4 k}{(2\pi)^4} \tilde{S}_F(k) e^{-ik \cdot x}, \quad (2.12)$$

where the function \tilde{S}_F is the Fourier transformation of the function S_F . It is important to notice that Eqs. (2.9), (2.10) and (2.12) are relations among non-interacting fields. Interacting fields are going to be summarized in Sec. 2.6.2.

As mentioned at the beginning of this section, Dirac equation enables us to describe spin $\frac{1}{2}$ particles such as the electrons. Furthermore, the simplest interaction between these particles, presented in the Sec. 2.3, is given through the interchange of photons. This interaction has been described for years through the minimal coupling, which is given through the operator

$$D_\mu = \partial_\mu + ieA_\mu, \quad (2.13)$$

where A^μ is the 4-potential of the electromagnetic field. This can be reached through an elegant mechanism called *gauge symmetry*, which arises from demanding the Lagrangian to be invariant under local $U(1)$ transformations.

2.3 Quantum Electrodynamics

As it was mentioned above, the QED Lagrangian is locally invariant under $U(1)$ gauge group actions, i.e., invariant under the transformation $\psi \rightarrow e^{i\alpha(x)}\psi$. It becomes evident that the second term $m\bar{\psi}\psi$ in Eq. (2.8) is invariant under such a transformation, however, the term containing the derivative of ψ can be worked out with a unimodular scalar function connecting two points x and y , $U(y, x)$, which transforms as

$$U(y, x) \rightarrow e^{i\alpha(y)}U(y, x)e^{-i\alpha(x)}. \quad (2.14)$$

This is due to the fact that, for any directional derivative with direction n^μ ,

$$n^\mu \partial_\mu \psi = \lim_{\epsilon \rightarrow 0} \frac{1}{\epsilon} (\psi(x + \epsilon n) - \psi(x)). \quad (2.15)$$

Thus, defining the covariant derivative D_μ as

$$n^\mu D_\mu \psi = \lim_{\epsilon \rightarrow 0} \frac{1}{\epsilon} (\psi(x + \epsilon n) - U(x + \epsilon n, x)\psi(x)), \quad (2.16)$$

it is possible to expand the argument of the limit with its Taylor series with respect to ϵ , $U(x + \epsilon n, x) = 1 - ie n^\mu A_\mu \epsilon + \mathcal{O}(\epsilon^2)$, where e is the electric charge of the fermion field ψ

and the vector field, A_μ , represents the electromagnetic field, namely, the photon. Then, we obtain

$$D_\mu = \partial_\mu + ieA_\mu, \quad (2.17)$$

where the minimal coupling, presented in Eq. (2.13), becomes explicit. In the same manner, expanding the transformation of the function $U(y, x)$, the gauge field A_μ transforms as

$$A_\mu \rightarrow A_\mu - \frac{1}{e}\partial_\mu\alpha. \quad (2.18)$$

It is important to recall that, with the transformation presented in Eq. (2.18), a mass term, such as $A_\mu A^\mu$, is not gauge invariant and thus, a massive term for A_μ would break the gauge invariance of the Lagrangian of the theory. Therefore, imposing gauge symmetry would not allow, in principle, massive gauge bosons.

From its definition, Eq. (2.16), the covariant derivative of the field ψ , $D_\mu\psi$ transforms according to

$$D_\mu(e^{i\alpha(x)}\psi) \rightarrow e^{i\alpha(x)}D_\mu\psi. \quad (2.19)$$

In this manner, the local gauge invariance is recovered if one performs the replacement $\partial_\mu \rightarrow D_\mu$. Besides the Lagrangian obtained from this replacement, a kinetic term for the field A_μ is still needed. As the local transformation law Eq. (2.14) holds, the covariant derivative transforms similarly. Furthermore, the second covariant derivative and the commutator transform as

$$[D_\mu, D_\nu]\psi \rightarrow e^{i\alpha(x)}[D_\mu, D_\nu]\psi. \quad (2.20)$$

Direct computation of the commutator of covariant derivatives yields to

$$[D_\mu, D_\nu] = ie(\partial_\mu A_\nu - \partial_\nu A_\mu) = ieF_{\mu\nu}. \quad (2.21)$$

Hence, the electromagnetic tensor $F_{\mu\nu}$ is locally gauge invariant. This is how the full QED Lagrangian can be obtained from the local gauge invariance of the free field Lagrangian Eq. (2.8), namely,

$$\mathcal{L}_{QED} = \bar{\psi}(i\not{D} - m)\psi - \frac{1}{4}F_{\mu\nu}F^{\mu\nu}. \quad (2.22)$$

As expected, it can be noticed that there is no quadratic term in A^μ , i.e., there is no mass term for the photon field. Hence, imposing gauge invariance leads to an elegant construction of the interaction of massive electrons with massless photons, as it appears to be in Nature.

It is interesting to see that the interactions between charged particles and photons can be read directly in QED Lagrangian, Eq. (2.22), in the term embedded in the covariant derivative, which is proportional to

$$\bar{\psi}\not{A}\psi, \quad (2.23)$$

where the electromagnetic 4-potential A^μ is coupled to two charged fermions ψ and $\bar{\psi}$. This can be represented through the diagram in Fig. 2.1 which is an example of the well-known Feynman diagrams, relating diagrams to analytical expressions through the Feynman rules, presented in Appendix A.

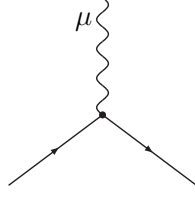


Figure 2.1: Interaction vertex in QED.

Eqs. (2.9) and (2.10) can be written in the so-called *chiral representation* (also known as *Weyl representation*), where

$$\psi = \begin{pmatrix} \psi_L \\ \psi_R \end{pmatrix}, \quad (2.24)$$

where ψ_L and ψ_R are called *chiral spinors* of the wave function ψ . This representation splits the wave function ψ into a left and right components, and these components can be obtained from the wave function ψ with the aid of the matrix $\gamma^5 = i\gamma^0\gamma^1\gamma^2\gamma^3$, through the projector operators

$$P_R = \frac{1 + \gamma^5}{2}, \quad P_L = \frac{1 - \gamma^5}{2}. \quad (2.25)$$

In this chiral representation, Dirac equation is written in the form

$$(i\not{\partial} - m)\psi = \begin{pmatrix} -m & i(\partial_0 + \boldsymbol{\sigma} \cdot \boldsymbol{\nabla}) \\ i(\partial_0 - \boldsymbol{\sigma} \cdot \boldsymbol{\nabla}) & -m \end{pmatrix} \begin{pmatrix} \psi_L \\ \psi_R \end{pmatrix} = 0. \quad (2.26)$$

It becomes evident that the left and right chiral spinors are coupled through the mass term. Thus, if we work with massless fermions, the chiral spinors decouple leading to the chiral equations,

$$i\bar{\sigma} \cdot \partial\psi_L = 0, \quad i\sigma \cdot \partial\psi_R = 0. \quad (2.27)$$

From the three fundamental interactions described by the Standard Model, QED is the simplest one, being a QFT with a Lagrangian invariant under $U(1)$ transformations. QED interactions are mediated by photons and they couple to fermions through their electric charge, while photons are massless neutral particles. Regarding the other two interactions, Quantum Chromodynamics (QCD) and Weak interactions, some words should be given. In QCD, gauge bosons, called *gluons* are color-charged particles leading to gluon interactions and, as shown in this section, an Abelian gauge theory cannot lead to gauge bosons interactions. With respect to Weak interactions, gauge bosons are massive, which is a characteristic property of this force. As it is going to be shown in the next section, non-Abelian QFTs also lead to massless gauge bosons, and thus a mechanism for gauge bosons to acquire mass is needed. This mechanism, known as *Higgs mechanism*, is explained in Sec. 2.5.1. Nevertheless, in order to have a theory with both charged gauge bosons and massive gauge bosons, it is necessary to introduce non-Abelian gauge theories and, in fact, Nature seems to be well described by them.

2.4 Non-Abelian gauge theories

Non-Abelian gauge theories are based on special unitary groups such as $SU(2)$ and $SU(3)$. An analogue procedure as that presented in the last section can be developed in order to calculate the invariant Lagrangian for these theories. To begin with the computations, it is important to consider the generators of the group, \mathbf{T}^a . As $SU(N)$ group can be represented by the set of $N \times N$ complex matrices M with $\det(M) = 1$, there are $N^2 - 1$ independent

parameters for M , and thus, $N^2 - 1$ generators for this group. This is an important fact, as the number of different gauge bosons is directly related to the number of generators of the group. For instance, for QED, a $U(1)$ gauge invariant theory, there is just one generator related to the photon, while in QCD, being an $SU(3)$ gauge invariant theory, there are 8 different generators, hence, 8 different gluons. Additionally, the generators must be Hermitian and satisfy the condition

$$\text{tr}[\mathbf{T}^a] = 0. \quad (2.28)$$

The commutator of two generators fullfills a Lie algebra relation as

$$[\mathbf{T}^a, \mathbf{T}^b] = \imath f^{abc} \mathbf{T}^c, \quad (2.29)$$

where the coefficients f^{abc} are the structure constants. By definition, structure constants are anti-symmetric.

Following the ideas of invariance under Abelian gauge groups, the transformation of the field ψ is now given in the form $\psi \rightarrow \exp[\imath \alpha_a \mathbf{T}^a] \psi$, in such a way that the function U is transformed as

$$U(y, x) \rightarrow \exp[\imath \alpha^a(y) \mathbf{T}^a] U(y, x) \exp[-\imath \alpha^a(x) \mathbf{T}^{a\dagger}]. \quad (2.30)$$

The function U can be expanded as $U(x + \epsilon n, x) = 1 + \imath g_S \epsilon n^\mu A_\mu^a \mathbf{T}^a + \mathcal{O}(\epsilon^2)$, where g_S is the charge of the interaction (similar to the electric charge e in QED). Comparing this expansion with the QED expansion, it is seen that in non-Abelian gauge theories $-g_S \mathbf{T}^a$ plays the role of e in QED, this is, $-g_S \mathbf{T}^a$ is the charge associated to this interaction. In this way, the covariant derivative is given by

$$D_\mu = \partial_\mu - \imath g_S A_\mu^a \mathbf{T}^a. \quad (2.31)$$

After expanding the transformation of the function U and comparing the terms of order ϵ , it is possible to obtain the transformation of the vector field,

$$A_\mu^a \mathbf{T}^a \rightarrow \exp[\imath \alpha^a(x) \mathbf{T}^a] \left(A_\mu^a \mathbf{T}^a - \frac{\imath}{g_S} \partial_\mu \right) \exp[-\imath \alpha^a(x) \mathbf{T}^{a\dagger}]. \quad (2.32)$$

Hence, it is then possible to arrive to the invariance of the covariant derivative in a non-Abelian theory, namely

$$D_\mu(\exp[\imath \alpha^a(x) \mathbf{T}^a] \psi) = \exp[\imath \alpha^a(x) \mathbf{T}^a] D_\mu \psi. \quad (2.33)$$

As usual, the field strength tensor is defined by the commutator of the covariant derivatives, through the relation $-\imath g_S F_{\mu\nu}^a \mathbf{T}^a = [D_\mu, D_\nu]$ or, more explicitly

$$F_{\mu\nu}^a = \partial_\mu A_\nu^a - \partial_\nu A_\mu^a + g_S f^{abc} A_\mu^b A_\nu^c. \quad (2.34)$$

The last term of Eq. (2.34) should not be identified as a mass term of the gauge field A_μ . This is due to the anti-symmetry property of the structure constants f^{abc} . Hence, the gauge fields A_μ is still massless, just as in the theory of QED.

It is then found that for a non-Abelian theory, such as that in Yang-Mills theory, the lagrangian is given by

$$\mathcal{L}_{YM} = \bar{\psi}(\imath \not{D} - m)\psi - \frac{1}{4} F_{\mu\nu}^a F_a^{\mu\nu}. \quad (2.35)$$

The last term in the field strength tensor, Eq. (2.34), involves explicitly the boson-boson interaction, which is not present in Eq. (2.21) for QED, because the latter is an Abelian gauge theory, and whence yields to non-self-interacting photons.

It is still needed to quantize the non-Abelian gauge field. This can be done through the formalism developed by Faddeev and Popov [39]. Starting with a pure gauge theory, without fermions, we have the functional integral

$$\int \mathcal{D}A \exp \left[i \int d^4x \left(-\frac{1}{4} (F_{\mu\nu}^a)^2 \right) \right]. \quad (2.36)$$

In this formalism, a gauge transformation is fixed within the Feynman path integral computations through the function $G(A) = 0$, so that it is harmless to introduce the constriction through the functional integral identity

$$\int \mathcal{D}\alpha \delta(G(A^\alpha)) \det \left(\frac{\delta G(A^\alpha)}{\delta \alpha} \right) = 1, \quad (2.37)$$

where A^α and A are related through a finite transformation, namely

$$(A^\alpha)_\mu^a = e^{i\alpha^a t^a} \left[A_\mu^b t^b + \frac{i}{g_S} \partial_\mu \right] e^{-i\alpha^a t^a}, \quad (2.38)$$

of in its infinitesimal form

$$(A^\alpha)_\mu^a = A_\mu^a + \frac{1}{g_S} \partial_\mu \alpha^a + f^{abc} A_\mu^b \alpha^c = A_\mu^a + \frac{1}{g_S} D_\mu \alpha^a, \quad (2.39)$$

with D the covariant derivative. It is worth noticing that the functional derivative $\delta G(A)/\delta \alpha$ in Eq. (2.37) is independent of α whenever $G(A)$ is linear. As the Lagrangian is gauge invariant, and by means of unitarity and linearity of the transformation in Eq. (2.38) (this equation represents a linear shift followed by a rotation of the components of A_μ^a), the integration measure is preserved, $\mathcal{D}A = \mathcal{D}A^\alpha$, so that

$$\int \mathcal{D}A e^{iS[A]} = \int \mathcal{D}A e^{iS[A]} \delta(G(A)) \det \left(\frac{\delta G(A)}{\delta \alpha} \right). \quad (2.40)$$

Fixing this gauge to the so called *Lorentz gauge*¹, namely, taking $G(A) = \partial^\mu A_\mu^a - \omega^a$, leads to the propagator of the field A_μ^a , namely,

$$\langle A_\mu^a A_\nu^b \rangle = \int \frac{d^4k}{(2\pi)^4} \frac{-i}{k^2 + i0} \left(g_{\mu\nu} - (1 - \xi) \frac{k_\mu k_\nu}{k^2} \right) \delta^{ab} e^{-ik \cdot (x-y)}, \quad (2.41)$$

where δ^{ab} is the Kronecker delta function and ξ is a parameter that fixes the gauge. In particular, the Feynman-t'Hooft gauge is obtained from Eq. (2.41) using $\xi = 1$.

Interesting to see is that inserting Eq. (2.38) into Eq. (2.37) leads to

$$\frac{\delta G(A)}{\delta \alpha} = \frac{1}{g_S} \partial^\mu D_\mu, \quad (2.42)$$

and so, the functional determinant gives rise to a field-like Lagrangian structure,

$$\det \left(\frac{1}{g_S} \partial^\mu D_\mu \right) = \int \mathcal{D}c \mathcal{D}\bar{c} \exp \left[i \int d^4x \bar{c} (-\partial^\mu D_\mu) c \right], \quad (2.43)$$

¹Some other possible gauges are presented in QFT textbooks. We exhort the interested reader to follow the references [40–43]

namely, the anticommuting fields c and \bar{c} that are scalars under Lorentz transformations. These are called *Faddeev-Popov ghosts*, whose Lagrangian is explicitly given by

$$\mathcal{L}_{\text{ghost}} = \bar{c}^a (-\partial^2 \delta^{ab} - g_S \partial^\mu f^{abc} A_\mu^b) c^c, \quad (2.44)$$

from which we identify the first term as a kinematic term, giving rise to the propagator

$$\langle c^a(x) \bar{c}^b(y) \rangle = \int \frac{d^4 k}{(2\pi)^4} \frac{i}{k^2} \delta^{ab} e^{-ik \cdot (x-y)}, \quad (2.45)$$

This is how the perturbative theory of non-Abelian gauge theories is obtained, leading to the QCD Lagrangian (where it is customary to define $G_{\mu\nu}^a \equiv F_{\mu\nu}^a$)

$$\mathcal{L}_{QCD} = -\frac{1}{4} (G_{\mu\nu}^a)^2 + \frac{1}{2\xi} (\partial^\mu A_\mu^a)^2 + \bar{\psi} (i\not{D} - m) \psi + \bar{c}^a (\partial^\mu D_\mu^{ab}) c^b \quad (2.46)$$

In an analogous way as in Sec. 2.3, Feynman rules for QCD can be extracted directly from the Lagrangian in Eq. (2.46). These rules are presented in Appendix A.

The relations presented up to this point give the framework to describe kinematics of fundamental particles of SM. However, it is still necessary to describe the mass generation mechanism of particles, as well as the description of the Weak interactions. Both rely on the symmetry breaking mechanism, and is presented in the next Section.

2.5 QFT at work: The Standard Model

Physics of SM is presented as a local, unitary and renormalizable QFT describing the fundamental interactions between fermions and bosons. These interactions can be understood by means of the gauge symmetry defined by

$$SU(3)_C \otimes SU(2)_L \otimes U(1)_Y, \quad (2.47)$$

with $SU(3)_C$ the group associated to Quantum Chromodynamics (QCD) governing the strong interactions and $SU(2)_L \otimes U(1)_Y$ is the group associated to the Electroweak (EW) interactions. The study of QED and QCD Lagrangians are presented in Sec. 2.3 and 2.4, respectively. The description of the Weak interaction is given by means of breaking the gauge symmetry. Also, without the weak interactions, the mass of each particle might be accepted as an arbitrary term in each Lagrangian. This is why symmetry breaking mechanisms are presented in this Section, where we are interested to show how $SU(2)_L$ group is broken, as it is the case in the SM. We also present different ways of breaking an arbitrary $SU(2)$ group, in order to highlight the different results obtained by changing the representation of the associated scalar field.

2.5.1 Breaking symmetries and mass generation in the SM

One of the gauge symmetry breaking mechanisms is the so-called *Higgs mechanism*. Let us begin the overview of Higgs mechanism with a scalar field doublet ϕ within the $SU(2)_L$ group, with expectation value ϕ_0 , parametrized by

$$\phi(x) = U(x) \frac{1}{\sqrt{2}} \begin{pmatrix} 0 \\ \phi_0 + h(x) \end{pmatrix}, \quad (2.48)$$

where the second component of the doublet in the right hand side is real, with a real fluctuation $h(x)$ around ϕ_0 , so that $\langle h \rangle = 0$, and U is an arbitrary $SU(2)$ transformation which makes $\phi(x)$ an arbitrary 2-component complex doublet. Being the Lagrangian an

$SU(2)$ invariant expression, it is possible to eliminate this transformation through a second gauge transformation, obtaining only one degree of freedom for ϕ ¹. For a non-vanishing expectation value ϕ_0 , it is possible to write down the Lagrangian

$$\mathcal{L} = |D_\mu\phi|^2 + \mu^2\phi^\dagger\phi - \lambda(\phi^\dagger\phi)^2, \quad (2.49)$$

so that it is possible to obtain the expectation value ϕ_0 , namely,

$$\phi_0 = \sqrt{\frac{\mu^2}{\lambda}}. \quad (2.50)$$

Substituting Eq. (2.48) into the potential energy terms of Eq. (2.49), we obtain the terms

$$-\mu^2h^2 - \lambda\phi_0h^3 - \frac{1}{4}\lambda h^4 = -\frac{1}{2}m_h^2h^2 - \sqrt{\frac{\lambda}{2}}m_hh^3 - \frac{1}{4}\lambda h^4. \quad (2.51)$$

The particle related to the field h is the so-called *Higgs boson*, which is scalar with mass

$$m_h = \sqrt{\frac{\lambda}{2}}\phi_0. \quad (2.52)$$

The presence of Higgs boson plays a central role in describing Weak interaction in an spontaneous broken symmetry.

In order to give a look on Higgs mechanism, let us consider a set of n scalar fields ϕ_i , each of which having an expectation value

$$\langle\phi_i\rangle = (\phi_0)_i, \quad (2.53)$$

described through an invariant Lagrangian under a gauge group G of transformations of the form

$$\phi_i \rightarrow (1 + i\alpha^a t^a)_{ij}\phi_j, \quad (2.54)$$

so that the transformations t^a are purely imaginary Hermitian transformations. Hence, it is possible to define a real antisymmetric transformation

$$T_{ij}^a = -it_{ij}^a, \quad (2.55)$$

leading to a covariant derivative of the form

$$(D_\mu\phi)_i = (\partial_\mu + gA_\mu^a T_{ij}^a)\phi_j, \quad (2.56)$$

for some gauge field A_μ^a and coupling g . Then, the kinematic term is given by

$$\frac{1}{2}|D_\mu\phi|^2 = \frac{1}{2}|\partial_\mu\phi|^2 + \partial_\mu\phi_i T_{ij}^a\phi_j + \frac{1}{2}g^2 A_\mu^a A^{b\mu} (T^a\phi)_i (T^b\phi)_i. \quad (2.57)$$

Expanding Eq. (2.57) around $(\phi_0)_i$, it is obtained a mass-like term for the gauge field A_μ^a , namely

$$\frac{1}{2}g^2 (T^a\phi_0)_i (T^b\phi_0)_i A_\mu^a A^{b\mu} = \frac{1}{2}m_{ab}^2 A_\mu^a A^{b\mu}. \quad (2.58)$$

We see that the matrix m_{ab}^2 has non-negative diagonal entries in any basis, as for $a = b$, the corresponding matrix element is given by $g^2 (T^a\phi_0)^2 \geq 0$. Some generators might vanish under the expectation vacuum of ϕ , $T^a\phi_0 = 0$, while the other generators

¹A full discussion on the degrees of freedom demands the study of Goldstone theorem, which relates other degrees of freedom to bosons called *Goldstone bosons*. In this work we do not attempt to describe this theorem.

will contribute to gauge bosons masses as expressed in Eq. (2.67).

As an example of the non-Abelian gauge theory, we can take the $SU(2)$ gauge group, so that $t^a = \sigma^a/2$. Thus, if the scalar field ϕ , transforming as a spinor under $SU(2)$ action, reaches an expectation value given by

$$\langle \phi \rangle = \frac{1}{\sqrt{2}} \begin{pmatrix} 0 \\ \phi_0 \end{pmatrix}, \quad (2.59)$$

the covariant derivative $D_\mu = \partial_\mu - igA_\mu^a t^a$ leads to a term of the form

$$\Delta\mathcal{L} = \frac{1}{2}g^2(\phi_0)^2 t^a t^b \begin{pmatrix} 0 \\ \phi_0 \end{pmatrix} A_\mu^a A^{b\mu}, \quad (2.60)$$

which can be simplified through the algebra satisfied by Pauli matrices to the mass term

$$\Delta\mathcal{L} = \frac{g^2\phi_0^2}{8} A_\mu^a A^{a\mu}. \quad (2.61)$$

Eq. (2.61) shows that all generators of $SU(2)$ are broken, and each of the three associated gauge bosons acquire a mass

$$m_A = \frac{g\phi_0}{2}. \quad (2.62)$$

Nevertheless, if the scalar field ϕ transforms as in the vector representation of $SU(2)$ and with expectation value pointing in a fixed arbitrary direction (let us assume this is the third axis) $\langle \phi \rangle_c = (\phi_0)_c \delta_{c3}$, then the covariant derivative takes the form $(D_\mu\phi)_a = \partial_\mu\phi_a - ig\epsilon_{abc}A_\mu^b\phi_c$, and hence the kinetic energy term of this scalar field in the Lagrangian leads to the mass terms

$$\Delta\mathcal{L} = \frac{1}{2}g^2(\epsilon_{abc}A_\mu^a(\phi_0)_c)^2 = \frac{1}{2}g^2(\phi_0)_3^2((A_\mu^1)^2 + (A_\mu^2)^2), \quad (2.63)$$

in such a way that the gauge boson related to the third generator remains massless while the other two become massive, with the same mass

$$m_1 = m_2 = g(\phi_0)_3. \quad (2.64)$$

In this manner, the way Higgs mechanism spontaneously breaks a gauge symmetry depends directly on the representation of the scalar field ϕ .

Now, let us begin with the description of Weak interactions following the well-known Glashow-Weinberg-Salam (GWS) approach [44, 45]. This is given in a $SU(2)$ gauge symmetry and a spontaneously symmetry breaking through a scalar field in the spinor representation as shown in Eq. (2.59). As presented in Eqs. (2.61) and (2.62), this leads to no massless gauge boson, although one is required due to experimental data (the photon), so an additional $U(1)$ gauge symmetry is imposed, where the scalar field has a charge $+1/2$. Then, the complete gauge transformation is given by

$$\phi \rightarrow e^{i\alpha^a t^a} e^{i\beta/2} \phi, \quad (2.65)$$

where $t^a = \sigma^a/2$. In particular, for $\alpha^1 = \alpha^2 = 0$ and $\alpha^3 = \beta$, the vacuum expectation value of ϕ remains invariant, leading to a massless gauge boson associated to this linear combination of the generators. Also, as $U(1)$ and $SU(2)$ transformations commute with

one another, their coupling constants might be different, so that the covariant derivative takes the form

$$D_\mu \phi = (\partial_\mu - igA_\mu^a t^a - i\frac{1}{2}g'B_\mu)\phi. \quad (2.66)$$

The mass terms for the gauge bosons come from the square of this covariant derivative, and are given by

$$\Delta\mathcal{L} = \frac{1}{2}[g^2(A_\mu^1)^2 + g^2(A_\mu^2)^2 + (-gA_\mu^3 + g'B_\mu)^2], \quad (2.67)$$

where the substitution $t^a = \sigma^a/2$ has been performed explicitly. Thus, from Eq. (2.67) we can extract the gauge fields masses, where the vector bosons

$$W_\mu^\pm = \frac{1}{\sqrt{2}}(A_\mu^1 \mp iA_\mu^2) \quad (2.68)$$

acquire the mass $m_W = gv/2$, the vector boson

$$Z_\mu^0 = \frac{1}{\sqrt{g^2 + g'^2}}(gA_\mu^3 - g'B_\mu) \quad (2.69)$$

acquires the mass $m_Z = \sqrt{g^2 + g'^2}v/2$, and the fourth vector boson, which must be orthogonal to Z_μ^0 ,

$$A_\mu = \frac{1}{\sqrt{g^2 + g'^2}}(g'A_\mu^3 + gB_\mu) \quad (2.70)$$

is massless. Now, for a fermion field in a general $SU(2)$ representation with $U(1)$ charge Y , the covariant derivative reads

$$D_\mu = \partial_\mu - igA_\mu^a t^a - ig'YB_\mu, \quad (2.71)$$

or, defining $T^\pm = t^1 \pm it^2$, Eq. (2.71) can be written in terms of the mass eigenstates (2.68), (2.69) and (2.70), namely,

$$\begin{aligned} D_\mu = \partial_\mu - i\frac{g}{\sqrt{2}}(W_\mu^+ T^+ + W_\mu^- T^-) - i\frac{1}{\sqrt{g^2 + g'^2}}Z_\mu(g^2 t^3 - g'^2 Y) \\ - i\frac{gg'}{\sqrt{g^2 + g'^2}}A_\mu(T^3 + Y). \end{aligned} \quad (2.72)$$

From the last term in this equation we can associate A_μ to the photon field, identifying the charge quantum number

$$Q = T^3 + Y, \quad (2.73)$$

and the electron charge

$$e = \frac{gg'}{\sqrt{g^2 + g'^2}}. \quad (2.74)$$

It is customary to introduce the *weak mixing angle* θ_w , which comes from the relations among (Z_μ^0, A_μ) and (A^3, B) , namely

$$\begin{pmatrix} Z^0 \\ A \end{pmatrix} = \begin{pmatrix} \cos\theta_w & -\sin\theta_w \\ \sin\theta_w & \cos\theta_w \end{pmatrix} \begin{pmatrix} A^3 \\ B \end{pmatrix}, \quad (2.75)$$

so that

$$\cos\theta_w = \frac{g}{\sqrt{g^2 + g'^2}}, \quad \sin\theta_w = \frac{g'}{\sqrt{g^2 + g'^2}}, \quad (2.76)$$

and the covariant derivative takes the form

$$D_\mu = \partial_\mu - i\frac{g}{\sqrt{2}}(W_\mu^+ T^+ + W_\mu^- T^-) - i\frac{g}{\cos\theta_w}(T^3 - \sin^2\theta_w Q) - ieA_\mu Q. \quad (2.77)$$

In GWS theory of Weak interactions, we separate left- and right-handed fermions, being the former described as doublets of $SU(2)$ and the latter described as singlets of the same group. Thus we can think of them as distinct particles, being mixed by the mass term. We can describe left-handed leptons and quarks through the doublets

$$E_L = \begin{pmatrix} \nu_e \\ e_L \end{pmatrix}, \quad Q_L = \begin{pmatrix} u_L \\ d_L \end{pmatrix}, \quad (2.78)$$

in such a way that the kinetic energy of the fermions can be described by the Lagrangian

$$\mathcal{L} = \bar{E}_L i \not{D} E_L + \bar{e}_R i \not{D} e_R + \bar{Q}_L i \not{D} Q_L + \bar{u}_R i \not{D} u_R + \bar{d}_R i \not{D} d_R, \quad (2.79)$$

which, after the substitution of the covariant derivative, Eq. (2.77), reads

$$\begin{aligned} \mathcal{L} = & \bar{E}_L i \not{\partial} E_L + \bar{e}_R i \not{\partial} e_R + \bar{Q}_L i \not{\partial} Q_L + \bar{u}_R i \not{\partial} u_R + \bar{d}_R i \not{\partial} d_R \\ & + g(W_\mu^+ J_W^{\mu+} + W_\mu^- J_W^{\mu-} + Z_\mu^0 J_Z^\mu) + eA_\mu J_{EM}^\mu, \end{aligned} \quad (2.80)$$

where the currents are defined as

$$\begin{aligned} J_W^{\mu+} &= \frac{1}{\sqrt{2}}(\bar{\nu}_L \gamma^\mu e_L + \bar{u}_L \gamma^\mu d_L), \\ J_W^{\mu-} &= \frac{1}{\sqrt{2}}(\bar{e}_L \gamma^\mu \nu_L + \bar{d}_L \gamma^\mu u_L), \\ J_Z^\mu &= \frac{1}{\cos\theta_w} \left[\bar{\nu}_L \gamma^\mu \left(\frac{1}{2} \right) \nu_L + \bar{e}_L \gamma^\mu \left(-\frac{1}{2} + \sin^2\theta_w \right) e_L + \bar{e}_R \gamma^\mu (\sin^2\theta_w) e_R \right. \\ & \quad + \bar{u}_L \gamma^\mu \left(\frac{1}{2} - \frac{2}{3} \sin^2\theta_w \right) u_L + \bar{u}_R \gamma^\mu \left(-\frac{2}{3} \sin^2\theta_w \right) u_R \\ & \quad \left. + \bar{d}_L \gamma^\mu \left(-\frac{1}{2} + \frac{1}{3} \sin^2\theta_w \right) d_L + \bar{d}_R \gamma^\mu \left(\frac{1}{3} \sin^2\theta_w \right) d_R \right] \\ J_{EM}^\mu &= \bar{e} \gamma^\mu (-1) e + \bar{u} \gamma^\mu \left(\frac{2}{3} \right) u + \bar{d} \gamma^\mu \left(-\frac{1}{3} \right) d. \end{aligned} \quad (2.81)$$

GWS theory is a chiral gauge theory, and the involved particles are described by multiplets of the form $(E_L, e_R, Q_L, u_R, d_R)$, usually called *generation* of quarks and leptons. This is in a good agreement with the lack of evidence of right-handed neutrinos. The full consistency of the theory requires that all quarks and leptons appear in Nature following the same structure of the generations of fermions. In the SM, the description of particle physics is given by three generations of quarks and leptons, four gauge bosons (photons, gluons, W^\pm and Z^0), and Higgs boson, as described in Fig. 2.2.

The reader might have noticed that the fermion mass terms, proportional to $\bar{f}_L f_R + \bar{f}_R f_L$ for a fermion f , presents the issue of being described by two different representations of the $SU(2)$ gauge group, hence violating gauge symmetry. Nevertheless, it is possible to couple left- and right-handed spinors in a gauge-invariant term through the spinor representation of Higgs boson ϕ , for instance, for the electron,

$$- \lambda_e \bar{E}_L \cdot \phi e_R + \text{h.c.}, \quad (2.82)$$

where h.c. stands for *hermitian conjugate*, λ_e is a dimensionless coupling constant and the $SU(2)$ indices of ϕ and E_L are contracted. Thus, after expanding this expression about the vacuum expectation value of ϕ , Eq. (2.59), it is obtained

$$\Delta\mathcal{L} = -\frac{1}{\sqrt{2}} \lambda_e \phi_0 \bar{e}_L e_R + \text{h.c.} + \dots \quad (2.83)$$

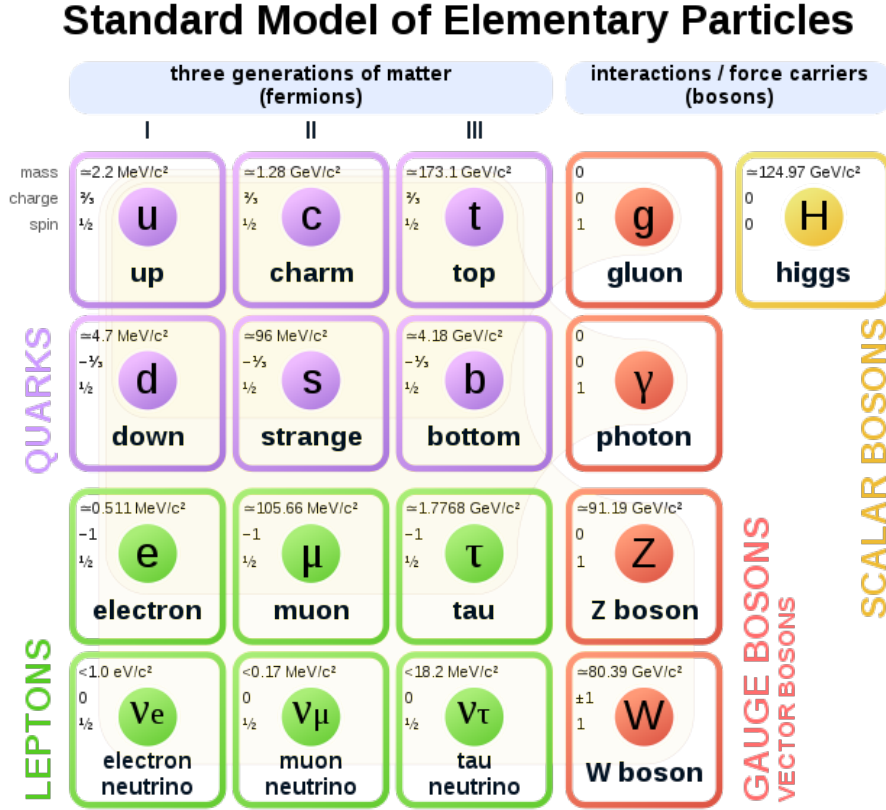


Figure 2.2: Standard Model of particle physics. Taken from Wikipedia https://en.wikipedia.org/wiki/Standard_Model

We notice that we obtain a mass term for the electron, where its mass is given by

$$m_e = \frac{1}{\sqrt{2}} \lambda_e \phi_0. \quad (2.84)$$

However, the SM includes coupling terms that mix the three generations. Let $u_L^i = (u_L, c_L, t_L)$ and $d_L^i = (d_L, s_L, b_L)$ be the up-like and down-like left-handed quarks in their original basis, and let $u_L'^i$ and $d_L'^i$ be the quarks in such a basis that diagonalizes their Higgs couplings¹. If we denote by U_u^{ij} and U_d^{ij} the changing basis matrices, this is

$$u_L^i = U_u^{ij} u_L'^j, \quad d_L^i = U_d^{ij} d_L'^j, \quad (2.85)$$

then the W current in this new basis is written in the form

$$J_W^{\mu+} = \frac{1}{\sqrt{2}} \bar{u}_L^i \gamma^\mu d_L^i = \frac{1}{\sqrt{2}} \bar{u}_L'^i \gamma^\mu (U_u^\dagger U_d)_{ij} d_L'^j, \quad (2.86)$$

where the unitary matrix,

$$V \equiv U_u^\dagger U_d, \quad (2.87)$$

is the so-called *Cabibbo-Kobayashi-Maskawa* (CKM) matrix [46, 47], and its off-diagonal elements allow weak interactions between generations.

¹This basis diagonalizes the mass matrix. This is a physical basis.

2.6 Computation of physical observables

Physics, as a phenomenological science, needs to be always confronted with experimental results. In this spirit, every theory within physics shall give theoretical predictions that have to be in agreement with experimental measurements in order to assure a correct interpretation of the natural phenomena. In this manner, the theory of the SM shall lead to a well-defined procedure for the computation of physical observables, which are experimentally accessible quantities. As this theory is based on QFT, determinism is not expected. Instead, the probabilistic property of Nature raises as it does in every quantum theory. In the specific case of particle physics, scattering processes are the natural way of studying the predictions of any QFT. As it is usual in quantum mechanics, the operator relating an initial state with a final state is called the scattering matrix, or briefly, the S -matrix, whose elements are known as *scattering amplitudes*. These amplitudes are used to compute the probability (colloquially known as the *cross-section*) of a certain scattering process to occur. The needed precision of the theoretical computations in nowadays research involve an intricate interplay between mathematical infinities and finite contributions. In this section we present the computational tools used in QFTs to obtain measurable quantities, and we give insight on how the divergences appear.

2.6.1 Scattering matrix and cross sections

As mentioned above, scattering processes are a natural way to study particle physics. For a given scattering process, the initial state of the colliding particles can be described by the vector (or *ket*) $|a\rangle = |p_1, \dots, p_n\rangle$, while the final state of the emerging particles can be described by $|b\rangle = |p'_1, \dots, p'_m\rangle$. It must be pointed out that both are free-particle states, namely, no interaction takes place. One possible outcome is that the initial particles do not interact, hence $|a\rangle = |b\rangle$. All other possibilities are regarded as interactions. In this manner, the probability that the interactions between the particles in $|a\rangle$ lead to the state $|b\rangle$ can be written as

$$S_{ba} = \langle b | S | a \rangle = \delta_{ba} + iT_{ba}, \quad (2.88)$$

where the second term is associated to the interactions, and includes the momentum conservation condition, i.e.,

$$T_{ba} = (2\pi)^4 \delta \left(\sum_{k \in b} p'_k - \sum_{k \in a} p_k \right) \mathcal{M}(a \rightarrow b), \quad (2.89)$$

where $\mathcal{M}(a \rightarrow b)$ is called the *invariant amplitude* of the process and it represents the probability amplitude of the occurrence of this process. The construction of the invariant amplitude follows the ideas of Feynman and it is formed by a collection of propagators, vertices and wavefunctions.

In particle physics, scattering processes are used as experimental probes to confront theory with Nature. In order to provide theoretical predictions to be compared with experiments, the differential cross section σ is given by

$$d\sigma = \frac{|\mathcal{M}|^2}{F} d\Pi, \quad (2.90)$$

where $d\Pi$ is an element of the phase space and F is called the *flux factor*, which depends on the kinematics of the experiment. Although Eq. (2.90) seems particularly simple, it is hidden the fact that \mathcal{M} is not exactly computable with nowadays techniques. Nevertheless, in certain kinematic regimes, it is possible to *approximate* its value with the aid of a technique called *perturbation theory*.

2.6.2 Perturbation theory and Feynman diagrams

Perturbation theory is a mathematical tool that enables to extract approximate solutions to problems that are analytically unsolvable, in the sense of a lack of mathematical approaches to reach exact solutions. Also, it is useful when the computations are cumbersome or complex. In this manner, perturbation theory makes it possible to approximate the exact solution of a problem. This approximation can be developed as a power series around a small parameter of the theory.¹

In order to present an overview of perturbation theory, let $H = H_0 + H_I$ be the Hamiltonian of a given system, with H_0 the Hamiltonian of a free field and H_I the terms of the Hamiltonian containing the interactions. This approach, called *interaction picture* can be used to simplify the computations, and to extract relations between interacting fields. For a given quantized field in the Heisenberg picture ϕ , its relation with its interaction picture ϕ_I is mediated by a unitary operator U , so that

$$\phi(x) = U^\dagger \phi_I(x) U. \quad (2.91)$$

The U operator is related with the interaction Hamiltonian H_I and with the interaction Lagrangian L_I through

$$U(t, t_0) = T \left\{ \exp \left[-i \int_{t_0}^t dt' H_I(t') \right] \right\} = T \left\{ \exp \left[i \int_{t_0}^t dt' L_I(t') \right] \right\}, \quad (2.92)$$

where the time ordered operator is understood to act on each term in the Taylor expansion of the exponential function.

In general, the ground state $|\Omega\rangle$ of the Hamiltonian H is different from the ground state $|0\rangle$ of H_0 . In fact, if $E_0 = \langle \Omega | H | \Omega \rangle$, then we can perform the expansion

$$e^{-iHT} |0\rangle = e^{-iE_0T} |\Omega\rangle \langle \Omega | 0 \rangle + \sum_{n \neq 0} e^{-iE_nT} |n\rangle \langle n | 0 \rangle. \quad (2.93)$$

Since $E_n > E_0$ for $n > 0$, it is possible to vanish the contribution of the first term if we take the limit $T \rightarrow \infty(1 - i0)$, where 0 represents a parameter which is sent to the number 0 eventually. Fortunately, the expectation values of time ordered products of two fields for the ground states $|\Omega\rangle$ and $|0\rangle$ are related by

$$\langle \Omega | T \phi(x) \phi(y) | \Omega \rangle = \lim_{t \rightarrow \infty(1-i0)} \frac{\langle 0 | T \{ \phi_I(x) \phi_I(y) U(t, -t) \} | 0 \rangle}{\langle 0 | T \{ U(t, -t) \} | 0 \rangle}. \quad (2.94)$$

From this result, it is possible to conclude that it is enough to compute observables in the interaction picture, as it will be used in the rest of this section. Therefore, the index I is dropped from now on. Eq. (2.94) gives the two-point correlation function for the field ϕ with the Hamiltonian H . In order to generalize this expression, it is important to realize that the field ϕ is a superposition of positive and negative frequencies, ϕ^+ and ϕ^- , satisfying the relations

$$\phi^+ |0\rangle = 0 \quad , \quad \langle 0 | \phi^- = 0. \quad (2.95)$$

From Eq. (2.95) it is possible to follow Wick's theorem [40], which is formulated on the interaction picture, in which we introduce the *normal ordered product*, $:\phi(x_1)\phi(x_2):$,

¹It is customary to take the coupling factor α in QFT as the small parameter.

related with the time ordered product, where all the positive-frequency components of the field are written in the far right of the term. Taking into account the commutation relations (for bosons) and the anti-commutation relations (for fermions), the contraction of a field in two points is defined as follows

$$\begin{aligned}\overline{\phi(x)\phi(y)} &= \begin{cases} [\phi^+(x), \phi^-(y)], & x^0 > y^0, \\ [\phi^+(y), \phi^-(x)], & y^0 > x^0, \end{cases} \\ \overline{\psi(x)\bar{\psi}(y)} &= \begin{cases} \{\psi^+(x), \bar{\psi}^-(y)\}, & x^0 > y^0, \\ -\{\bar{\psi}^+(y), \psi^-(x)\}, & y^0 > x^0. \end{cases}\end{aligned}\quad (2.96)$$

The relation between the normal ordered product and the time ordered product is the main result of Wick's theorem, which states

$$T(\phi(x_1)\dots\phi(x_n)) =: \phi(x_1)\dots\phi(x_n) + \text{all possible contractions} :. \quad (2.97)$$

Eq. (2.97) is valid for bosons as well as for fermions. It is important to notice that the contraction between equal fields is their propagator. Hence, the contractions can be rewritten as

$$\overline{\phi(x)\phi(y)} = G_F(x-y), \quad \overline{\psi(x)\bar{\psi}(y)} = S_F(x-y). \quad (2.98)$$

As it was mentioned in Section 2.2, the given solutions apply only for the ground state of non-interacting particles. Given a particle in the state $|p\rangle$, it is possible to obtain the relations

$$\phi^+(x)|p\rangle = e^{-ip\cdot x}|0\rangle, \quad \langle 0|\phi^-(x) = e^{ip\cdot x}, \quad (2.99)$$

and can be written as contractions of the form

$$\overline{\phi(x)|p\rangle} = e^{-ip\cdot x}, \quad \langle p|\phi(x) = e^{ip\cdot x}. \quad (2.100)$$

In an analogous way, the Dirac field gives the contractions

$$\overline{\psi|p,s\rangle} = u_s(p), \quad \overline{\bar{\psi}|k,s\rangle} = \bar{v}_s(k), \quad \langle p,s|\bar{\psi} = \bar{u}_s(p), \quad \langle k,s|\psi = v_s(k). \quad (2.101)$$

Recalling Eq. (2.94), the numerator $\langle 0|T(\phi(x)\phi(y)U(t,-t))|0\rangle$ can be studied by means of Wick's theorem. Therefore, each term in the expansion of this numerator can be associated with a so called *Feynman diagram*. These diagrams can be constructed for each term in the expansion starting with the fields outside the operator U , that are depicted as external particles. The expansion of the operator U up to a desired order in the parameter $\alpha = g^2/4\pi$ (for QED, $\alpha = e^2/4\pi$ is the well known fine structure constant) involve extra field factors that are represented by internal particles. The way all internal and external particles are related in the diagram is through their contractions, each of which represents a propagator for internal particles, spinors for external fermions and polarization vectors for external bosons. Thus each term in the expansion can be represented by a Feynman diagram. In fact, the relation is satisfied in both directions. This is, for each Feynman diagram, a set of rules called *Feynman rules*, gives the mathematical representation of the corresponding term in the expansion of Eq. (2.94). Feynman rules are presented in Appendix A. It is important to highlight that Feynman diagrams and rules depend on the theory they describe, so that the same rules are satisfied for every diagram within the same theory.

Different kinds of Feynman diagrams arise from Wick's theorem. One of these is the one-particle-irreducible (1PI) diagrams, being those that removing one internal edge will

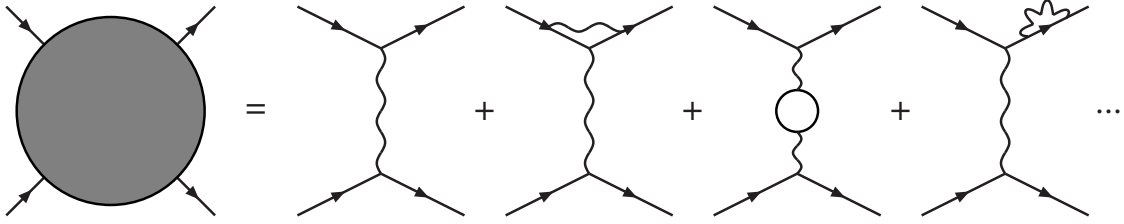


Figure 2.3: Electron-electron scattering in perturbative theory up to one loop.

not break it into two disjoint diagrams. Another one is the vacuum polarization diagrams, that are those lacking external particles. Eq. (2.94) can be rewritten in such a way that only 1PI contributes. Within these contributions, Feynman diagrams are also classified as *loop* diagrams, that are those containing a close path following adjacent propagators, and *tree-level* diagrams, containing no such close paths.

In summary, Feynman diagrams are pictorial representations of the perturbative computation of a given amplitude. For instance, in a purely QED theory, Eq. (2.22), the scattering of two electrons can be depicted as in Fig. 2.3.

The perturbative expansion given in Fig. 2.3 exhibits the usual procedure for the computation of an amplitude up to a given order in the interaction coupling α . First, all possible Feynman diagrams obtained from the theory with the corresponding number of vertices are depicted. Then, the application of Feynman rules gives the mathematical expression of these diagrams so that the computation can be developed. In view of the structure of Klein-Gordon, Dirac and gauge propagators, Eqs. (2.4), (2.12) and (2.41) respectively, divergences emerge naturally for the computation of some of the terms in a perturbative expansion, such as the second and third terms in Fig. 2.3. These divergences arise from the integration of rational functions on the loop momenta.

Several astonishing results arise from the computation of an n -point function $\langle \Omega | T \{ \phi(x_1) \dots \phi(x_n) \} | \Omega \rangle$. One of these is the Callan-Symanzik equation, which encodes the evolution of the factors known as *running couplings*. These running couplings show correlations between the intensity of the interactions and the energy at which the experiment is performed. Surprisingly, non-Abelian gauge theories, just like QCD, show a running coupling that decreases in value as the energy of the experiment increases. This is the reason of two particular properties related with QCD, known as *confinement* and *asymptotic freedom*.

Confinement and asymptotic freedom are two faces of the same phenomenon, which is the running of the coupling with negative rate with the energy. The interaction between two color-charged particles, as well as for any other interaction, depends on the energy, or equivalently, on the distance between these particles. In particular, for QCD, the shorter the distance, the weaker the interaction and vice-versa (the greater the distance, the stronger the interaction). Thus, on one hand, if the particles are close enough, the strength of the interaction becomes so soft that they behave as free particles (*asymptotic freedom*). This asymptotic freedom is the theoretical tool that allows us to perform perturbative calculations for QCD in the high-energy regime. On the other hand, when these color-charged particles are not so close one from another, the interaction becomes very strong. If the distance between them becomes large enough, the energy of the interaction takes such a great value that the creation of a new pair of color-charged particles is ener-

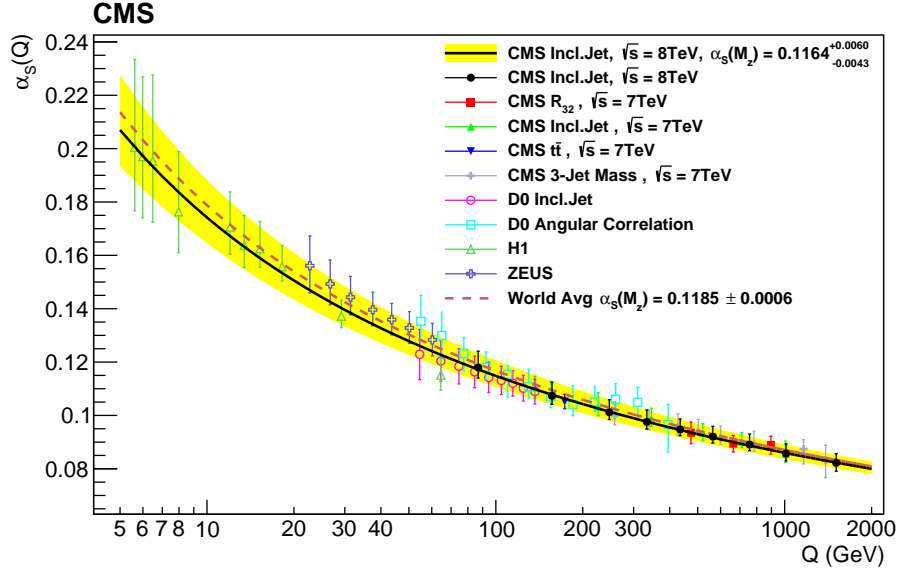


Figure 2.4: Comparison between theoretical predictions and experimental data for QCD running coupling α_s . Extracted from Ref. [49]

getically favourable, leading to two bounded systems. This is the qualitative explanation of confinement. Both confinement and asymptotic freedom lead to the conclusion that color-charged particles are never isolated. Whether the interaction between two particles creates another pair of particles as one tries to isolate one of them, or the only possibility to describe an isolated color-charged particle is to have this close to another one. It is important to stress that this is not just a mathematical consequence of the theory, but is in a remarkable agreement with experimental data as it can be seen in Fig. 2.4. D. J. Gross, H. D. Politzer and F. Wilczek won the Nobel Prize due to this explanation in QCD [38, 48]¹.

Perturbation theory gives us an elegant method to compute scattering amplitudes in order to compare theoretical results with experimental data. It is worth noting that every internal particle with momentum p and mass m has a Feynman propagator proportional to $(p^2 - m^2 + i0)^{-1}$. For on-shell particles (those with definite momentum), momentum and mass satisfy the Einstein equation, $p^2 = m^2$. For off-shell particles (those with undetermined momentum, appearing in loop-level diagrams) has an arbitrary momentum p which is not constrained by Einstein equation, but it should be integrated along all its possible values. For instance, in a production of three jets, $g \rightarrow gq\bar{q}$, a tree-level contribution is sketched in Fig. 2.5, where the final gluon has momentum p' and the final quark has momentum p and mass m . In this case, the internal quark has a propagator of the form

$$S_F(p + p') \propto \frac{\not{p} + \not{p}' + m}{(p + p')^2 - m^2 + i0} = \frac{\not{p} + \not{p}' + m}{2p \cdot p' + i0}. \quad (2.102)$$

Eq. (2.102) reflects an undesirable behaviour. For instance, if the gluon is soft, this is, if $p' \simeq 0$, the propagator in Eq. (2.102) tends to diverge. In general, computations of scattering amplitudes involve the presence of different kind of divergences. Some of these divergences have physical meaning, while some of them have not. A concrete explanation of the divergences appearing in the theory is given in the Sec. 3.1.

¹G. 't Hooft discovered first these phenomena, but did not publish his results.

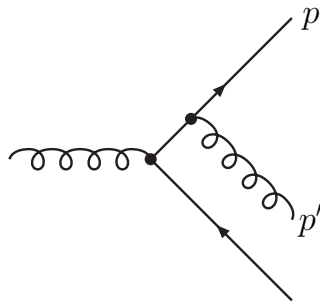


Figure 2.5: Three jets production through $g \rightarrow gq\bar{q}$.

Chapter 3

Singularities in QFT

Perturbative expansion gives rise to ill-defined expressions, meaning that their computations lead to *singularities* (or *divergences*) due to the mathematical structure of the propagators of the SM particles. These divergences can be removed with the aid of different regularisation procedures. In this chapter, the traditional Dimensional Regularisation (DREG) [50, 51] is described, and the mathematical properties are studied in order to tackle their cancelation at cross-section level.

3.1 The origin of divergences

Loop Feynman diagrams have unrestricted internal four-momenta. In order to obtain the scattering amplitude, integrals over all possible values of these four-momenta are mandatory. Formally speaking, an L -loop N -point function can be represented by the integral

$$\mathcal{A}(\{p_i\}_N) = \left(\prod_{i=1}^L \int \frac{d^4 \ell_i}{(2\pi)^4} \right) \prod_j f_j(\{\ell_k\}_L, \{p_i\}_N), \quad (3.1)$$

where ℓ_{kL} is the set of all loop momenta, p_{iN} is the set of all external momenta, and each of the functions f_j is a rational function of the loop and external momenta. It is important to stress that the final N -point function depends only on the external momenta.

For different processes, divergences of different nature could emerge. One of these divergences appear in the high-energy domain or, equivalently, in short distances (just like the force between two point-like charged particles in classical electrodynamics). This kind of divergence is called *ultraviolet* (UV). An example of the UV divergences appears for the scalar 1-loop 2-point function $L^{(1)}(p)$, as depicted in Fig. 3.1 (notice that \mathcal{A} is used for amplitudes while L is written for scalar functions).

The analytical expression for this function for massless internal particles is given by the integral

$$L^{(1)}(p) = -i \int \frac{d^4 \ell}{(2\pi)^4} \frac{1}{(\ell^2 + i0)((\ell + p)^2 + i0)}. \quad (3.2)$$

From Eq. (3.2) it is possible to perform a power counting on ℓ^2 , leading to the so-called *superficial degree of divergence*, which helps as an insight of possible UV divergences. In the UV limit, $\ell + p \simeq \ell$, the integrand is approximately $(\ell^2)^{-2}$. Also, the integration measure is of order $(\ell^2)^2$. Thus, the integral in Eq. (3.2) diverges logarithmically in the UV regime. Although the superficial degree of divergence is a good estimator of the level

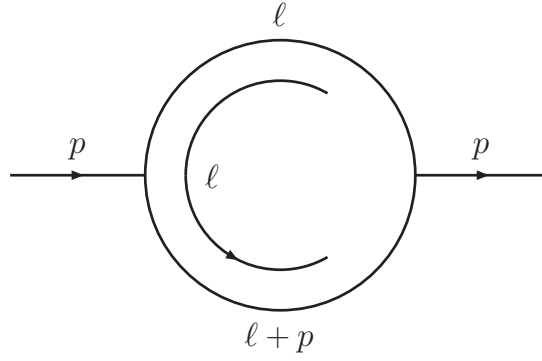


Figure 3.1: Scalar 1-loop 2-point function.

of the divergence of an object, sometimes it does not determine it correctly beyond one loop, particularly when there is a divergent sub-diagram.

There are other kinds of divergences, such as the *infrared* (IR) ones. These divergences appear when there are massless fields involved, since possible degenerate states can be found. IR divergences are associated with two different phenomena. One of them takes place when zero energy particles are radiated. As the experiment is blind for these particles, the emission of them makes no difference for the obtained data. In this respect, the experiment does not recognize the number of these *soft* particles, although mathematically it would be possible to reach a singularity with an arbitrary large number of them. This kind of divergence is called *soft*.

Another phenomenon appears in a similar way. In this case, a massless radiated particle could be emitted in the same direction as the massless radiating particle, being both parallel, whence these divergences are called *collinear*. In this scenario, the experiment would not distinguish between two particles with their own momenta, or one particle with its momentum being the sum of both. From a theoretical perspective, if both particles are massless, it is possible to look at the divergence in the propagator of the radiating particle before the radiation as shown in Fig. 3.2. The propagator would be of the form $G_F^{-1}(q) = 2q \cdot p + i0$, obtaining thus the divergences for $p \rightarrow 0$, or else, for $q_0 p_0 = \mathbf{q} \cdot \mathbf{p}$, respectively for soft or collinear divergences. It should be noted that these divergences were here described for real emissions, but these can occur just as well as for virtual (loop) amplitudes. This becomes evident when writing a loop amplitude as an integral over all possible values of the loop momenta.

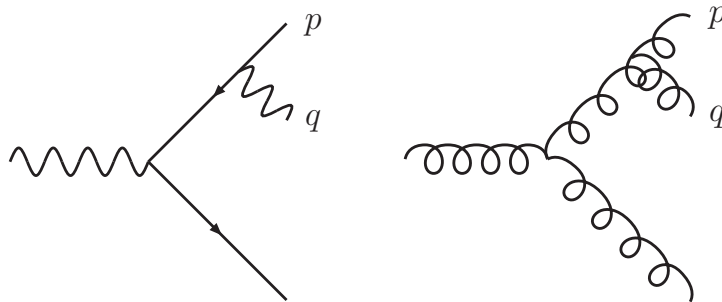


Figure 3.2: Examples of Feynman diagrams with IR divergences.

Other kind of divergences show up for particular configurations of momenta. These particular configurations leads to the so called *threshold* singularities. In the case of loop-level computations, thresholds singularities are interpreted as the intersection of two surfaces in a d -dimensional phase-space, corresponding to the equations $G_F^{-1}(q_i) = 0$ and $G_F^{-1}(q_j) = 0$. For the case of three or more simultaneous on-shell conditions, these divergences are known as *anomalous thresholds* [5]. The anomalous thresholds will be analysed later in this document.

The divergences studied up to here are the most common singularities found in high-precision computations. There are other divergences that have no physical meaning. These kinds of divergences are called *spurious* singularities, and should cancel between each other. In what follows, it will be shown how spurious singularities cancel in a natural way. This is a surprising result of the Loop-Tree Duality framework.

Physical measurable quantities are naturally finite, so that the divergences obtained arise due to the calculation methods, and theoretical predictions of these observables should be free of any divergence. In order to work with these divergences, a regularisation scheme must be taken into account. These regularisation schemes are the framework used to isolate divergences so that it is possible to avoid them or, if possible, remove them. Several regularisation schemes have been developed, for instance, introducing a non-physical particle with an arbitrary mass (usually written also as Λ , which is the regulator in the UV regime) defining the so-called *Pauli-Villars scheme* [52]. Among other regularisation schemes, they usually present fundamental issues (like violating fundamental principles, as it is the case of Lattice [53], which violates Lorentz invariance, or Pauli-Villars scheme, which introduces non-physical quantities) and sometimes they make the computations too complicated. *Dimensional Regularisation* (DREG) does not show the issues presented in other schemes.

3.2 Dimensional regularisation

DREG is a widely used regularisation scheme, introduced simultaneously and independent one to another by Giambiagi and Bollini [50], and by 't Hooft and Veltman [51]. The simplicity of its principles makes it a very powerful tool for high-precision computations within perturbation theory.

DREG consists on the analytical extension of the integration space (whether it is the space-time or energy-momentum coordinates) to an arbitrary dimension d ¹. This implies a consistent modification of other quantities. At the end of any computation, the limit $d \rightarrow 4$ is assumed to be taken in order to recover the theoretical predictions for high energy experiments. It is worth mentioning that this is a mathematical tool rather than a model of the physical nature of space-time. This modification introduces a parameter μ for each loop integral, so that the total dimension is fixed to four,

$$\int \frac{d^4 \ell}{(2\pi)^4} \rightarrow \mu^{4-d} \int \frac{d^d \ell}{(2\pi)^d} . \quad (3.3)$$

It is customary to write $d = 4 - 2\epsilon$, so that the limit $d \rightarrow 4$ is now written in the form $\epsilon \rightarrow 0$ (other conventions can be used, as it could be $d = 4 \pm \epsilon$). Being DREG an

¹Formally, being DREG an analytic continuation of the theory, it is mandatory to take $d \in \mathbb{C}$. Moreover, being an analytic continuation, each object obtained in this framework satisfies Cauchy-Riemann conditions. In this manner, every limit can be developed through any path, so that it is possible to think of d as being purely real, as we are interested in the limit $d \rightarrow 4$. However, there is no mathematical limitation on such limit, as in the examples given below.

analytical extension of the theory on the space-time dimension, it is important to notice that no divergence can be found for $d \neq 4$. With these ideas, any possible divergences can be isolated as poles in the parameter ϵ , i.e., functions of the form $1/\epsilon^n$.

As an example of the computations with DREG and customary techniques, let us compute the integral in Eq. (3.2). We start the computation with the so-called *Feynman parameters*, which relies on the identity

$$\frac{1}{AB} = \int_0^1 dx dy \frac{\delta(1-x-y)}{(xA+yB)^2}, \quad (3.4)$$

or in general,

$$\prod_{i=1}^n \frac{1}{A_i^{m_i}} = \int_0^1 \left(\prod_{i=1}^n \frac{x_i^{m_i-1} dx_i}{\Gamma(m_i)} \right) \delta \left(1 - \sum_{i=1}^n x_i \right) \frac{\Gamma \left(\sum_{i=1}^n m_i \right)}{\left(\sum_{i=1}^n x_i A_i \right)^{\sum_{i=1}^n m_i}}, \quad (3.5)$$

where Γ is the Euler Gamma function. Thus, Eq. (3.2) reads

$$\begin{aligned} L^{(1)}(p) &= -i\mu^{4-d} \int \frac{d^d \ell dx}{(2\pi)^d} \frac{1}{(x(\ell^2 + i0) + (1-x)((\ell+p)^2 + i0)^2)} \\ &= -i\mu^{4-d} \int \frac{d^d Q dx}{(2\pi)^d} \frac{1}{(Q^2 + x(1-x)p^2 + i0)^2}, \end{aligned} \quad (3.6)$$

with $Q = \ell + (1-x)p$.

Then, it is possible to perform the well-known *Wick rotation*, which formally implies a promotion of the energy-component of the integration momentum Q_0 into the complex numbers \mathbb{C} , and then integrate along a contour enclosing the first and third quadrant. Thus, we change the variable $Q_0 \rightarrow iQ'_0$, so that $d^d Q = i d^d Q'$ and $Q^2 = Q_0^2 - \mathbf{Q}^2 = -(Q_0'^2 + \mathbf{Q}^2)$, obtaining a 4 dimensional Euclidean momentum $Q' = (Q'_0, \mathbf{Q})$. Then, Eq. (3.6) can be rewritten as

$$\begin{aligned} L^{(1)}(p) &= \mu^{4-d} \int \frac{d^d Q' dx}{(2\pi)^d} \frac{1}{(-Q'^2 + x(1-x)p^2 + i0)^2} \\ &= \mu^{4-d} \int \frac{d\Omega dQ'^2 dx}{2(2\pi)^d} \frac{(Q'^2)^{\frac{d}{2}-1}}{(-Q'^2 + x(1-x)p^2 + i0)^2}, \end{aligned} \quad (3.7)$$

where $d\Omega$ is a solid-angle element of a $(d-1)$ -dimensional sphere. We can see that the integrand is isotropic, in such a way that the integral with respect to the solid angle factors out, leading to

$$\int \frac{d\Omega}{(2\pi)^d} = \frac{2}{(4\pi)^{\frac{d}{2}} \Gamma(\frac{d}{2})}. \quad (3.8)$$

After the change of variables $Q'^2 = (-x(1-x)p^2 - i0)t$, the integral takes the form

$$L^{(1)}(p) = \frac{\mu^{4-d}}{(4\pi)^{\frac{d}{2}} \Gamma(\frac{d}{2})} \int dx (-x(1-x)p^2 - i0)^{\frac{d}{2}-2} \int dt \frac{t^{\frac{d}{2}-1}}{(1+t)^2}. \quad (3.9)$$

The integral with respect to t is the Euler Beta function. Regarding the integral with respect to x , it is important to notice that the sign of the real part of the integrand does not change, and hence it is possible to factorize

$$-x(1-x)p^2 - i0 = x(1-x)(-p^2 - i0). \quad (3.10)$$

With this information, and after substituting $d = 4 - 2\epsilon$, it is possible to write down

$$L^{(1)}(p) = \frac{\mu^{2\epsilon}}{(4\pi)^{2-\epsilon}\Gamma(2-\epsilon)} B(2-\epsilon, \epsilon) (-p^2 - i0)^{-\epsilon} \int dx x(1-x)^{-\epsilon}. \quad (3.11)$$

Now the integral with respect to x also gives rise to a new Beta function, namely,

$$\int dx x^{-\epsilon}(1-x)^{-\epsilon} = B(1-\epsilon, 1-\epsilon), \quad (3.12)$$

leading to the result

$$L^{(1)}(p) = \frac{\mu^{2\epsilon}\Gamma(\epsilon)\Gamma^2(1-\epsilon)}{(4\pi)^{2-\epsilon}\Gamma(2-2\epsilon)} (-p^2 - i0)^{-\epsilon}, \quad (3.13)$$

or else, taking advantage of the multiplicative property of the gamma function, $x\Gamma(x) = \Gamma(1+x)$, the integral of Eq. (3.2) computed within DREG leads to

$$L^{(1)}(p) = c_\Gamma \frac{\mu^{2\epsilon}}{\epsilon(1-2\epsilon)} (-p^2 - i0)^{-\epsilon}, \quad (3.14)$$

with the coefficient c_Γ the d -dimensional volume factor of 1-loop computations, given by

$$c_\Gamma = \frac{\Gamma(1+\epsilon)\Gamma(1-\epsilon)^2}{(4\pi)^{2-\epsilon}\Gamma(1-2\epsilon)}. \quad (3.15)$$

It is important to notice that the volume factor c_Γ is finite when the limit $\epsilon \rightarrow 0$ is taken. In Eqs. (3.14) and (3.15) the dependence of the integral in Eq. (3.2) with the dimension of the integration space is exhibited. The divergence explicitly appear with the factor ϵ in the denominator, in such a way that the massless scalar 1-loop two-point function diverges for $d = 4$, as expected. This is the usual procedure when working with DREG in higher-order computations in perturbation theory.

Simpler examples such as the integral of the functions $(x+1)^{-1}$ and x^{-1} over the positive real numbers are quite instructive. For instance,

$$I_1 = \int_0^\infty \frac{dx}{x+1} \rightarrow \mu^{1-d} \int_{(\mathbb{R}^+)^d} \frac{d^d x}{x+1} = \mu^{1-d} \int_\Omega d\Omega_d \int_0^\infty \frac{x^{d-1}}{x+1} dx, \quad (3.16)$$

where Ω is the angular region of integration in d -dimensions. It is important to notice that the integral in the right hand side of the arrow in Eq. (3.16) is divergent in the limit $d \rightarrow 1$, where the integral in the left hand side of the arrow is recovered. The computation of the factor of the integral with respect to x is not mandatory, although it is instructive to follow. As the integrand does not depend on any angle, the angular integration can be computed directly from the integration of the complete solid angle in d -dimensions,

$$\int d\Omega_d = \frac{2\pi^{d/2}}{\Gamma(d/2)}, \quad (3.17)$$

where the integration is computed over the full solid angle. As the integration in Eq. (3.16) is performed only over positive real space, the region Ω is not the full solid angle. Rather, the angular integration over the region Ω leads to

$$\int_\Omega d\Omega_d = \frac{\pi^{d/2}}{2^{d-1}\Gamma(d/2)}, \quad (3.18)$$

in such a way that

$$I_1 = \frac{\mu^{1-d}\pi^{d/2}}{2^{d-1}\Gamma(d/2)} \int_0^\infty \frac{x^{d-1}}{x+1} dx = \frac{\mu^{1-d}\pi^{d/2}}{2^{d-1}\Gamma(d/2)} B(d, 1-d), \quad (3.19)$$

where B is the customary Beta function, so that $0 < \text{Re}(d) < 1$. As the beta function is related to the gamma function, it implies that

$$B(d, 1-d) = \Gamma(d)\Gamma(1-d) = \frac{\pi}{\sin(\pi d)}, \quad (3.20)$$

and we obtain

$$I_1 = \frac{\mu^{1-d}\pi^{d/2}}{2^{d-1}\Gamma(d/2)} \frac{\pi}{\sin(\pi d)}. \quad (3.21)$$

The first factor of Eq. (3.21), $\mu^{1-d}\pi^{d/2}/(2^{d-1}\Gamma(d/2))$ is finite with the limit $d \rightarrow 1$ and approaches 1. However, the second factor has a vanishing denominator for $d = 1$. Therefore, there is a pole in the parameter d . This result exhibits an explicit divergence in the space dimension. Although the condition $0 < \text{Re}(d) < 1$ follows from the definition of the beta function, it is possible to handle this result for every $d \in \mathbb{C}$, recalling DREG is an analytical continuation.

Another example also gives insight of the computations within DREG. The integral can be expanded, as well, as follows

$$I_2 = \int_0^\infty \frac{dx}{x} \rightarrow \mu^{1-d} \int_{(\mathbb{R}^+)^d} \frac{d^d x}{x} = c \int_0^\infty \frac{dx}{x^{2-d}}, \quad (3.22)$$

where the factor c is similar to the first factor of Eq. (3.21), which is finite for the limit $d \rightarrow 1$, and also includes the measure μ^{1-d} . It is explicit in Eq. (3.22) that if $\text{Re}(d) = 1$, it diverges logarithmically both for $x \ll 1$ and $x \rightarrow \infty$; furthermore, if $\text{Re}(d) > 1$, it is divergent for $x \approx 0$; and if $\text{Re}(d) < 1$, the integral is divergent for $x \rightarrow \infty$. These divergences are not meant to appear in an analytical continuation such as DREG, so the integral must be treated differently. From all different values of d , the only different result from the integral arises at $d = 1$. Therefore, it is possible to split the integration domain into two disjoint intervals, such that

$$\int_0^\infty \frac{dx}{x^{2-d}} = \int_0^1 \frac{dx}{x^{2-d}} + \int_1^\infty \frac{dx}{x^{2-d}} = \frac{1}{d-1} \Big|_{\text{Re}(d)<1} - \frac{1}{d-1} \Big|_{\text{Re}(d)>1}. \quad (3.23)$$

The conditions $\text{Re}(d) > 1$ and $\text{Re}(d) < 1$ can be relaxed, again, as this computation is developed within an analytical continuation. Finally, it is seen that the integral cancels, in such a way that $I_2 = 0$, which is clear by means of DREG.

In general, DREG preserves fundamental symmetries, such as gauge invariance, leading to more compact results compared with other regularisation schemes [50, 51]. This makes it an advantage of barely finding quantities with no physical meaning in the intermediate steps, as it is the case of Paulli-Villars scheme. Even more, as it was sketched in the last example of DREG computations, sometimes, the IR and UV divergences can cancel each other.

It is important to emphasize that these divergences that appear in diagram-by-diagram computations, the sum of all contributing diagrams to a given physical process should be free of divergences, in such a way that the theoretical predictions can be confronted with experimental data.

3.3 Cancellation of UV and IR divergences

Quantum corrections of physical observables within perturbation theory involve contributions with virtual states. These corrections demand the summation over all possible virtual configurations, including those states with unbounded energy. Studying those unbounded energy states implies the scan of short-distance interactions. Thus, this limit gives rise to the UV divergences.

UV divergences naturally arise from the computations of quantum corrections, and it is possible to isolate them through a process called *renormalization*. This process implies the absorption of infinities in new definitions within the Lagrangian parameters. Hence, it is possible to define the *bare Lagrangian* \mathcal{L}_0 which includes the singularities, and another Lagrangian \mathcal{L}_{ren} , defined as the one satisfying the equation

$$\mathcal{L}_{ren} = \mathcal{L}_0 - \mathcal{L}_{cnt}, \quad (3.24)$$

where both \mathcal{L}_0 and \mathcal{L}_{cnt} diverge, while \mathcal{L}_{ren} is the physical Lagrangian and provides finite theoretical predictions. In the renormalization process, in order to define physical observables, it is mandatory to introduce an energy scale, μ_{ren} , and thus all these predictions will depend on this parameter. Nevertheless, this dependence is not arbitrary, and is determined through the renormalization group equation. Examples of these equations are the running of the couplings and the mass evolution of the involved particles.

The kernels of these equations, the beta function and the anomalous dimensions, can be computed in a perturbative approach. For instance, the computation of the beta function in a gauge theory can be developed through the expansion

$$\frac{d \ln \alpha(\mu^2)}{d \log \mu^2} = -\alpha(\beta_0 + \beta_1 \alpha + \dots), \quad (3.25)$$

where the first terms are given by [54]

$$\begin{aligned} \beta_0 &= \frac{11C_A - 2N_f}{12\pi}, \\ \beta_1 &= \frac{17C_A^2 - 5C_A N_f - 3C_F N_f}{24\pi^2}. \end{aligned} \quad (3.26)$$

This approach holds below an energy scale, Λ_{QCD} , such that the coupling remains in the perturbative regime and, in order to determine such an evolution, it is customary used a reference scale, and the experimental value of α_{QCD} can be obtained ($\alpha_{QCD}(m_Z) = 0.1180 \pm 0.0007$). In general, all the counterterms included in \mathcal{L}_{cnt} (those cancelling the singularities of the parameters in a bare theory) need to be computed to determine the renormalization of a theory through the computation of self-energy corrections.

3.4 Threshold singularities and the optical theorem

Regarding threshold singularities, it is important to mention that these are integrable divergences. As mentioned in Sec. 3.3, these singularities correspond to particular configuration of internal and external momenta, and their interplay can be studied by means of the well known *optical theorem*.

The computation of observables needs the calculation of invariant matrix elements \mathcal{M} , which are given by the integrals arriving from Feynman rules. It has been mentioned also that divergences naturally appear when computing the integrals given by Feynman

diagrams with loops. With respect to these divergences, there is an interesting result concerning threshold singularities. In order to show this result, it is necessary to deepen a bit more in the properties of the S -matrix.

Recalling from Section 2.6, the S -matrix can be written as $S = 1 + iT$ and has to be Hermitian. Hence,

$$S^\dagger S = (1 - iT^\dagger)(1 + iT) = 1 \implies T - T^\dagger = iT^\dagger T. \quad (3.27)$$

Then, comparing a scattering process from an initial state $|a\rangle$ to a final state $|b\rangle$ as given in Section 2.6 (namely, $|a\rangle = |p_1, \dots, p_n\rangle$ and $|b\rangle = |p'_1, \dots, p'_m\rangle$), it is given that

$$\langle b | (T - T^\dagger) | a \rangle = i \langle b | T^\dagger T | a \rangle. \quad (3.28)$$

Therefore, introducing a complete set of intermediate states $|f\rangle = |p_{f,1}, \dots, p_{f,r}\rangle$ and a phase-space factor Π_f , the right hand side of Eq. (3.28) becomes

$$i \langle b | T^\dagger T | a \rangle = i(2\pi)^4 \delta \left(\sum_k p'_k - \sum_k p_k \right) \sum_f \int d\Pi_f \langle b | T^\dagger | f \rangle \langle f | T | a \rangle, \quad (3.29)$$

where the overall delta function ensures the momentum conservation from the state $|a\rangle$ to the state $|b\rangle$. Thus it is obtained

$$\mathcal{M}(a \rightarrow b) - \mathcal{M}^*(b \rightarrow a) = i \sum_f \int d\Pi_f \xi \mathcal{M}^*(b \rightarrow f) \mathcal{M}(a \rightarrow f), \quad (3.30)$$

where the factor ξ is given by

$$\xi = (2\pi)^4 \delta \left(\sum_k p_{f,k} - \sum_a p_a \right), \quad (3.31)$$

assuring the momentum conservation between the state $|a\rangle$ and the intermediate state $|f\rangle$. Eq. (3.30) is called the *generalised optical theorem* [40], and it is satisfied order by order in perturbation theory. In particular, for the case where $|a\rangle = |b\rangle$, it is obtained

$$2\text{Im}(\mathcal{M}(a \rightarrow a)) = \sum_f \int d\Pi_f |\mathcal{M}(a \rightarrow f)|^2. \quad (3.32)$$

Eq. (3.30) itself is an important result. The optical theorem relates forward scattering amplitudes to the total cross section for production of every final state. In particular, we know that the imaginary part of the forward scattering amplitude should be proportional to the probability of the scattering process since it gives the attenuation of the forward wave through the collision. For instance, for an elastic scattering of two particles, this leads to the relation

$$\text{Im}(\mathcal{M}(p_1, p_2 \rightarrow p_1, p_2)) = 2E_{\text{cm}} p_{\text{cm}} \sigma_{\text{total}}(p_1, p_2 \rightarrow \text{anything}), \quad (3.33)$$

where E_{cm} is the total energy in the center of mass frame and p_{cm} is the momentum of either particles in the same frame. Also, it is easy to show, following the Sokhotski-Plemelj theorem, that for a single particle with momentum q , it is satisfied

$$\text{Im} \frac{1}{q^2 - m^2 + i0} = -\pi \delta(q^2 - m^2). \quad (3.34)$$

Regarding the evaluation of the imaginary part of loop diagrams, we can rely on the so-called *Cutkosky's cutting rules* [55]. These rules provide the evaluation of the imaginary part of an arbitrary amplitude in an algorithmic way. This algorithm consists on setting on-shell internal particles whenever momentum conservation holds. Then, perform the replacement $G_F(q) \rightarrow -2i\pi\delta(q^2 - m^2)$ for each cut particle with momentum q and mass m . Then, the sum of all cuts gives rise to the integrable discontinuity, which is twice the imaginary part of the original amplitude with the opposite sign.

Both optical theorem and Cutkosky's cutting rules are of great interest to distinguish between causal and non-causal divergences. Roughly speaking, non-causal singularities are those arising in the intermediate steps of the computation of a given scattering amplitude and should cancel each other, while causal singularities are those having an associated cut in terms of Cutkosky's cutting rules. It is worth noticing that causal singularities arise when the energy flow of intermediate states corresponds with the time evolution of the process, and non-causal singularities demand an opposite orientation of these two flows. In terms of Feynman diagrams, causal singularities arise when internal particles reach their on-shell energy and their momentum flow are all outgoing from or incoming to a common vertex, as sketched in Fig. 3.3. In the following chapters, a method developed to perform multi-loop integrals, regarding the topology of the diagram and not the number of loops, is presented and it will be shown this naturally reproduces the causal cuts.

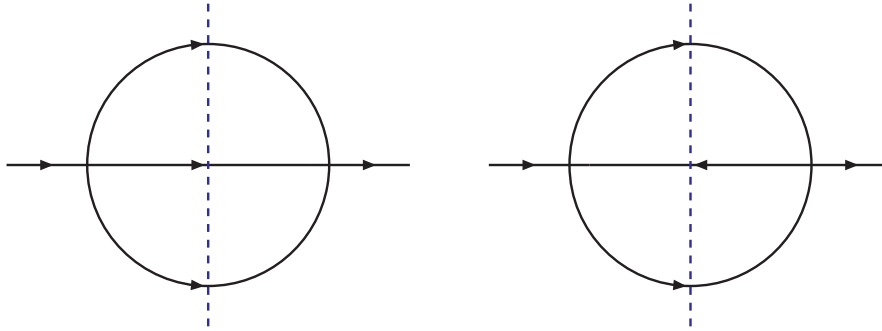


Figure 3.3: Causal (left) and non-causal (right) singularities arising from different configurations of on-shell internal momenta for the sunrise diagram. In the left diagram, all the internal particles have a momentum flow oriented outgoing from the left vertex and incoming to the right vertex.

Chapter 4

The Loop-Tree Duality at higher perturbative orders

The Loop-Tree Duality (LTD) [56–62] is a mathematical framework that exhibits interesting properties with respect to the customary Feynman representation of multi-loop scattering amplitudes [63–68]. Based on Cauchy’s residue theorem, LTD can be applied to any QFT in Minkowski space with arbitrary d space-time dimensions. This framework allows to transform an L -loop integral over an Ld -dimensional Minkowski space into an integral over an $L(d - 1)$ -dimensional integration space. LTD can be easily applied to an arbitrary L -loop Feynman diagram, LTD tells us how to cut internal lines in such a way that the study of this diagram can be rephrased to the study of a sum of tree-level diagrams. Furthermore, cancellation of non-physical divergences becomes explicit in this formalism. In this Chapter, an introduction to the LTD groundwork is given for a scalar theory. An extensive study on the mathematical subtleties are given in Chapter 5.

4.1 Loop-Tree Duality in a nutshell

As mentioned before, LTD framework is based on Cauchy’s residue theorem, which states: *Let $f : \mathbb{C} \rightarrow \mathbb{C}$ be a meromorphic function with poles $\alpha = \{z_1, \dots, z_n\}$. Let C be a contour within \mathbb{C} enclosing a subset β of the poles α . Then,*

$$\int_C f(z)dz = 2\pi i \sum_{j \in \beta} \Gamma_j \text{Res}(f, \{z, j\}), \quad (4.1)$$

where Γ_j is the winding number of C for a point z_j inside C , defined by

$$\Gamma_j = \int_C \frac{dz}{z - z_j}. \quad (4.2)$$

For the case of Feynman integrals (which are integrals over a real Minkowski space), it is possible to promote the energy component of the loop momenta to the complex plane and, as a convention, the contour of integration will be always a simple closed contour surrounding the lower half plane as shown in Fig. 4.1, so that the positive real part of the energy is taken into account. In this manner, $\Gamma_j = -1$ for all j and all of these integrations.

A full study of 1- and 2-loop scalar diagrams is quite instructive for the application of LTD formalism and will give insight to what is expected in the following.

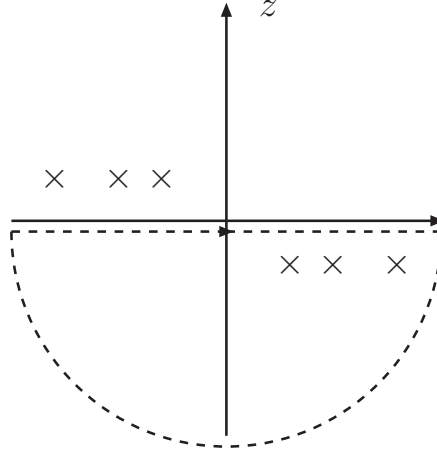


Figure 4.1: Standard integration contour.

4.1.1 The Loop-Tree Duality at one loop

In this section, basic concepts of LTD formalism are given. With the aim of doing so, the computations are performed within DREG scheme, and a short-hand notation is used. In this manner, the integration measure will be denoted by

$$\begin{aligned}
 \int_{\ell} \bullet &= -i\mu^{4-d} \int \frac{d^d \ell}{(2\pi)^d} \bullet, \\
 \int_{\ell} \bullet &= \int_{\vec{\ell}} \int_{\ell_0} \bullet, \\
 \int_{\ell_0} \bullet &= \int \frac{d\ell_0}{2\pi} \bullet.
 \end{aligned} \tag{4.3}$$

Let $L^{(1)}$ be a scalar N -point 1-loop integral as shown in Fig. 4.2. Let also $\alpha = \{1, \dots, N\}$ be the set of indices of the internal particles, each of which having momentum

$$q_i = \ell + \sum_{k=1}^i p_k, \quad i \in \alpha, \tag{4.4}$$

where the overall conservation of momenta holds, so that

$$\sum_{k=1}^N p_k = 0. \tag{4.5}$$

It is straightforward to note that $q_N = \ell$, and that $q_i - q_j = p_{j+1} + \dots + p_i$ (for $i > j$) is independent of the loop momentum. As we shall see, this difference appears in every computation of residues, in such a way that it is convenient to give a recursive definition of the function

$$p_{1,1} = 0, \quad p_{1,i} = p_{1,i-1} + p_i, \quad p_{i,j} = p_{1,i} - p_{1,j}. \tag{4.6}$$

The function $p_{i,j}$ satisfies the relations $p_{i,i} = 0$, $p_{i,j} = -p_{j,i}$ and $p_{i,j} + p_{j,k} = p_{i,k}$. With this notation, the integral $L^{(1)}$ can be written in the form

$$L^{(1)}(\{p_i\}_N) = \int_{\ell} \prod_{i \in \alpha} G_F(q_i). \tag{4.7}$$

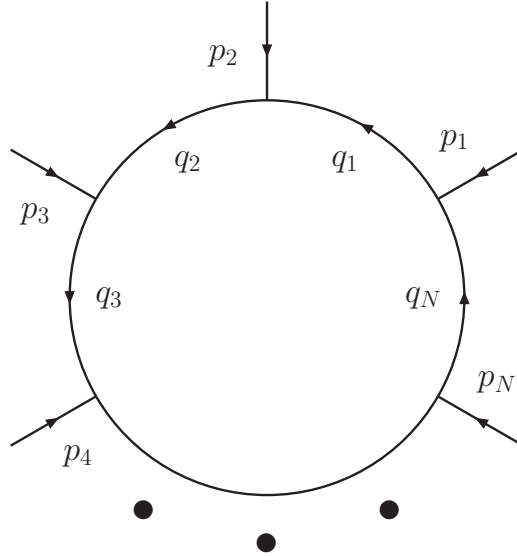


Figure 4.2: General scalar 1-loop diagram.

Each of the Feynman propagators can be written in the form

$$G_F(q_i) = \frac{1}{q_i^2 - m_i^2 + i0} = \frac{1}{(q_{i,0} - q_{i,0}^{(+)}) (q_{i,0} + q_{i,0}^{(+)})}, \quad (4.8)$$

where $q_{i,0}^{(+)} = \sqrt{\vec{q}_i^2 + m_i^2} - i0$ is the positive on-shell energy¹. It is important to emphasize that this definition is independent of the number of loops in Feynman diagram and that $\text{Im}(q_{i,0}^{(+)})$, by definition, is always negative. Thus, the integral can be rewritten in the form

$$L^{(1)}(\{p_i\}_N) = \int_{\ell} \prod_{i \in \alpha} \left((\ell_0 + p_{1,i,0} - q_{i,0}^{(+)}) (\ell_0 + p_{1,i,0} + q_{i,0}^{(+)}) \right)^{-1}, \quad (4.9)$$

where the third index of $p_{i,j}$ is related to the energy component of the 4-momentum. In order to apply Cauchy's residue theorem, let ℓ_0 be promoted to the complex plane. It is important to notice that, for non-vanishing external momenta $\{p_i\}_N$, all the poles are simple poles, as shown in Fig. 4.3.

Therefore, Cauchy's residue theorem can be applied with the contour enclosing the lower half-plane, selecting the poles $q_{i,0}^{(+)}$. Then, $L^{(1)}$ has the form

$$L^{(1)}(\{p_i\}_N) = \sum_{i \in \alpha} \int_{\vec{\ell}} \frac{1}{2q_{i,0}^{(+)}} \prod_{\substack{j \in \alpha \\ j \neq i}} G_F(q_{i,0}^{(+)} - p_{j,i,0}, \vec{q}_j). \quad (4.10)$$

with $G_F(q_{i,0}^{(+)} - p_{j,i,0}, \vec{q}_j)$ being the propagator of a particle with energy $q_{i,0}^{(+)} - p_{j,i,0}$ and momentum \vec{q}_j .

¹It is important to stress that Feynman propagator depends on a 4-momentum q , which means that it depends on four parameters, say the energy component of the 4-momentum q_0 and its 3 components of the 3-momentum \vec{q} (in general, a function of the 4 coordinates of the 4-vector q). This is, Feynman propagators can be written as functions of a 4-momentum $G_F(q)$, as well as functions of the energy and the 3-momentum $G_F(q_0, \vec{q})$.

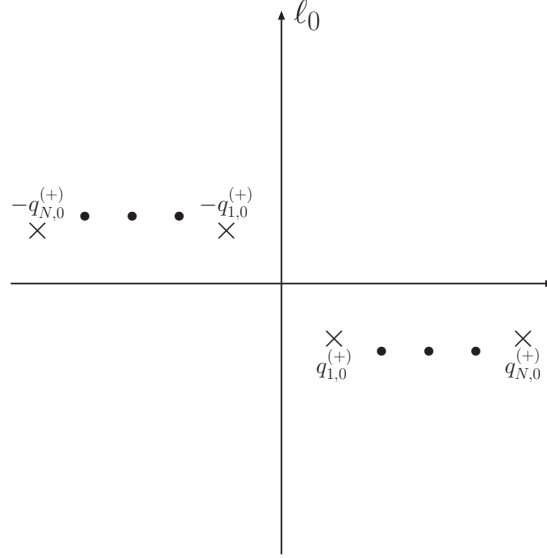


Figure 4.3: Pole structure of a 1-loop diagram.

Interesting is to see from Eq. (4.10) that each factor $(2q_{i,0}^{(+)})^{-1}$ represents one internal particle which has been set on shell. The usual representation of this procedure consists on opening the loop diagram into all possible trees by cutting only one internal line. This, in graph theory, correspond to study a diagram with cyclomatic number 1 by studying all its spanning trees. This is an interesting result that will appear in every diagram with L loops.

For higher-order poles, let $p_1 = \dots = p_{j-1} = 0$, in such a way that $q_1 = \dots = q_{j-1} = q_N \equiv q$ so that the propagator $G_F(q)$ acquires a multiplicity j within the integrand, with $q_0^{(+)}$ the negative-imaginary-part root of $G_F^{-1}(q) = 0$. Then the relation

$$G_F^j(q) = \frac{1}{(j-1)!} \frac{\partial^{j-1}}{\partial (q_0^{(+)2})^{j-1}} G_F(q) \quad (4.11)$$

can be used in such a way that

$$L^{(1)}(\{p_i\}_N) = \int_{\vec{\ell}} \frac{1}{(j-1)!} \frac{\partial^{j-1}}{\partial (q_0^{(+)2})^{j-1}} \int_{\ell_0} \prod_{i=j}^N G_F(q_i). \quad (4.12)$$

Then, Eq. (4.12) shows that the computation of integrals with higher order poles can be derived directly from integrals containing only simple poles. In this manner, the most general study can be obtained from the knowledge of simple poles.

As an example of these computations, for $N = 2$, which is the usual 1-loop 2-point function, with $p_1 = -p_2 = p$, the LTD representation

$$L^{(1)}(p) = \int_{\vec{\ell}} \left(\frac{1}{2q_{1,0}^{(+)}} \frac{1}{(q_{1,0}^{(+)} + p_0)^2 - (q_{2,0}^{(+)})^2} + \frac{1}{2q_{2,0}^{(+)}} \frac{1}{(q_{2,0}^{(+)} - p_0)^2 - (q_{1,0}^{(+)})^2} \right) \quad (4.13)$$

is obtained.

After splitting the integrand of Eq. (4.13) through partial fractions, it is obtained the expression

$$L^{(1)}(p) = - \int_{\vec{\ell}} \frac{1}{\prod_{i=1}^2 2q_{i,0}^{(+)}} \left(\frac{1}{q_{1,0}^{(+)} + q_{2,0}^{(+)} + p_0} + \frac{1}{q_{1,0}^{(+)} + q_{2,0}^{(+)} - p_0} \right). \quad (4.14)$$

Eq. (4.14) has interesting properties due to the fact that $\text{Re}(q_{i,0}^{(+)}) > 0$. First, it can be observed that threshold divergences are present for different energies of the external particles. If $p_0 > 0$, the divergence manifestly appear in the second term, when $q_{1,0}^{(+)} + q_{2,0}^{(+)} = p_0$. Else, if $p_0 < 0$, the divergence appears evidently in the first term, when $q_{1,0}^{(+)} + q_{2,0}^{(+)} = -p_0$. Second, it is evident that non-causal singularities, Sec. 3.4, are not present in the integrand of Eq. (4.14). Only causal thresholds appear, so that the integrand of Eq. (4.14) exhibits the *causal representation* of the scalar 1-loop 2-point function.

Causal structure of any diagram is naturally obtained from LTD. This is an astonishing result which turns out to be deduced from the residues of Feynman integrands with respect to the energy components of the loop momenta. Nevertheless, some ideas of the formal mathematical proof are given below.

The structure of Eq. (4.10) gives an important insight of what to expect for an arbitrary L -loop diagram. This structure shows that, even in a 1-loop level diagram, the complexity of obtaining the causal structure becomes higher whenever the number of vertices within the loop structure of the diagram increases.

4.1.2 The Loop-Tree Duality at two loops

The next case of interest is the scalar 2-loop diagram, with an arbitrary number of external legs N . This diagram is depicted in Fig. 4.4. In this diagram, several internal momenta have the same dependence on the loop momenta ℓ_1 and ℓ_2 . These sets of internal momenta can be defined by indices as follows:

$$\begin{aligned} 1 &= \{ \ell_1 + p_{1,i} \quad | 1 \leq i \leq r \}, \\ 2 &= \{ \ell_2 + p_{r+1,j} \quad | r+1 \leq j \leq l \}, \\ 3 &= \{ \ell_1 + \ell_2 + p_{l+1,k} \quad | 1 \leq k \leq N \}. \end{aligned} \quad (4.15)$$

With these sets, let us define a Feynman-propagator function as the product of Feynman propagators of each set,

$$G_F(i) = \prod_{q_j \in i} G_F(q_j). \quad (4.16)$$

In addition, it is possible to define products of these Feynman functions as

$$G_F(i_1, \dots, i_n) = \prod_{j=1}^n G_F(i_j). \quad (4.17)$$

Therefore, the scalar 2-loop integral can be written in a compact form as

$$L^{(2)}(\{p_k\}_N) = \int_{\ell_1, \ell_2} G_F(1, 2, 3), \quad (4.18)$$

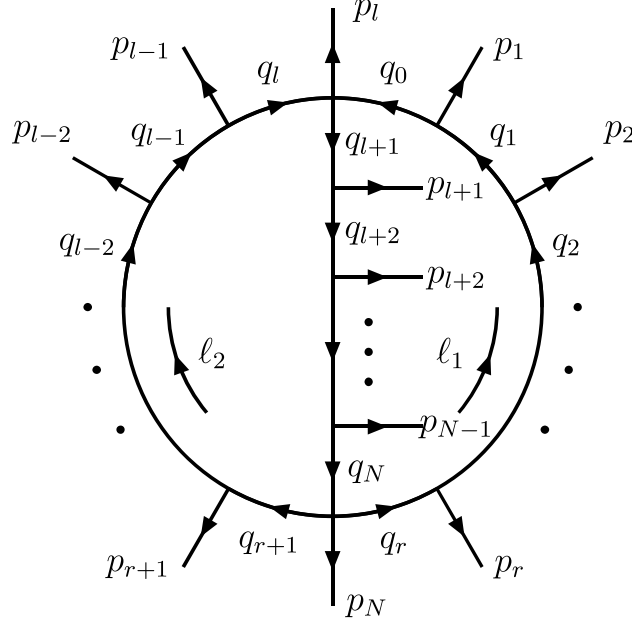


Figure 4.4: General 2-loop diagram.

where the double indices in the integral stands a nested integration

$$\int_{\ell_1, \ell_2} \bullet = \int_{\ell_1} \int_{\ell_2} \bullet. \quad (4.19)$$

According to the previous definitions, the integral can be split as

$$L^{(2)}(\{p_k\}_N) = \int_{\ell_1} G_F(1) \int_{\ell_2} G_F(2, 3). \quad (4.20)$$

The integral with respect to ℓ_2 is a 1-loop-like integration, where it would be possible to interpret the ℓ_1 momentum as a shift of every external momenta in the set 3. With this in mind, the computation of the residue with respect to the energy component of the loop momentum ℓ_2 will lead to an expression involving several terms (one for each internal momentum in the loop depending on ℓ_2). This expression will have a similar structure to that of Eq. (4.10), so that the causal structure of this expression could be found. In order to present a concrete example, let us assume that $1 = \{q_1\}$, $2 = \{q_2\}$ and $3 = \{q_1 + q_2 + p\}$. For this case, it is given

$$L^{(2)}(p) = \int_{q_1} \frac{1}{q_{1,0}^2 - q_{1,0}^{(+2)}} \int_{q_2} \frac{1}{(q_{2,0}^2 - q_{2,0}^{(+2)}) \left((q_{1,0} + q_{2,0} + p_0)^2 - q_{3,0}^{(+2)} \right)}. \quad (4.21)$$

Then, applying Cauchy's residue theorem to the integrand with respect to $q_{2,0}$ and recalling the result of the 1-loop case shows that,

$$\begin{aligned} \frac{1}{(q_{2,0}^2 - q_{2,0}^{(+2)}) \left((q_{1,0} + q_{2,0} + p_0)^2 - q_{3,0}^{(+2)} \right)} &\rightarrow \frac{1}{2q_{2,0}^{(+)}} \frac{1}{(q_{1,0} + q_{2,0}^{(+)} + p_0)^2 - q_{3,0}^{(+2)}} \\ &+ \frac{1}{2q_{3,0}^{(+)}} \frac{1}{(-q_{1,0} - p_0 + q_{3,0}^{(+)})^2 - q_{2,0}^{(+2)}}, \end{aligned} \quad (4.22)$$

where the arrow represents the computation of the sum of the residues in all the poles with negative imaginary part. Each term of the right hand side of Eq. (4.22) gives rise to

$$\begin{aligned} I_{q_{2,0}^{(+)}} &= \int_{q_1, \vec{q}_2} \frac{1}{2q_{2,0}^{(+)}} \frac{1}{\left(q_{1,0}^2 - q_{1,0}^{(+2)}\right) \left(\left(q_{1,0} + q_{2,0}^{(+)} + p_0\right)^2 - q_{3,0}^{(+2)}\right)}, \\ I_{q_{3,0}^{(+)}} &= \int_{q_1, \vec{q}_2} \frac{1}{2q_{3,0}^{(+)}} \frac{1}{\left(q_{1,0}^2 - q_{1,0}^{(+2)}\right) \left(\left(q_{1,0} + p_0 - q_{3,0}^{(+)}\right)^2 - q_{2,0}^{(+2)}\right)}, \end{aligned} \quad (4.23)$$

respectively. Both integrals in Eq. (4.23) have a common subtle issue about the position of the poles. The poles of the first integral are located in

$$\text{Poles} \left[I_{q_{2,0}^{(+)}} \right] = \left\{ \pm q_{1,0}^{(+)}, \pm q_{3,0}^{(+)} - q_{2,0}^{(+)} - p_0 \right\}, \quad (4.24)$$

while the poles of the second integral are found in

$$\text{Poles} \left[I_{q_{3,0}^{(+)}} \right] = \left\{ \pm q_{1,0}^{(+)}, \pm q_{2,0}^{(+)} + q_{3,0}^{(+)} - p_0 \right\}. \quad (4.25)$$

Both integrals have a common pole $q_{3,0}^{(+)} - q_{2,0}^{(+)} - p_0$. It has been mentioned before that, from the definition of $q_{i,0}^{(+)}$, it always holds that $\text{Im} \left(q_{i,0}^{(+)} \right) < 0$, and being p an external momentum, $\text{Im}(p) = 0$. Still, the imaginary part of the difference of two $q_{i,0}^{(+)}$ is not necessarily constant in sign, it rather runs over the remaining integrals. Actually, this sign depends deeply in both 3-momenta \vec{q}_1 and \vec{q}_2 . These poles with non-constant sign for their imaginary part are called *displaced poles*. The reason of this name will be evident in the Sec. 5.1. This is why, for the application of Cauchy's residue theorem with respect to $q_{1,0}$, the selection of negative imaginary part poles can be imposed by multiplying every residue by a Heaviside theta function evaluated on the negative of the imaginary part of the pole. Thus, for an arbitrary integrand $I(q_0)$ with the set of poles $P_I = \{q_1^{(+)}, \dots, q_n^{(+)}\}$, we use

$$I(q_0) \rightarrow \sum_{q_i^{(+)} \in P_I} \text{Res} \left(I(q_0), \left\{ q_0, q_i^{(+)} \right\} \right) \theta \left(-\text{Im} \left(q_i^{(+)} \right) \right). \quad (4.26)$$

Computing the residues of both integrands in Eq. (4.23) at the pole $q_{3,0}^{(+)} - q_{2,0}^{(+)} - p_0$, it is obtained

$$\begin{aligned} \frac{1}{\left(q_{1,0}^2 - q_{1,0}^{(+2)}\right) \left(\left(q_{1,0} + q_{2,0}^{(+)} + p_0\right)^2 - q_{3,0}^{(+2)}\right)} &\rightarrow \frac{1}{2q_{3,0}^{(+)}} \frac{\theta \left(-\text{Im} \left(q_{3,0}^{(+)} - q_{2,0}^{(+)} - p_0 \right) \right)}{\left(q_{3,0}^{(+)} - q_{2,0}^{(+)} - p_0\right)^2 - q_{1,0}^{(+2)}}, \\ \frac{1}{\left(q_{1,0}^2 - q_{1,0}^{(+2)}\right) \left(\left(q_{1,0} + p_0 - q_{3,0}^{(+)}\right)^2 - q_{2,0}^{(+2)}\right)} &\rightarrow \frac{-1}{2q_{2,0}^{(+)}} \frac{\theta \left(-\text{Im} \left(q_{3,0}^{(+)} - q_{2,0}^{(+)} - p_0 \right) \right)}{\left(q_{3,0}^{(+)} - q_{2,0}^{(+)} - p_0\right)^2 - q_{1,0}^{(+2)}}. \end{aligned} \quad (4.27)$$

If both residues of Eq. (4.27) are introduced into Eq. (4.26), it can be noticed that

$$\begin{aligned} \text{Res} \left[\text{Res} \left[G_F(1, 2, 3), \left\{ q_{2,0}, q_{2,0}^{(+)} \right\} \right], \left\{ q_{1,0}, q_{3,0}^{(+)} - q_{2,0}^{(+)} - p_0 \right\} \right] &= \\ -\text{Res} \left[\text{Res} \left[G_F(1, 2, 3), \left\{ q_{2,0}, q_{3,0}^{(+)} - q_{1,0} - p_0 \right\} \right], \left\{ q_{1,0}, q_{3,0}^{(+)} - q_{2,0}^{(+)} - p_0 \right\} \right]. \end{aligned} \quad (4.28)$$

Surprisingly, Eq. (4.28) is not a lucky result, it is an important one that shall be strictly proven below. Up to now, every computation has been developed only for simple poles and, as it was pointed out before, this is enough for these computations. However, it should be remarked that Eq. (4.28) also holds for higher-order poles. Furthermore, Eq. (4.28) is valid for every displaced pole (and every order of these poles), as it will be shown in the Sections 5.1 and 5.2. The full computation of the second residue gives the expression

$$\begin{aligned}
G_F(1, 2, 3) \rightarrow & \frac{1}{4q_{1,0}^{(+)} q_{2,0}^{(+)}} \frac{1}{\left(q_{1,0}^{(+)} + q_{2,0}^{(+)} + p_0\right)^2 - q_{3,0}^{(+)^2}} \\
& + \frac{1}{4q_{1,0}^{(+)} q_{3,0}^{(+)}} \frac{1}{\left(q_{1,0}^{(+)} - q_{3,0}^{(+)} + p_0\right)^2 - q_{2,0}^{(+)^2}} \\
& + \frac{1}{4q_{2,0}^{(+)} q_{3,0}^{(+)}} \frac{1}{\left(q_{2,0}^{(+)} + q_{3,0}^{(+)} - p_0\right)^2 - q_{1,0}^{(+)^2}}.
\end{aligned} \tag{4.29}$$

Eq. (4.29) shows the dual expansion of the function $G_F(1, 2, 3)$. This expression exhibits that the computation of the residues cuts two internal lines in such a way that the 2-loop diagram can be studied through tree-level diagrams, i.e., its spanning trees. Furthermore, if each of its terms is split through partial fractions, it is obtained

$$L^{(2)}(p) = \int_{\vec{\ell}_1, \vec{\ell}_2} \frac{1}{8q_{1,0}^{(+)} q_{2,0}^{(+)} q_{3,0}^{(+)}} \left(\frac{1}{q_{1,0}^{(+)} + q_{2,0}^{(+)} + q_{3,0}^{(+)} + p_0} + \frac{1}{q_{1,0}^{(+)} + q_{2,0}^{(+)} + q_{3,0}^{(+)} - p_0} \right). \tag{4.30}$$

Comparing Eq. (4.14) with Eq. (4.30) it can be noticed that the causal structure of both diagrams, Fig. 4.2 and Fig. 4.4, are deeply related. These diagrams shall be related through their topology.

4.1.3 Topological classification of multi-loop Feynman diagrams

High precision computations involve multi-loop Feynman diagrams. The application of LTD to these diagrams together with an algebraic simplification gives, in turn, their causal representation. This causal representation, as shown in Eq. (4.14) and (4.30), motivates a topological classification of 1PI diagrams, regardless the number of loops, whenever the causal structure remains the same. This classification is given by the topology of the 1PI diagram. In order to give insight of this classification, a scalar theory shall be used, although it has been studied for the theories within the SM.

In order to present the following results, it is important to introduce a set of definitions or notation. This notation is inspired on the fact that the results can be extracted by looking only at the pole structure of the integrands and of the intermediate expressions, together with the fact that Feynman propagators have a quadratic structure on the energy component of the momentum of the particle, $(q_0^2 - q_0^{(+)^2})^{-1}$. In this new notation the following rules are given:

1. Having two or more indices together in the s -th argument of the propagator function G_F means that the s -th internal propagator depends on the sum of the loop momenta indicated by those indices. For instance, the scalar sunrise diagram can be written in the form,

$$G_F(1, 2, 12) = \frac{1}{\left(q_{1,0}^2 - q_{1,0}^{(+)^2}\right) \left(q_{2,0}^2 - q_{2,0}^{(+)^2}\right) \left((q_{1,0} + q_{2,0} + p_0)^2 - q_{3,0}^{(+)^2}\right)}. \tag{4.31}$$

2. A bar above an index means an inversion on the variable it represents $x \rightarrow -x$. This we call the *bar convention*, and the set of indices together with their bars (whenever they have) is called *bar structure*. For example,

$$G_F(1, 2, \bar{1}\bar{2}) = \frac{1}{\left(q_{1,0}^2 - q_{1,0}^{(+2)}\right) \left(q_{2,0}^2 - q_{2,0}^{(+2)}\right) \left((q_{1,0} - q_{2,0} + p_0)^2 - q_{3,0}^{(+2)}\right)}. \quad (4.32)$$

3. Sub-indices imply a summation over the on-shell energies indicated by them. They also satisfy the bar convention. As an example,

$$G_F(1, 2, \bar{3}\bar{4}) = \frac{1}{\left(q_{1,0}^2 - q_{1,0}^{(+2)}\right) \left(\left(q_{2,0} + q_{3,0}^{(+)} - q_{4,0}^{(+)}\right)^2 - q_{2,0}^{(+2)}\right)}. \quad (4.33)$$

4. The function G_D , called *dual propagator*, is understood as the residue of a Feynman propagator or another dual propagator at one of all its negative imaginary part poles. If the selected pole comes from the propagator indicated by the i -th argument, then we write this explicitly substituting this argument with $0_{(i)}$. For instance,

$$G_D(0_{(1)}, \dots) \equiv \text{Res} \left[G_{F,D}(1, \dots), \left\{ q_{1,0}, q_{1,0}^{(+)} \right\} \right], \quad (4.34)$$

where $G_{F,D}$ means that it could be a Feynman propagator function as well as another dual propagator.

5. After the computation of some residues, the energy of some internal lines will not depend on loop energies. In this case, the argument is given by a 0 with some sub-indices, according to the bar convention. For instance, the dual expansion of the scalar 2-loop diagram in Eq. (4.29) can be written in the form

$$L^{(2)}(p) = \int_{\vec{\ell}_1, \vec{\ell}_2} \left(G_D(0_{(1)}, 0_{(2)}, 0_{12}) + G_D(0_{(1)}, 0_{\bar{1}\bar{3}}, 0_{(3)}) + G_D(0_{23}, 0_{(2)}, 0_{(3)}) \right). \quad (4.35)$$

This notation can also be applied to a Heaviside theta function. As the only parameters containing imaginary parts are the $q_{i,0}^{(+)}$ on-shell energies¹, it is defined

$$\theta(i\bar{j}) = \theta \left(-\text{Im} \left(q_{i,0}^{(+)} - q_{j,0}^{(+)} \right) \right). \quad (4.36)$$

The quadratic structure of Feynman propagators gives rise to the properties $G_F(i_j) = G_F(\bar{i}\bar{j})$ and $G_F(\bar{i}\bar{j}) = G_F(i\bar{j})$. Also, it is possible to develop arithmetic with this notation by the rules

$$\bar{\bar{i}} = i \quad , \quad i\bar{i} = 0. \quad (4.37)$$

This arithmetic gives an efficient method to compute residues, and also gives a simpler method to identify displaced poles and negative imaginary part poles. As an example, the scalar 2-point 2-loop function is developed again, but with this new notation. It begins with the integrand $G_F(1, 2, 1\bar{2})$. This integrand, as a function of $q_{2,0}$ has the poles at $q_{2,0}^{(+)}$, arising from the second argument, and $q_{3,0}^{(+)} - q_{1,0} - p_{1,0}$, from the third argument. With this notation, the first pole is reached when the condition

$$2 = 0_2 \quad (4.38)$$

¹In these computations, we assume that there is a unique complex variable in the integration computation. This is, only one loop energy is assumed to be complex in each iteration of the application of Cauchy residue theorem, while the others remain real.

holds. Thus, this pole contributes with the full residue with the term obtained after the substitution of this index equation, namely $G_D(1, 0_{(2)}, 1_2)$. The second pole is reached if

$$1_2 = 0_3. \quad (4.39)$$

From this index equation it can be obtained

$$\bar{1}(1_2) = \bar{1}(0_3) \Rightarrow 2 = \bar{1}_3. \quad (4.40)$$

Then, the substitution of this index equation concludes to the term $G_D(1, \bar{1}_3, 0_{(3)})$ which, followed by the quadratic structure of the Feynman propagator, can be written in the form $G_D(1, 1_{\bar{3}}, 0_{(3)})$. Hence, Cauchy's residue theorem applied to $G_F(1, 2, 1_2)$ with respect to $q_{2,0}$ for a contour enclosing the lower half plane gives

$$G_F(1, 2, 1_2) \rightarrow G_D(1, 0_{(2)}, 1_2) + G_D(1, 1_{\bar{3}}, 0_{(3)}). \quad (4.41)$$

Then, from Eq. (4.41), it is now needed to apply the Cauchy's residue theorem for $q_{1,0}$. In order to do so, it is mandatory to analyze term by term. The first term, $G_D(1, 0_{(2)}, 1_2)$, gives a pole arising from the first argument, namely

$$1 = 0_1. \quad (4.42)$$

After the substitution of this index equation it is obtained the term $G_D(0_{(1)}, 0_{(2)}, 0_{12})$. From the third argument of this term, it is obtained a pole when

$$1_2 = 0_3 \rightarrow 1 = 0_{\bar{2}3}. \quad (4.43)$$

This pole is a displaced pole, as this notation represents the pole in $q_{3,0}^{(+)} - q_{2,0}^{(+)} - p_{1,0}$, already studied in the last section. From the second term, $G_D(1, 1_{\bar{3}}, 0_{(3)})$, the first argument gives the pole located at $q_{1,0} \rightarrow q_{1,0}^{(+)} = 0_1$. The substitution of this index equation contributes to Cauchy's residue theorem with the term $G_D(0_{(1)}, 0_{1\bar{3}}, 0_{(3)})$. The second argument of this term gives the poles

$$\begin{aligned} 1_{\bar{3}} &= 0_2, \\ 1_{\bar{3}} &= 0_{\bar{2}}. \end{aligned} \quad (4.44)$$

It is seen that the second index equation gives rise to the same displaced pole, $1 = 0_{\bar{2}3}$. The first index equation produces to a negative imaginary part pole $1 = 0_{23}$. This pole contributes with Cauchy's residue theorem with the term $G_D(0_{23}, 0_{(2)}, 0_{(3)})$. This notation leads, after the iterated application of the residues, to the expressions

$$\begin{aligned} G_F(1, 2, 1_2) &= \frac{1}{\left(q_{1,0}^2 - q_{1,0}^{(+2)}\right) \left(q_{2,0}^2 - q_{2,0}^{(+2)}\right) \left((q_{1,0} + q_{2,0} + p_0)^2 - q_{3,0}^{(+2)}\right)}, \\ G_D(0_{(1)}, 0_{(2)}, 0_{12}) &= \frac{1}{4q_{1,0}^{(+)} q_{2,0}^{(+)}} \frac{1}{\left(q_{1,0}^{(+)} + q_{2,0}^{(+)} + p_0\right)^2 - q_{3,0}^{(+2)}}, \\ G_D(0_{(1)}, 0_{1\bar{3}}, 0_{(3)}) &= \frac{1}{4q_{1,0}^{(+)} q_{3,0}^{(+)}} \frac{1}{\left(q_{1,0}^{(+)} - q_{3,0}^{(+)} + p_0\right)^2 - q_{2,0}^{(+2)}}, \\ G_D(0_{23}, 0_{(2)}, 0_{(3)}) &= \frac{1}{4q_{2,0}^{(+)} q_{3,0}^{(+)}} \frac{1}{\left(q_{2,0}^{(+)} + q_{3,0}^{(+)} - p_0\right)^2 - q_{1,0}^{(+2)}}. \end{aligned} \quad (4.45)$$

Each factor $2\pi i$ coming from the application of Cauchy's residue theorem cancels with the integration measure of the integrals over the loop 4-momenta, leading naturally to

the 3-momentum integration measure. In summary, the iterated application of Cauchy's residue theorem to each energy component of the loop momenta and expressed with this new notation reads

$$G_F(1, 2, 12) \rightarrow G_D(0_{(1)}, 0_{(2)}, 0_{12}) + G_D(0_{(1)}, 0_{1\bar{3}}, 0_{(3)}) + G_D(0_{23}, 0_{(2)}, 0_{(3)}). \quad (4.46)$$

This computation can be shortened even more by noticing some facts. First, through the computation of the residues it is seen that if one of the arguments of a term has a sub-index without a bar, then the associated poles are one positive imaginary part pole and a displaced pole. This is due to the fact that, if $i\alpha_j$ is the k -th argument of some term (where α is some set of indices with or without bar), then the poles are given by the equations $i\alpha_j = 0_k$ and $i\alpha_j = 0_{\bar{k}}$, as this represents the propagator

$$\frac{1}{\left(q_{i,0} + \sum_{r \in \alpha} (-1)^{\sigma_r} q_{r,0} + q_{j,0}^{(+)} + p_0\right)^2 - q_{k,0}^{(+)2}}, \quad (4.47)$$

where $\sigma_r \in \{0, 1\}$, corresponding to the bar configuration of α , and the poles of this propagator are located in

$$q_{i,0} = \pm q_{k,0}^{(+)} - q_{j,0}^{(+)} - \sum_{r \in \alpha} (-1)^{\sigma_r} q_{r,0} - p_0. \quad (4.48)$$

The first of these index equations gives $i = \bar{\alpha}_{\bar{j}k}$, so that this pole depends on $q_{k,0}^{(+)} - q_{j,0}^{(+)}$, being this a displaced pole. The second index equation gives $i = \bar{\alpha}_{\bar{j}\bar{k}}$. This pole depends on $-q_{k,0}^{(+)} - q_{j,0}^{(+)}$, and thus having a positive imaginary part. Then, if at least one of the sub-indices of an argument does not have a bar, then this argument does not contribute to Cauchy's residue theorem. In other words, only the arguments with all its sub-indices with a bar, or without sub-indices, contribute with Cauchy's residue theorem. Regarding arguments with all its sub-indices with bar, something similar happens. In this case, let $i_{\bar{j}}$ be the k -th argument of a dual propagator G_D , representing the factor

$$\frac{1}{\left(q_{i,0} - q_{j,0}^{(+)}\right)^2 - q_{k,0}^{(+)2}}. \quad (4.49)$$

Then, its poles are given by $i_{\bar{j}} = 0_k$ and $i_{\bar{j}} = 0_{\bar{k}}$. The first index equation gives the pole $i = 0_{jk}$ which is a negative imaginary part pole and thus contributes to Cauchy's residue theorem. The second index equation gives the pole $i = 0_{\bar{j}\bar{k}}$. Being this last pole a displaced pole, its contribution cancels the contribution of another displaced pole.

The second important fact to notice is that the bar configuration of the sub-indices can be deduced by the number of indices in each argument. For instance, let α and β be sets of indices such that $\alpha \cap \beta = \emptyset$, and let α be the i -th argument and $\alpha \cup \beta$ the j -th argument of a given dual propagator G_D in such a way that the integrand includes the factor

$$\frac{1}{\left(\left(\sum_{r \in \alpha} q_{r,0}\right)^2 - q_{i,0}^{(+)2}\right) \left(\left(\sum_{r \in \alpha} q_{r,0} + \sum_{s \in \beta} q_{s,0}\right)^2 - q_{j,0}^{(+)2}\right)}. \quad (4.50)$$

On one hand, the pole of the i -th argument is given by the index equation $\alpha = 0_i$, and thus the computation of the residue will give $0_{(i)}$ in the i -th argument and β_i in the j -th

argument of the function G_D , which leads to the factor

$$\frac{1}{2q_{i,0}^{(+)}} \frac{1}{\left(q_{i,0}^{(+)} + \sum_{s \in \beta} q_{s,0}\right)^2 - q_{j,0}^{(+)2}}. \quad (4.51)$$

On the other hand, the pole of the j -th argument is given by the index equation $\alpha \cup \beta = 0_j$. Then this pole contributes with a term G_D with $0_{(j)}$ in the j -th argument and $\bar{\beta}_j = \beta_{\bar{j}}$ in the i -th argument, or equivalently, with a term with the factor

$$\frac{1}{2q_{j,0}^{(+)}} \frac{1}{\left(\sum_{s \in \beta} q_{s,0} - q_{j,0}^{(+)}\right)^2 - q_{i,0}^{(+)2}}. \quad (4.52)$$

Thus, it can be noticed that, if the i -th argument has fewer or the same number of indices than the j -th argument, and if the residue is developed with respect to the pole of the i -th argument, then the pole of the first argument is written as an index without a bar, else, if the residue is computed with respect to the pole associated to the j -argument, the pole is written with a bar. For instance, in Eq. (4.41) it can be observed that the application of Cauchy's residue theorem to the integrand $G_F(1, 2, 12)$ has two arguments with 2, the second and the third. As the second argument has only one index and the second has two indices, then one term has a sub-index 2 in the third argument and the other term has a sub-index $\bar{3}$ in the second argument.

In compliance with this notation, the classification of Feynman diagrams with respect to their topology can be presented. The classification is based on the concept of *topological complexity* k of a Feynman diagram with v vertices, defined by $k = v - 1$. Then, for $k = 1$, the L -loop diagram is called the *Maximal-Loop-Topology* (MLT(L)) diagram, in the sense that this diagram can be interpreted as a topological simplification of every other family of diagrams with higher topological complexity. This diagram is shown in Fig. 4.5, where external particles are omitted, and its integrand is given by

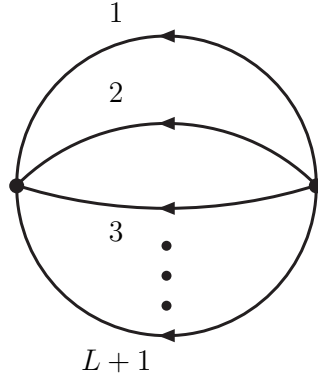
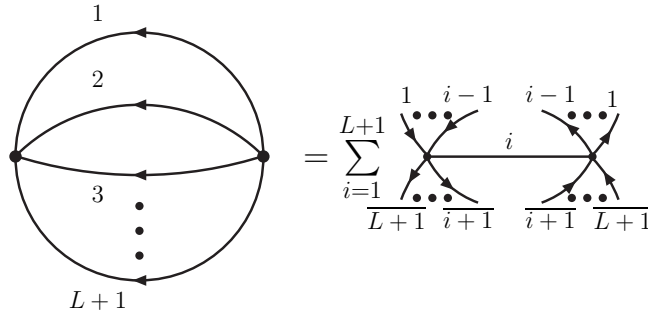
$$\mathcal{I}_{\text{MLT}}^{(L)}(p_1) = G_F(1, \dots, L, 1 \dots L) = G_F(1, \dots, L + 1), \quad (4.53)$$

where $L + 1 = \overline{1 \dots L}$, this is, the internal momenta of the set $L + 1$ have the form $-\sum_i q_i + k$ with k beign a linear combination of external momenta. We would like to recall that each argument of the propagator function G_F represents a product of different propagators with the same dependence on the loop momenta. In other words, an arbitrary configuration of external particles are assumed to be attached to the internal sets with indices $1, \dots, L + 1$, and the vertices.

The computation of Cauchy's residue theorem over the energy components in an iterated way brings the relation

$$\mathcal{I}_{\text{MLT}}^{(L)}(p_1) \rightarrow \sum_{i=1}^n G_D(0_{(1)}, \dots, 0_{(i-1)}, 0_{1 \dots (i-1) \overline{(i+1) \dots (L+1)}}, 0_{(i+1)}, \dots, 0_{(L+1)}). \quad (4.54)$$

Eq. (4.54) can be deduced through mathematical induction, and will be deduced in the Sec. 5.1. It is interesting to notice that each of the terms involved in the summation symbol has L internal lines on-shell. Diagrammatically, this is represented as the cut of all but one internal lines, as shown in Fig. 4.6. This is, LTD formalism opens the MLT(L) diagram into all its spanning trees.

Figure 4.5: Feynman diagram for the MLT(L) topology.Figure 4.6: Action of the nested residue to a MLT(L) diagram. External momenta are omitted in order to easily see what nested residues do to the sets of internal momenta.

If there is only one propagator in each set and external particles are attached to the two vertices adding up an external momentum p_1 , so that $q_{L+1} = -\sum q_i + p_1$, this relation of the MLT diagram can be reduced through partial fractioning into the relation

$$\mathcal{I}_{\text{MLT}}^{(L)}(p_1) \rightarrow \frac{1}{\prod_{i=1}^{L+1} (2q_{i,0}^{(+)})} \left(\frac{1}{\sum_{i=1}^{L+1} q_{i,0}^{(+)} + p_{1,0}} + \frac{1}{\sum_{i=1}^{L+1} q_{i,0}^{(+)} - p_{1,0}} \right), \quad (4.55)$$

in accordance with Eqs. (4.14) and (4.30), for the cases $L = 1$ and $L = 2$ respectively.

Eq. (4.55) shows the causal representation of the MLT diagram with L loops. In light of Eq. (4.55), it can be remarked that both $L^{(1)}(p)$ and $L^{(2)}(p)$ are particular cases of MLT diagrams, with $L = 1$ and $L = 2$ respectively. The first factor appears in a natural way in every topological family. Hence, it is convenient to define the factor

$$x_k = \prod_{i=1}^k (2q_{i,0}^{(+)}). \quad (4.56)$$

Besides, it can be defined the function

$$\lambda_{\Gamma}^{\pm} = \sum_{i=1}^{L+1} q_{i,0}^{(+)} \pm p_{1,0}, \quad (4.57)$$

which represents the causal thresholds of the MLT(L) diagram as a natural generalization of Eqs. (4.14) and (4.30). This is the reason why these functions are called *causal denominators*. Finally, according to this notation, the causal representation of MLT diagrams

can be written in the compact form,

$$\mathcal{I}_{\text{MLT}}^{(L)}(p_1) \rightarrow \frac{1}{x_{L+1}} \left(\frac{1}{\lambda_1^+} + \frac{1}{\lambda_1^-} \right). \quad (4.58)$$

It is important to notice that all the $q_{i,0}^{(+)}$ terms in Eq. (4.57) have positive real part. This can be interpreted as all the internal momenta flow incoming or outgoing from a vertex. In this manner, Eq. (4.55) and (4.58) are diagrammatically depicted in Fig. 4.7.

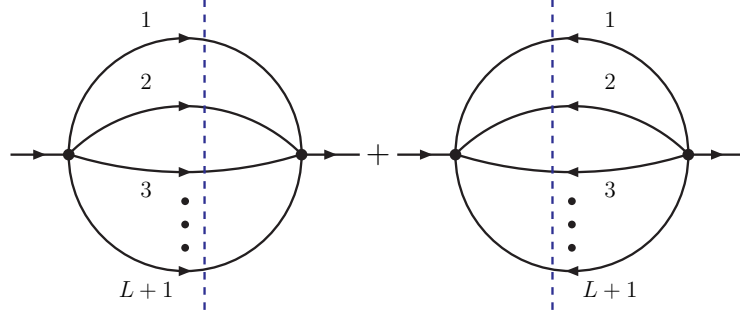


Figure 4.7: Graphical interpretation of the causal representation of the MLT(L) diagram.

In order not to overload the notation, from now on the contributions of external momenta are not going to be explicitly written as super-indices when they make it difficult to follow the computation. Although, we recall that this multi-leg scenario has been considered in the following. Hence, from now on, no super-indices, meaning the presence of external momenta, are going to be written explicitly.

The diagram with the next topological complexity corresponds to the L -loop *Next-to-Maximal Loop Topology* (NMLT(L)) diagram. This diagram is depicted in Fig. 4.8 where, as in the MLT topological family, $L + 1 = \overline{1 \dots L}$, and also $L + 2 = \overline{12}$, whose integrand is given by the function

$$\mathcal{I}_{\text{NMLT}}^{(L)} = G_F(1, \dots, L, 1 \dots L, 12) = G_F(1, \dots, L + 2). \quad (4.59)$$

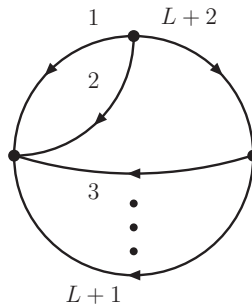


Figure 4.8: Feynman diagram of the NMLT(L) topology.

As mentioned before, LTD formalism cuts internal lines in such a way that all spanning trees of the given graph are taken into account. Also, the insertion of MLT diagrams into higher topological complexity diagrams can be thought as a single propagator. In this manner, it is possible to consider only the NMLT diagram with the minimum number of loops, which is the NMLT(1) diagram. In order to make it evident, the set of propagators $\{3, \dots, L + 1\}$ represents an MLT($L - 2$), while both propagators 1 and 2 form an MLT(1) insertion. Thus, after the reduction of the MLT insertions into a single propagator, the

full NMLT(L) diagram is equivalent to a triangle diagram, and thus there is a relation between NMLT(L) integrand and a triangle integrand,

$$\mathcal{I}_{\text{NMLT}}(p_1, p_2, p_3) \sim G_F(1). \quad (4.60)$$

The application of LTD formalism to the NMLT(L) integrand gives an interesting relation. If the residues are applied to the energies with indices $L, L-1, \dots, 3$, the MLT insertion can be substituted by a propagator-like function

$$G_F(3, \dots, L, 1 \dots L) \rightarrow G_{3 \dots (L+1)}^*(12) \sim \frac{1}{(q_{1,0} + q_{2,0})^2 - (q_{3,0}^{(+)} + \dots + q_{L+1,0}^{(+)})^2}. \quad (4.61)$$

Then, after all residues have been taken, it is obtained the relation

$$\begin{aligned} \mathcal{I}_{\text{NMLT}}^{(L)}(p_1, p_2, p_3) &\rightarrow G_D(1, 2, 12) \otimes G_{3 \dots (L+1)}^*(12) \\ &+ G_D(1, 2) \otimes G_{3 \dots (L+1)}^*(0_{(3 \dots (L+1))}) \otimes G_D(12), \end{aligned} \quad (4.62)$$

which can be depicted as a factorization relation as shown in Fig. 4.9.

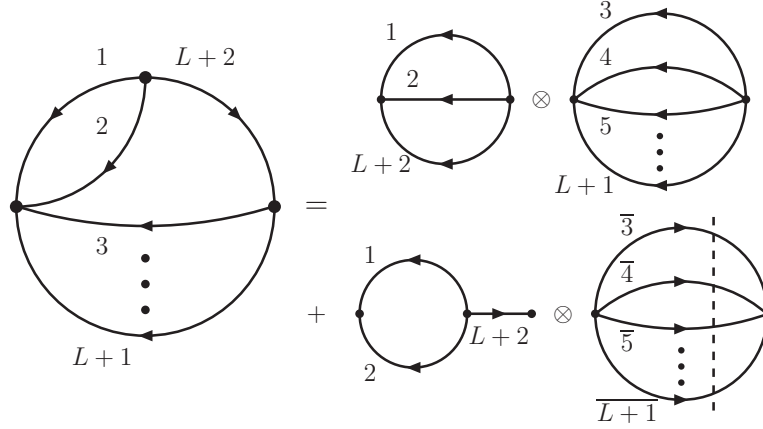


Figure 4.9: Dual decomposition of NMLT(L) in terms of loop configurations with lower topological complexity.

Convolution symbols in Eq. (4.62) are defined by

$$\begin{aligned} &G_D(1, 2, 12) \otimes G_{3 \dots (L+1)}^*(12) \\ &= \sum_{i=3}^{L+1} G_D(0_{\overline{2(L+2)}}, 0_{(2)}, \dots, 0_{(i-1)}, 0_{\overline{3 \dots (i-1)(i+1) \dots (L+2)}}, 0_{(i+1)}, \dots, 0_{(L+1)}, 0_{(L+2)}) \\ &+ \sum_{i=3}^{L+1} G_D(0_{(1)}, 0_{\overline{1(L+2)}}, 0_{(3)}, \dots, 0_{(i-1)}, 0_{\overline{3 \dots (i-1)(i+1) \dots (L+2)}}, 0_{(i+1)}, \dots, 0_{(L+1)}, 0_{(L+2)}) \\ &+ \sum_{i=3}^{L+1} G_D(0_{(1)}, \dots, 0_{(i-1)}, 0_{\overline{1 \dots (i-1)(i+1) \dots (L+1)}}, 0_{(i+1)}, \dots, 0_{(L+1)}, 0_{(12)}), \end{aligned} \quad (4.63)$$

and,

$$\begin{aligned} &G_D(1, 2) \otimes G_{3 \dots (L+1)}^*(0_{(3 \dots (L+1))}) \otimes G_D(12) \\ &= G_D(0_{\overline{2 \dots (L+1)}}, 0_{(2)}, \dots, 0_{(L+1)}, 0_{\overline{3 \dots (L+1)}}) \\ &+ G_D(0_{(1)}, 0_{\overline{13 \dots (L+1)}}, 0_{(3)}, \dots, 0_{(L+1)}, 0_{\overline{3 \dots (L+1)}}). \end{aligned} \quad (4.64)$$

Both definitions given in Eqs. (4.63) and (4.64) seem to be intricate, yet they have a natural meaning in terms of the spanning trees of the NMLT diagram. Recalling Fig. 4.9, spanning trees are obtained after cutting L internal lines. The cut lines can be divided into two sets, the set where one of the lines $3, \dots, L+1$ is off shell, or equivalently, cut¹, and the set where all the lines $3, \dots, L+1$ are cut. The first set is represented by the first of the definitions. As the diagram has $L+2$ lines and already has one off-shell line, it must have another line off shell, and it can be the line 1, the line 2 or the line $L+2$, which corresponds to the first, second and third sum of this definition, respectively. As the lines $3, \dots, L+1$ have an MLT structure, as well as the lines 1, 2 and $L+2$, it is natural to represent this set as the convolution of two MLT diagrams. It is important to notice that the evaluation of the $G_{3\dots(L+1)}^*$ function off shell depends deeply on which internal lines have been set on shell (or equivalently, have been cut). With respect to the second set, it is represented by the second definition. In this case, already $L-1$ lines have been cut, in such a way that only one line of the lines 1, 2 and $L+2$ has to be cut. Moreover, the line $L+2$ cannot be cut in order to obtain a spanning tree, otherwise, the obtained graph would be disconnected (in particular, the vertex adjacent to lines 3, $\dots, L+2$ would be disconnected from the other two vertices). Thus in this second set, there are only two contributions: one obtained after cutting the line 1 and one obtained after cutting the line 2, corresponding to the first and the second term of this definition, respectively. In this case, the line $L+2$ is always off shell, while the lines 1 and 2 have an MLT structure, as well as the lines $3, \dots, L+1$. Thus, it is natural to represent this contribution as an MLT formed by the lines 1 and 2 with a propagator $L+2$ in convolution with an fully cut MLT formed by the lines $3, \dots, L+1$. It becomes important to notice that Eq. (4.62) relates an NMLT(L) diagram with a sum of the convolution of an MLT(2) diagram with an MLT($L-2$) diagram and the convolution of an MLT(1) diagram with a fully opened MLT($L-2$) diagram. This is, Eq. (4.62) shows that the NMLT(L) diagram can be studied in terms of lower complexity diagrams and fewer loops, as shown in Fig. 4.9.

Analogously to the MLT(L) and NMLT(L) diagrams, it is possible to define the L -loop *Next-to-Next-to-Maximal Loop Topology* ($N^2\text{MLT}(L)$) diagram as sketched in Fig. 4.10, where $L+1 = \overline{1\dots L}$, $L+2 = \overline{12}$ and also $L+3 = \overline{23}$, which is defined by its integrand

$$\begin{aligned} \mathcal{I}_{N^2\text{MLT}}^{(L)}(p_1, p_2, p_3, p_4) &= G_F(1, \dots, L, 1\dots L, 12, 23) \\ &= G_F(1, \dots, L+3). \end{aligned} \quad (4.65)$$

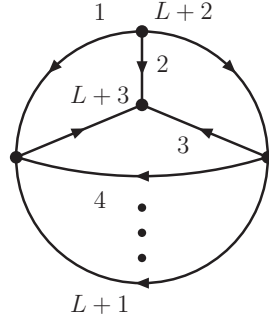
$N^2\text{MLT}(L)$ diagram is a generalization of the well-known *Mercedes-Benz* diagram which, in this classification, is the $N^2\text{MLT}(3)$ diagram.²

It is important to notice that this topological class cannot be reached with one loop, as the case of the NMLT topological family. Actually, the minimal diagram of the $N^2\text{MLT}(L)$ diagram is the Mercedes-Benz, implying that every diagram with 1 or 2 loops cannot be included in the $N^2\text{MLT}(L)$ classification. For the general $N^2\text{MLT}(L)$ diagram, one obtains the LTD expression,

$$\begin{aligned} \mathcal{I}_{N^2\text{MLT}}^{(L)}(p_1, \dots, p_4) &\rightarrow G_D(1 \cup L+3, 2, L+2 \cup 3) \otimes G_{4\dots(L+1)}^*(123) \\ &\quad + G_D(1, 2, 3, L+2, L+3) \otimes G_{4\dots(L+1)}^*(0_{(4\dots(L+1))}), \end{aligned} \quad (4.66)$$

¹Notice that, if two of these lines are kept off shell, then there would still be a loop in the remaining term.

²The computation of the nested residues can be developed using the ideas behind this notation, and a code in MATHEMATICA with the aim of computing it for the $N^2\text{MLT}(L)$ is presented in Appendix B.

Figure 4.10: $N^2MLT(L)$ diagram with L loops.

where the convolution symbols are defined as follows:

$$\begin{aligned}
& G_D(1 \cup L+3, 2, L+2 \cup 3) \otimes G_{4\dots(L+1)}^*(123) \\
&= G_D(0_{(1)}, 0_{\overline{1(L+2)}}, 0_{(3)}, 0_{(L+2)}, 0_{\overline{13(L+2)}}) \\
&\times \sum_{i=4}^{L+1} G_D(0_{(4)}, \dots, 0_{(i-1)}, 0_{\overline{(L+2)3\dots(i-1)(i+1)\dots(L+1)}}, 0_{(i+1)}, \dots, 0_{(L+1)}) \\
&+ G_D(0_{\overline{2(L+2)}}, 0_{(2)}, 0_{(3)}, 0_{\overline{23}}) \\
&\times \sum_{i=4}^{L+1} G_D(0_{(4)}, \dots, 0_{(i-1)}, 0_{\overline{(L+2)3\dots(i-1)(i+1)\dots(L+1)}}, 0_{(i+1)}, \dots, 0_{(L+1)}) \\
&+ G_D(0_{\overline{3(L+2)(L+3)}}, 0_{\overline{3(L+3)}}, 0_{(3)}, 0_{(L+2)}, 0_{(L+3)}) \\
&\times \sum_{i=4}^{L+1} G_D(0_{(4)}, \dots, 0_{(i-1)}, 0_{\overline{(L+2)3\dots(i-1)(i+1)\dots(L+1)}}, 0_{(i+1)}, \dots, 0_{(L+1)}) \\
&+ G_D(0_{(1)}, 0_{(2)}, 0_{\overline{2(L+3)}}, 0_{12}, 0_{(L+3)}) \\
&\times \sum_{i=4}^{L+1} G_D(0_{(4)}, \dots, 0_{(i-1)}, 0_{\overline{1(L+3)4\dots(i-1)(i+1)\dots(L+1)}}, 0_{(i+1)}, \dots, 0_{(L+1)}) \\
&+ G_D(0_{(1)}, 0_{\overline{3(L+3)}}, 0_{(3)}, 0_{\overline{13(L+3)}}, 0_{(L+3)}) \\
&\times \sum_{i=4}^{L+1} G_D(0_{(4)}, \dots, 0_{(i-1)}, 0_{\overline{1(L+3)4\dots(i-1)(i+1)\dots(L+1)}}, 0_{(i+1)}, \dots, 0_{(L+1)}) \\
&+ G_D(0_{(1)}, 0_{\overline{1(L+2)}}, 0_{\overline{1(L+2)(L+3)}}, 0_{(L+2)}, 0_{(L+3)}) \\
&\times \sum_{i=4}^{L+1} G_D(0_{(4)}, \dots, 0_{(i-1)}, 0_{\overline{1(L+3)4\dots(i-1)(i+1)\dots(L+1)}}, 0_{(i+1)}, \dots, 0_{(L+1)}) \\
&+ G_D(0_{\overline{2(L+2)}}, 0_{(2)}, 0_{\overline{2(L+3)}}, 0_{(L+2)}, 0_{(L+3)}) \\
&\times \sum_{i=4}^{L+1} G_D(0_{(4)}, \dots, 0_{(i-1)}, 0_{\overline{2(L+2)(L+3)4\dots(i-1)(i+1)\dots(L+1)}}, 0_{(i+1)}, \dots, 0_{(L+1)}) \\
&+ G_D(0_{(1)}, 0_{(2)}, 0_{(3)}, 0_{12}, 0_{23}) \\
&\times \sum_{i=4}^{L+1} G_D(0_{(4)}, \dots, 0_{(i-1)}, 0_{\overline{1\dots(i-1)(i+1)\dots(L+1)}}, 0_{(i+1)}, \dots, 0_{(L+1)}),
\end{aligned} \tag{4.67}$$

and,

$$\begin{aligned}
& G_D(1, 2, 3, L+2, L+3) \otimes G_{4\dots(L+1)}^*(0_{4\dots(L+1)}) \\
&= G_D(0_{4\dots(L+1)(L+3)}, 0_{4\dots(L+1)(L+2)}, 0_{4\dots(L+1)(L+2)}, 0_{(4)}, \dots, 0_{(L+3)}) \\
&+ G_D(0_{(1)}, 0_{(2)}, 0_{124\dots(L+1)}, 0_{(4)}, \dots, 0_{(L+1)}, 0_{12}, 0_{14\dots(L+1)}) \\
&+ G_D(0_{(1)}, 0_{13\dots(L+1)}, 0_{(3)}, \dots, 0_{(L+1)}, 0_{3\dots(L+1)}, 0_{14\dots(L+1)}) \\
&+ G_D(0_{4\dots(L+1)(L+3)}, 0_{(2)}, 0_{2(L+3)}, 0_{(4)}, \dots, 0_{(L+1)}, 0_{24\dots(L+1)(L+3)}, 0_{(L+3)}) \quad (4.68) \\
&+ G_D(0_{2\dots(L+1)}, 0_{(2)}, \dots, 0_{(L+1)}, 0_{3\dots(L+1)}, 0_{24\dots(L+1)}) \\
&+ G_D(0_{(1)}, 0_{1(L+2)}, 0_{4\dots(L+1)}, 0_{(L+2)}, 0_{14\dots(L+1)}) \\
&+ G_D(0_{4\dots(L+1)(L+3)}, 0_{\bar{3}(L+3)}, 0_{(3)}, \dots, 0_{(L+1)}, 0_{3\dots(L+1)}, 0_{(L+3)}) \\
&+ G_D(0_{2(L+2)}, 0_{(2)}, 0_{4\dots(L+1)(L+2)}, 0_{(4)}, \dots, 0_{(L+2)}, 0_{24\dots(L+1)(L+2)}),
\end{aligned}$$

where, following the same ideas of the NMLT(L) diagram, the edges 1, 2, 3, $L+2$ and $L+3$ have been factorized in order to have a simpler reading.

As it was highlighted for the definitions of the convolution symbols given for the NMLT(L) diagram, these new definitions have simpler interpretations when they are presented diagrammatically. It is important to recall that the LTD formalism cuts a 1PI L -loop diagram (or, speaking in terms of graph theory, a multi-graph without loops and with cyclomatic number L) into its spanning trees. In the case of $N^2\text{MLT}(L)$ diagram, as it has L loops, there will be L cut internal lines. In terms of standard combinatorics, there shall be cuts that will give rise to a graph with two disconnected components. However, based on the LTD, it is found that disconnected topologies cannot occur. An evident example of this case is that the edges 1, 2 and $L+2$ cannot be cut simultaneously, as this shall disconnect the vertex adjacent to these three edges. In an analogous manner, the sets of edges $\{1, 4, \dots, L+1, L+3\}$, $\{3, 4, \dots, L+1, L+2\}$, $\{2, 3, L+3\}$, $\{1, 3, L+2, L+3\}$, together with $\{1, 2, L+2\}$, represent the cuts that cannot appear simultaneously. Remarkably, this gives rise to the same classification of cuts as the one given for the NMLT(L) diagram: one class with one of the edges 4, \dots , $L+1$ off-shell (notice that, if two of these edges are off-shell, then there will still exist a loop in the remaining term), and other class with all the edges 4, \dots , $L+1$ on-shell.

The first class is represented by the definition of the first convolution, given in Eq. (4.67). In this case, there are $L-3$ edges set on-shell. Then, the other three cut edges should be three in the set $\{1, 2, 3, L+2, L+3\}$. Consequently, there are 10 combinations of three of these edges, and two of them gives a disconnected graph, namely $\{1, 2, L+2\}$ and $\{2, 3, L+3\}$. Then, there are 8 different cuts for each of the off-shell lines in the set $\{4, \dots, L+1\}$, leading to the 8 summations in the definition of the second convolution symbol, Eq. (4.67).

Regarding the second class, there are already $L-2$ edges already on-shell, in such a way that there are two elements of the set $\{1, 2, 3, L+2, L+3\}$ on-shell. As a result, there are also 10 combinations of two elements from this set. However, two of these combinations will give rise to a disconnected graph, namely $\{1, L+3\}$ and $\{3, L+2\}$, leading to the eight terms of Eq. (4.68). It is important to highlight that Eq. (4.66) relates an $N^2\text{MLT}(L)$ diagram with the sum of the convolution of an NMLT(3) diagram with an MLT($L-3$) diagram and the convolution of an MLT(2) diagram with a fully opened MLT($L-3$) diagram. Thereby, an $N^2\text{MLT}(L)$ can be studied in terms of lower complexity diagrams with fewer loops, as it was the case for the NMLT(L) diagram.

Both convolutions defined in Eqs. (4.67) and (4.68) include the function $G_{4\dots(L+1)}^*$, which represents the explicit expression of the off-shell internal momenta in terms of the on-shell momenta. The relation given in Eq. (4.66) can be represented pictorially as shown in Fig. 4.11.

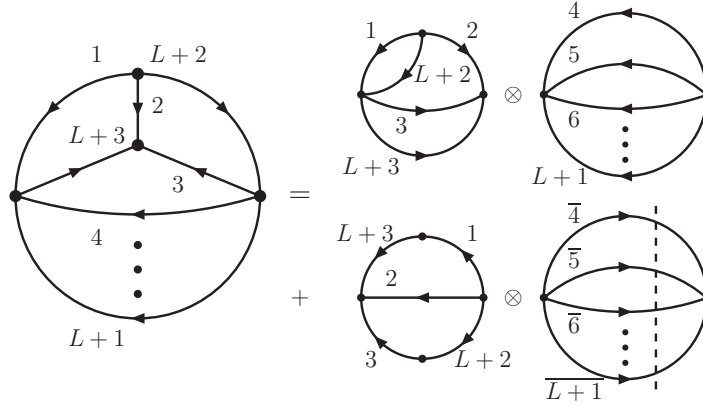


Figure 4.11: Dual expansion of a $N^2\text{MLT}(L)$ diagram.

In general, an arbitrary topological family with topological complexity k and L loops is denoted by $N^{k-1}\text{MLT}(L)$ (*Next-to-...-Next-To-Maximal Loop Topology*), and it is expected to have a dual expansion similar to Eq. (4.54), Eq. (4.62) and Eq. (4.66). Furthermore, it would be seen that the $N^{k-1}\text{MLT}(L)$ diagram can be studied in terms of diagrams with lower topological complexity and fewer loops.

In this chapter, the computational aspects of the LTD framework has been studied. It has been also presented a short-hand notation in order to give a compact representation of the results, together with a classification of Feynman diagrams in terms of the topology of the underlying graphs. This topological classification has shown to be a well suited structure to study a diagram with an arbitrary number L of loops.

Chapter 5

Mathematical properties of nested residues within the Loop-Tree Duality

In Chapter 4 it was presented that LTD formalism gives some astonishing interpretations for multi-loop multi-leg Feynman amplitudes, giving a trail to go from a Feynman diagram to its factorization formulae, removing in the intermediate steps the non-physical divergences of MLT diagrams and MLT insertions. In this chapter, the mathematical foundations of the computations given in Chapter 4 are presented. This represents a solid foundation to LTD formalism.

5.1 Iterated and nested residues

A well known procedure for the computation of integrals of an arbitrary function $f : \mathbb{R} \rightarrow \mathbb{C}$ consists on extending the domain of the function to the complex plane \mathbb{C} (likewise, \mathbb{R} is embedded in \mathbb{C}), obtaining the function $f : \mathbb{C} \rightarrow \mathbb{C}$, and then perform the integral with the aid of complex analysis techniques. One of the main results of complex analysis is Cauchy's residue theorem, stated in Sec. 4.1.

Let us start with an arbitrary rational function on L variables, $f : \mathbb{R}^L \rightarrow \mathbb{C}$, such that

$$f(\vec{x}) = \frac{\mathcal{N}(\vec{x})}{\prod_{i=1}^L (x_i^2 - y_i^2) \prod_{i=L+1}^m (z_i^2 - y_i^2)}, \quad (5.1)$$

where each z_i is a linear combination of (x_1, \dots, x_L) , $y_i \in \mathbb{C}$ such that $\text{Re}(y_i) > 0$ and every y_i has an infinitesimally small negative imaginary part. Also the numerator $\mathcal{N}(\vec{x})$ depends as well on some other real parameters. These properties are the basic characteristics of the integrand of an amplitude given by Feynman rules, where each x_i can be associated with each $q_{i,0}$ and each y_i with its respective on-shell energy $q_{i,0}^{(+)}$. Analogously, the z_i can be related to the linear combinations of the x_i variables that define a topological class.

The iterated application of Cauchy's residue theorem is developed with the algorithm called *iterated residue*, which is described as follows. We start with the function f given in Eq. (5.1). The natural inclusion operator,

$$i : \mathbb{C}^{\mathbb{R}^n \times \mathbb{C}^m} \rightarrow \mathbb{C}^{\mathbb{R}^{n-1} \times \mathbb{C}^{m+1}}, \quad (5.2)$$

maps a functions with n real ordered arguments and m complex ordered arguments into a function with $n-1$ real ordered arguments and $m+1$ complex ordered arguments such that $i(f(\vec{x})) = f(\vec{x})$, where $x_n \in \mathbb{C}$. Briefly, the natural inclusion operator promotes the last real argument of a function to the complex plane \mathbb{C} . In this manner, the natural inclusion operator is applied to the function f . The new function $i(f)$ is a function with its L -th argument in the complex plane. It is important to notice that this function is meromorphic in x_L , and let $\text{Poles}[f, x_L] = \{p_1, \dots, p_k\}$ be the set of all the poles in the variable x_L of the function $i(f)$. It is mandatory to define a function $\text{IRes} : \mathbb{C}^{\mathbb{R}^{L-1} \times \mathbb{C}} \rightarrow \mathbb{C}^{\mathbb{R}^{L-1}}$ through the relation

$$\text{IRes}(i(f(x_1, \dots, x_L))) = -2\pi i \sum_{p_s \in \text{Poles}[f, x_L]} \text{Res}(f(x_1, \dots, x_L), \{x_L, p_s\}) \theta(-\text{Im}(p_s)), \quad (5.3)$$

which represents the application of Cauchy's residue theorem to the function $i(f)$ along a contour enclosing the lower half plane, where the negative sign of the imaginary part of the pole is assured by the Heaviside theta function. It is important to notice that the right hand side of Eq. (5.3) does not depend on x_L anymore. In this manner, the functor

$$\text{IRes} \circ i : \mathbb{C}^{\mathbb{R}^n} \rightarrow \mathbb{C}^{\mathbb{R}^{n-1}}, \quad (5.4)$$

can be applied iteratively to the function f obtaining in each iteration a function with one less argument. This is represented by the algebraic diagram

$$\mathbb{C}^{\mathbb{R}^L} \xrightarrow{\text{IRes} \circ i} \mathbb{C}^{\mathbb{R}^{L-1}} \xrightarrow{\text{IRes} \circ i} \dots \xrightarrow{\text{IRes} \circ i} \mathbb{C}. \quad (5.5)$$

This is the full algorithm of the iterated residue. As expected, each application of the functor given in Eq. (5.4) is called *iteration* of the iterated residue. Now, with the notation given in Sec. 4.1, the right arrow is interpreted as any number of iterations of the iterated residues, and the poles where the residue has been computed is represented by $0_{(k)}$ in the k -th argument. As mentioned in the Sec. 4.1.2, an important result is the cancellation of the contribution of the displaced poles to the iterated residues. For simple poles, the proof is quite simple. Let

$$F_i(j) = \frac{1}{x_j^2 - y_i^2}, \quad (5.6)$$

and let $\text{IRes}(F_i(j), \{j, 0_k\})$ be the residue of the function $F_i(j)$ for the negative imaginary part pole $x_j = y_k$. In this manner,

$$\text{IRes}(F_i(k), \{k, 0_j\}) = \frac{\delta_{ij}}{2y_i}, \quad (5.7)$$

where δ_{ij} is the Kronecker's delta function. Also, if we define

$$\theta(i\bar{j}) \equiv \theta\left(-\text{Im}\left(q_{i,0}^{(+)} - q_{j,0}^{(+)}\right)\right), \quad (5.8)$$

a direct computation shows that

$$\text{IRes}(F_i(k_j), \{k, 0_{i\bar{j}}\}) = \frac{\theta(i\bar{j})}{2q_{i,0}^{(+)}} \quad , \quad \text{IRes}(G_j(k_{\bar{i}}), \{k, 0_{i\bar{j}}\}) = -\frac{\theta(i\bar{j})}{2q_{j,0}^{(+)}}. \quad (5.9)$$

In order to appreciate the potential use with arbitrary numerators, let us consider a meromorphic function h on the sets i and j , such that $h(0_i, j)$, $h(0_i, 0_{i\bar{k}})$ and $h(\bar{j}_k, j)$ are

well defined. From the relations in Eq. (5.9), direct computations lead to

$$\begin{aligned}
& \text{IRes}(\text{IRes}(h(i, j)F_i(i)F_k(ij), \{i, 0_i\}), \{j, 0_{\bar{i}k}\}) \\
&= \frac{1}{2y_i} \text{IRes}(h(0_i, j)F_k(j_i), \{j, 0_{\bar{i}k}\}) = h(0_i, 0_{\bar{i}k}) \frac{\theta(\bar{i}k)}{4y_i y_k}, \\
& \text{IRes}(\text{IRes}(h(i, j)F_i(i)F_k(ij), \{i, \bar{j}_k\}), \{j, 0_{\bar{i}k}\}) \\
&= \frac{1}{2y_k} \text{IRes}(h(\bar{j}_k, j)F_i(\bar{j}_k), \{j, 0_{\bar{i}k}\}) = h(0_i, 0_{\bar{i}k}) \left(-\frac{\theta(\bar{i}k)}{4y_i y_k} \right),
\end{aligned} \tag{5.10}$$

Both expressions in Eq. (5.10) explicitly show the cancellation of displaced poles for single poles. For higher-order poles, Eq. (5.9) can be used to derive the proof. The procedure is sketched as follows: let us assume that a function f has the pole y_i with order n , this is,

$$f(\vec{x}) \propto (z_i^2 - y_i^2)^{-n}. \tag{5.11}$$

Then, consider a new function \tilde{f} defined by

$$\tilde{f}(\vec{x}) = \frac{(z_i^2 - y_i^2)^n}{\prod_{j=1}^n \left(z_i^2 - \left(y_i + \sum_{k=1}^j a_k \right)^2 \right)} f(\vec{x}), \tag{5.12}$$

for some purely real constants a_k . In this manner, we split the n -th order pole into n different simple poles with the same imaginary part. In order to simplify the computations, it is possible to replace $a \equiv a_i$ for all $i \in \{1, \dots, n\}$, so that the poles for the denominators depending on z_i are given by

$$i = \{y_i + a, \dots, y_i + na\}. \tag{5.13}$$

From its definition, it is seen that $\tilde{f} \rightarrow f$ as $a \rightarrow 0$. Additionally, as the function \tilde{f} contains simple poles only, the cancellation of the contributions of its displaced poles to the iterated residues is assured by Eq. (5.10), and after the limit $a \rightarrow 0$, it is obtained the same result for an arbitrary n -th order pole. This is, for a function

$$F(x_i, x_j) = \frac{P(x_i, x_j)}{((x_i - k_i)^2 - y_i^2)^{\gamma_i} ((x_i + x_j - k_{ij})^2 - y_k^2)^{\gamma_k}}, \tag{5.14}$$

the next relation holds,

$$\begin{aligned}
& \text{IRes}(\text{IRes}(F(x_i, x_j), \{x_i, y_j + k_i\}), \{x_j, y_k - y_i + k_{ij} - k_i\}) = \\
& -\text{IRes}(\text{IRes}(F(x_i, x_j), \{x_i, y_k - x_j + k_{ij}\}), \{x_j, y_k - y_i + k_{ij} - k_i\}).
\end{aligned} \tag{5.15}$$

Hence, this cancellation holds step by step of the iterated residues, and thus, it does not depend on the residues already taken. This implies that this cancellation holds regardless the order of the previous iterations of the iterated residues. Eq. (5.15) assures that the bar configuration of the poles contributing to the iterated residues is the one without any bar. An alternate proof is given in Appendix C. In order to have a better idea of what is happening, let us focus on the vacuum 2-loop function

$$\mathcal{I}_{\text{MLT}}^{(2)} = G_F(1, 2, 3) = G_F(1, 2, 12), \tag{5.16}$$

as a function of $q_{2,0} \in \mathbb{C}$. The set of poles of the function $\mathcal{I}_{\text{MLT}}^{(2)}$ is given by $\text{Poles}[\mathcal{I}_{\text{MLT}}^{(2)}, q_{2,0}] = \{\pm q_{2,0}^{(+)}, \pm q_{3,0}^{(+)} - q_{1,0}\}$. Recalling that $q_{1,0} \in \mathbb{R}$, the poles $\pm q_{3,0}^{(+)} - q_{1,0}$ depend on the real parameter $q_{1,0}$, so that their imaginary part depend only on the sign of $q_{3,0}^{(+)}$. Also, their

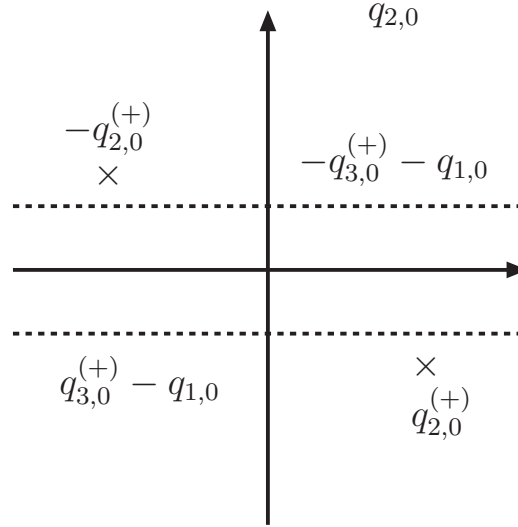


Figure 5.1: Pole structure of $\mathcal{I}_{\text{MLT}}^{(2)}$ as a function of $q_{2,0}$.

real part depends explicitly on $q_{1,0}$, so these poles are located in some point along two horizontal lines in the $q_{2,0}$ -complex plane. The pole structure of the function $\mathcal{I}_{\text{MLT}}^{(2)}$ can be sketched as in Fig. 5.1, where the dashed lines represent the poles $\pm q_{3,0}^{(+)} - q_{1,0}$.

Following the computations given in Sec. 4.1.2, the first iteration of the iterated residue leads to two terms, namely,

$$\begin{aligned}
 t_1 &= \frac{1}{2q_{2,0}^{(+)}} \frac{1}{\left(q_{1,0}^2 - q_{1,0}^{(+2)}\right) \left(\left(q_{1,0} + q_{2,0}^{(+)} + p_0\right)^2 - q_{3,0}^{(+2)}\right)}, \\
 t_2 &= \frac{1}{2q_{3,0}^{(+)}} \frac{1}{\left(q_{1,0}^2 - q_{1,0}^{(+2)}\right) \left(\left(q_{3,0}^{(+)} - q_{1,0} - p_0\right)^2 - q_{2,0}^{(+2)}\right)}.
 \end{aligned} \tag{5.17}$$

Each of the terms in Eq. (5.17) has its own pole structure. However, the displaced pole $q_{3,0}^{(+)} - q_{2,0}^{(+)}$ is common in both terms. Pole structures of t_1 and t_2 are depicted in Fig. 5.2, where the gray blob represents the location of the displaced pole, as the imaginary part is still indeterminate. From Fig. 5.2 it can be seen that all poles but the displaced pole of one term is the reflection of the poles of the other term with respect to the origin. This shows that t_1 and t_2 are related. It can be noticed that, closing the integration contour around the lower half-plane for one term is equivalent to close the integration contour around the upper half-plane, together with an overall opposite sign. As the displaced pole appears in both contours, it gives opposite contributions to the residue of each term, resulting on their cancellations.

Given the cancellation of the contributions of the displaced poles, it is possible to define an algorithm analogous to the iterated residue, but this time restricting the selection of the negative imaginary part poles to the non-displaced negative imaginary part poles. This algorithm is called the *nested residues*. Naturally, both iterated and nested residues lead to the same results. The main difference between iterated and nested residues is that displaced poles contribute to the former (and then their cancellation happens) while displaced poles are absent in the later. The iterated residues are the result of the direct

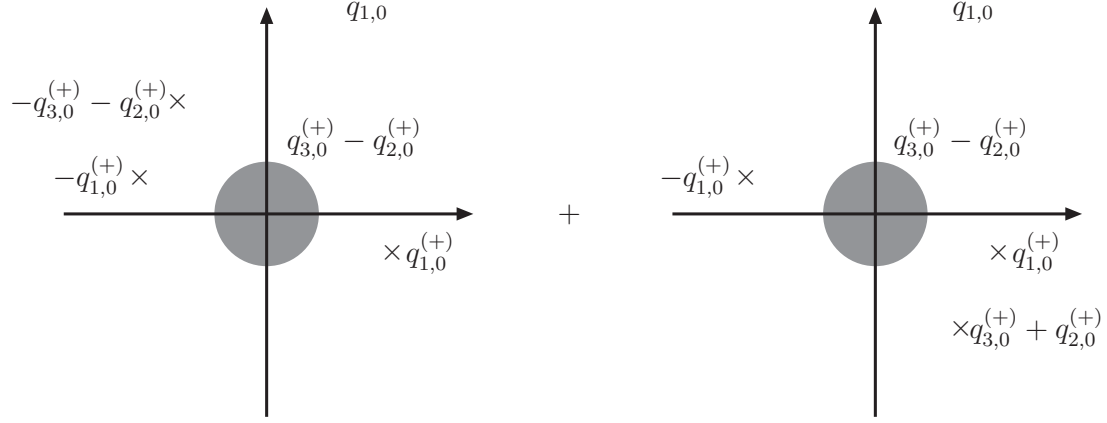


Figure 5.2: Pole structure of the first iteration of the iterated residues of $\mathcal{I}_{\text{MLT}}^{(2)}$ as a function of $q_{1,0}$ sketched term by term.

application of Cauchy residue theorem, while the nested residues account for the cancellation of displaced poles and lead to a more efficient implementation of LTD.

It is important to notice that, in both cases, iterated and nested residues, the order of the residues is not commutative and gives rise to different expressions. For example, for the sunrise diagram, a direct computation of the nested residues, first with respect to $q_{1,0}$ and then with respect to $q_{2,0}$, leads to

$$\begin{aligned}
\mathcal{I}_{\text{MLT}}^{(2)} &\rightarrow G_D(0_{(1)}, 0_{(2)}, 0_{12}) + G_D(0_{(1)}, 0_{13}, 0_{(3)}) + G_D(0_{2\bar{3}}, 0_{(2)}, 0_{(3)}) \\
&= \frac{1}{4q_{1,0}^{(+)} q_{2,0}^{(+)}} \frac{1}{\left(q_{1,0}^{(+)} + q_{2,0}^{(+)} + p_0\right)^2 - \left(q_{3,0}^{(+)}\right)^2} \\
&+ \frac{1}{4q_{1,0}^{(+)} q_{3,0}^{(+)}} \frac{1}{\left(q_{1,0}^{(+)} + q_{3,0}^{(+)} - p_0\right)^2 - \left(q_{2,0}^{(+)}\right)^2} \\
&+ \frac{1}{4q_{2,0}^{(+)} q_{3,0}^{(+)}} \frac{1}{\left(q_{2,0}^{(+)} - q_{3,0}^{(+)} + p_0\right)^2 - \left(q_{1,0}^{(+)}\right)^2}.
\end{aligned} \tag{5.18}$$

Comparing Eq. (5.18) with Eq. (4.29) it can be perceived that the expressions are different term by term. Fortunately, both expressions lead to the same causal representation, Eq. (4.30). If one starts the calculation of the nested residues with the $q_{L,0}$ energy, followed by $q_{L-1,0}$, and so on, one obtains the following general expression for the $\text{MLT}(L)$ integrand after the i -th iteration,

$$\begin{aligned}
G_F(1, \dots, L, L+1) &\rightarrow G_F(1, \dots, L-i) \\
&\times \sum_{j=L-i+1}^{L+1} G_D(0_{(L-i+1)}, \dots, 0_{(j-1)}, 1 \dots (L-i)_{(L-i+1)\dots(j-1)\overline{(j+1)\dots(L+1)}, 0_{(j+1)}, \dots, 0_{(L+1)}).
\end{aligned} \tag{5.19}$$

The proof of Eq. (5.19) is given by mathematical induction in Appendix D. In particular, for $i = L$, Eq. (5.19) gives

$$G_F(1, \dots, L+1) \rightarrow \sum_{i=1}^L G_D(0_{(1)}, \dots, 0_{(i-1)}, 0_{1\dots(i-1)\overline{(i+1)\dots(L+1)}, 0_{(i+1)}, \dots, 0_{(L+1)}), \tag{5.20}$$

as presented in Sec. 4.1. The i -th term of the right hand side of Eq. (5.19), after applying partial fractioning, can be written in the form

$$t_i = \frac{1}{x_{L+1}} \left(\frac{1}{\sum_{k=1}^{i-1} q_{k,0}^{(+)} - \sum_{k=i}^{L+1} q_{k,0}^{(+)} + p_0} - \frac{1}{\sum_{k=1}^i q_{k,0}^{(+)} - \sum_{k=i+1}^{L+1} q_{k,0}^{(+)} + p_0} \right). \quad (5.21)$$

Each term of Eq. (5.21) generates a divergence for some particular configuration of the loop 3-momenta. Some of these divergences do not have a physical meaning, and they cancel, as sketched below. The sum of the i -th and the $(i+1)$ -th term gives

$$t_i + t_{i+1} = \frac{1}{x_{L+1}} \left(\frac{1}{\sum_{k=1}^{i-1} q_{k,0}^{(+)} - \sum_{k=i}^{L+1} q_{k,0}^{(+)} + p_0} - \frac{1}{\sum_{k=1}^{i+1} q_{k,0}^{(+)} - \sum_{k=i+2}^{L+1} q_{k,0}^{(+)} + p_0} \right). \quad (5.22)$$

Comparing Eq. (5.21) with Eq. (5.22), it is possible to see the shift between the indices of the positive and the negative terms¹. This is, the negative term of Eq. (5.21) equals in magnitude the positive term of t_{i+1} . This is an explicit example of the cancellation of spurious divergences. Then, the causal representation of the MLT(L) diagram is obtained through these cancellations, leading to

$$G_F(1, \dots, L+1) \rightarrow \frac{1}{x_{L+1}} \left(\frac{1}{\lambda_1^+} + \frac{1}{\lambda_1^-} \right), \quad (5.23)$$

as presented in Eq. (4.55).

Let us recall the idea of obtaining the same causal representation for the MLT(L), independently on the order of integration. This is not a coincidence, but a formal result. Briefly, if the order of integration is changed, different terms are obtained, but they have the same functional structure as the one given in Eq. (5.20). Then, the cancellation of spurious divergences follows in the same fashion, where the difference rely on which momentum flow is fixed. Now, let us formalize these ideas. Let us assume that the order of integration is developed following a permutation $\pi = (\pi_1, \pi_2, \dots, \pi_L)$ of the standard order $I = (1, 2, \dots, L)$ and define $\pi_{L+1} = L+1$. Then, reordering the arguments of $G_F(1, \dots, L+1) = G_F(\pi_1, \dots, \pi_{L+1})$, an analogous relation to Eq. (5.20) is obtained, namely

$$G_F(\pi_1, \dots, \pi_{L+1}) \rightarrow \sum_{i=1}^{L+1} G_D(0_{(\pi_1)}, \dots, 0_{(\pi_{i-1})}, 0_{\pi_1 \dots \pi_{i-1} \overline{\pi_{i+1} \dots \pi_{L+1}}}, 0_{(\pi_{i+1})}, \dots, 0_{(\pi_{L+1})}). \quad (5.24)$$

The cancellation of spurious singularities follows from Eq. (5.24), where the fixed momentum flow is $q_{\pi_i,0}^{(+)}$ instead of $q_{i,0}^{(+)}$ as in Eq. (5.23). Then, the causal structure becomes

$$G_F(\pi_1, \dots, \pi_{L+1}) \rightarrow \frac{1}{\prod_{i=1}^{L+1} 2q_{\pi_i,0}^{(+)}} \left(\frac{1}{\sum_{i=1}^{L+1} q_{\pi_i,0}^{(+)} + p_0} + \frac{1}{\sum_{i=1}^{L+1} q_{\pi_i,0}^{(+)} - p_0} \right). \quad (5.25)$$

¹This can be thought as fixing the orientation of the momentum flow in the $(i+1)$ -th propagator.

Finally, recalling that $\pi^* = (\pi_1, \dots, \pi_{L+1})$ is just a permutation of $I_1 = (1, \dots, L+1)$, it is seen that the right hand side of Eq. (5.25) equals the right hand side of Eq. (5.23).

Eq. (5.23) is a particular case of the cancellations that take place in Eq. (5.19). There, each term has the form

$$t_{i,j} = \frac{1}{\prod_{\substack{k=L-i+1 \\ k \neq j}}^{L+1} 2q_{k,0}^{(+)}} \frac{G_F(1, \dots, L-i)}{\left(\sum_{k=1}^{L-i} q_{k,0} + \sum_{k=L-i+1}^{j-1} q_{j,0}^{(+)} - \sum_{k=j+1}^{L+1} q_{k,0}^{(+)} + p_0 \right)^2 - \left(q_{j,0}^{(+)} \right)^2}. \quad (5.26)$$

Recalling that this result is obtained after each iteration of the nested residues, each off-shell energy $q_{k,0}$ is a real parameter, so the variable

$$p'_0 = p_0 + \sum_{k=1}^{L-i} q_{k,0} \quad (5.27)$$

is real. Then, the summation of all $t_{i,j}$ terms over j gives

$$G_F(1, \dots, L+1) \rightarrow \frac{G_F(1, \dots, L-i)}{\prod_{k=L-i+1}^{L+1} 2q_{k,0}^{(+)}} \left(\frac{1}{\sum_{k=1}^{L-i} q_{k,0} + p_0 - \sum_{k=L-i+1}^{L+1} q_{k,0}^{(+)}} - \frac{1}{\sum_{k=1}^{L-i} q_{k,0} + p_0 + \sum_{k=L-i+1}^{L+1} q_{k,0}^{(+)}} \right). \quad (5.28)$$

Eq. (5.28) reveals a non-trivial simplification. In fact, both sides of Eq. (5.28) contain the factor $G_F(1, \dots, L-i)$. The rest of the right hand side of Eq. (5.28) is a propagator-like function which is called *auxiliary propagator*, $G_{(L-i+1)\dots(L+1)}^*$, defined by

$$G_{(L-i+1)\dots(L+1)}^*(1, \dots, L-i) = \frac{1}{\prod_{k=L-i+1}^{L+1} 2q_{k,0}^{(+)}} \left(\frac{1}{\sum_{k=1}^{L-i} q_{k,0} + p_0 - \sum_{k=L-i+1}^{L+1} q_{k,0}^{(+)}} - \frac{1}{\sum_{k=1}^{L-i} q_{k,0} + p_0 + \sum_{k=L-i+1}^{L+1} q_{k,0}^{(+)}} \right). \quad (5.29)$$

Auxiliary propagator, Eq. (5.29), is similar to a propagator with off-shell energy $q_{1,0} + \dots + q_{L-i} + p_0$ and on-shell energy $q_{L-i+1,0}^{(+)} + \dots + q_{L+1,0}^{(+)}$. This implies that if the iterations of the nested residues with respect to energies of MLT insertions is computed, it would give an analogous result to that with a single propagator instead, as shown in Fig. 5.3. It is important to notice that some spurious singularities are cancelled in order to reach the auxiliary propagator, and hence its substitution does not introduce any new singularity. Instead, the divergences of the diagram obtained through these substitutions are associated to the orientations of the momentum flow among the MLT insertions, as shown in Fig. 5.4, where an arbitrary MLT(L) subdiagram has been inserted in each internal line of the $N^2\text{MLT}(3)$ diagram.

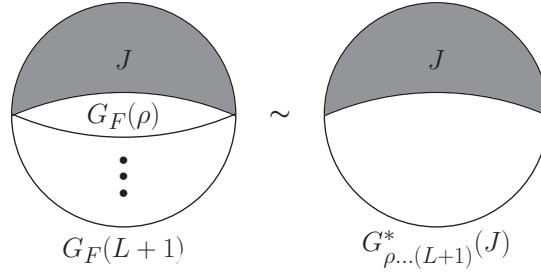


Figure 5.3: Causal simplification of an MLT insertion can be understood as merging all its propagators into a single auxiliary propagator G^* . The J blob contains any configuration of internal momenta.

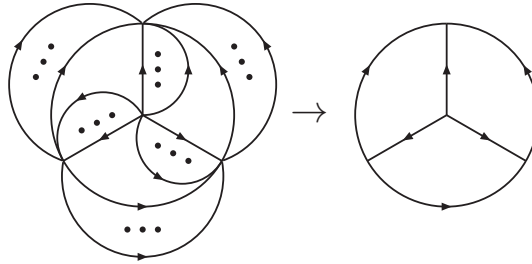


Figure 5.4: Reduction of an arbitrary $N^2\text{MLT}(L)$ diagram to the minimal diagram $N^2\text{MLT}(3)$. Each edge of the left hand side represents an MLT insertion and each arc in the right hand side represents the auxiliary propagator associated to the corresponding MLT insertion.

The interpretation of the auxiliary propagator with respect to MLT insertions can be understood as follows. Let us assume that an $N^k\text{MLT}$ diagram with L loops is to be computed, and let it have an $\text{MLT}(\rho)$ in the line $L + 1$ (it is not necessary to have the MLT insertion in the line $L + 1$, but this is taken this way in order to fix the ideas). Then, the integrand is given by

$$\mathcal{I}_{N^k\text{MLT}}^{(L)} = G_F(1, \dots, L - \rho, \dots, L, L + 1, \dots, m). \quad (5.30)$$

Let, also, $L - \rho, \dots, L$ be the momenta within the MLT insertion (if this is not the case, then a new labeling of the momenta will give the desired result). In this manner, the momenta $L + 2, \dots, m$ do not depend on the momenta $L - \rho, \dots, L$. Then it is possible to factorize the integrand in the way

$$\mathcal{I}_{N^k\text{MLT}}^{(L)} = G_F(1, \dots, L - \rho - 1, L + 2, \dots, m) G_F(L - \rho, \dots, L + 1). \quad (5.31)$$

Thus, the first ρ iterations of the nested residue only affect the second factor of the right hand side of Eq. (5.31). After these iterations are performed, it is obtained

$$\mathcal{I}_{N^k\text{MLT}}^{(L)} \rightarrow G_F(1, \dots, L - \rho - 1, L + 2, \dots, m) G_{(L-\rho)\dots(L+1)}^*(1 \dots (L - \rho - 1)). \quad (5.32)$$

The computations of the next iterations of the nested residues will produce two different terms, one with the auxiliary propagator off-shell and one with the auxiliary propagator on-shell. In order to give a representation of these two kinds of terms, it is important to

notice that the derivation of the definition of the auxiliary propagator implies that

$$\begin{aligned} & G_{(L-\rho)\dots(L+1)}^*(1\dots(L-\rho-1)) \\ &= \sum_{j=L-\rho}^{L+1} G_D(0_{(L-\rho)}, \dots, 0_{(j-1)}, 1\dots(L-\rho-1)_{(L-\rho)\dots(j-1)\overline{(j+1)\dots(L+1)}}, 0_{(j+1)}, \dots, 0_{(L+1)}). \end{aligned} \quad (5.33)$$

Now let $\beta = \beta_1 \dots \beta_{L-\rho-1}$ be the sum of some indices with their corresponding bar configuration, associated with the poles where the rest of the iterations of the nested residues are computed. Then $1\dots(L-\rho-1) = 0_\beta$. If $\beta_i \notin \{L-\rho, \dots, L+1\}$, then it is obtained

$$\begin{aligned} & G_{(L-\rho)\dots(L+1)}^*(0_\beta) \\ & \rightarrow \sum_{j=L-\rho}^{L+1} G_D(0_{(L-\rho)}, \dots, 0_{(j-1)}, 0_{\beta(L-\rho)\dots(j-1)\overline{(j+1)\dots(L+1)}}, 0_{(j+1)}, \dots, 0_{(L+1)}). \end{aligned} \quad (5.34)$$

Eq. (5.34) shows that when the auxiliary propagator is off-shell, it represents the set of all tree-level diagrams that differ only in which internal line in the MLT insertion is off-shell.

Regarding the case where the auxiliary propagator is on-shell, Eq. (5.29) shows that only one term survives, namely

$$G_{(L-\rho)\dots(L+1)}^*(0_{((L-\rho)\dots(L+1))})G_D(0_{(L-\rho)}, \dots, 0_{(L+1)}). \quad (5.35)$$

Eq. (5.35) manifests that when the auxiliary propagator is on-shell, it represents that all the internal particles $L-\rho, \dots, L+1$ are set on-shell. Both interpretations are in agreement with the explanation given at the end of Chapter 4. Also, with this interpretation, the notation used in Eq. (4.62) and in Eq. (4.66) becomes easier to understand. This function also gives some insight of how the factorization properties of higher topological families can be developed, this is, it might have one term with a factor $G_{(L-\rho)\dots(L+1)}^*$ off-shell and one term with this factor on-shell. It is important to notice that the auxiliary propagator gives some freedom in the study of a given topological class $\mathbb{N}^{k-1}\text{MLT}(L)$. Hence, the study of an arbitrary topological class can be reduced to the study of diagrams with the same topological complexity but with the fewest possible number of loops. For instance, the study of the $\mathbb{N}^2\text{MLT}(L)$ diagram can be reduced to the study of the Mercedes-Benz diagram $\mathbb{N}^2\text{MLT}(3)$. However, it is important to highlight that this result holds for scalar particles. When an arbitrary polynomial appears in the numerator, it is in general not possible to reduce the MLT insertion to a single propagator. For instance, if the numerator depends on one integration variable, the reduction leads to two propagators.

5.2 Higher-order poles

The analysis of the analytic structure of Feynman integrands is incomplete if the scenario with multiple poles is not considered. One of the results studied up to now is given in Appendix C. The cancellation of the contributions of displaced poles to the iterated residues for all order poles gives insight of the structure of the final results, as displaced poles are not expected to appear. It was mentioned before that the study of simple poles is enough for the analysis of n -th order poles.

The relation presented in Eq. (4.11) is very useful for the study of higher-order poles. Let us assume that, for $\alpha_1, \dots, \alpha_m \in \mathbb{N}$, a Feynman diagram gives the integrand

$$\tilde{\mathcal{I}}_{\mathbb{N}^{k-1}\text{MLT}}^{(L)} = \prod_{i=1}^m G_F^{\alpha_i}(q_i). \quad (5.36)$$

Applying Eq. (4.11), we obtain

$$\begin{aligned} \tilde{\mathcal{I}}_{\mathbb{N}^{k-1}\text{MLT}}^{(L)} &= \left(\prod_{i=1}^m \frac{1}{(\alpha_i - 1)!} \frac{\partial^{\alpha_i - 1}}{\partial (q_{i,0}^{(+2)})^{\alpha_i - 1}} \right) \prod_{i=1}^m G_F(q_i) \\ &= \left(\prod_{i=1}^m \frac{1}{(\alpha_i - 1)!} \frac{\partial^{\alpha_i - 1}}{\partial (q_{i,0}^{(+2)})^{\alpha_i - 1}} \right) \mathcal{I}_{\mathbb{N}^{k-1}\text{MLT}}^{(L)}, \end{aligned} \quad (5.37)$$

where $\mathcal{I}_{\mathbb{N}^{k-1}\text{MLT}}^{(L)}$ is the integrand of the $\mathbb{N}^{k-1}\text{MLT}(L)$ integrand with simple poles. In order to assure that this relation is useful, it is left to prove that

$$\begin{aligned} &\sum_{q_{j,0} \in \text{Poles}[\tilde{\mathcal{I}}_{\mathbb{N}^{k-1}\text{MLT}}^{(L)}, q_{i,0}]} \text{Res} \left[\frac{\partial^{\alpha_i - 1}}{\partial (q_{i,0}^{(+2)})^{\alpha_i - 1}} \mathcal{I}_{\mathbb{N}^{k-1}\text{MLT}}^{(L)}, \{q_{i,0}, q_{j,0}^{(+)}\} \right] \theta(-\text{Im}(q_{j,0}^{(+)})) \\ &= \sum_{q_{j,0} \in \text{Poles}[\tilde{\mathcal{I}}_{\mathbb{N}^{k-1}\text{MLT}}^{(L)}, q_{i,0}]} \frac{\partial^{\alpha_i - 1}}{\partial (q_{i,0}^{(+2)})^{\alpha_i - 1}} \text{Res} \left[\mathcal{I}_{\mathbb{N}^{k-1}\text{MLT}}^{(L)}, \{q_{i,0}, q_{j,0}^{(+)}\} \right] \theta(-\text{Im}(q_{j,0}^{(+)})), \end{aligned} \quad (5.38)$$

but using Cauchy residue theorem, the proof is simple, as Eq. (5.38) is equivalent to

$$\int dq_{i,0} \frac{\partial^{\alpha_i - 1}}{\partial (q_{i,0}^{(+2)})^{\alpha_i - 1}} \mathcal{I}_{\mathbb{N}^{k-1}\text{MLT}}^{(L)} = \frac{\partial^{\alpha_i - 1}}{\partial (q_{i,0}^{(+2)})^{\alpha_i - 1}} \int dq_{i,0} \mathcal{I}_{\mathbb{N}^{k-1}\text{MLT}}^{(L)}, \quad (5.39)$$

which holds as the boundary of the integration does not depend on $q_{i,0}^{(+)}$. Formally, let

$$\mathcal{F}_{L,m} = \left\{ \prod_{i=1}^m G_F^{\alpha_i}(q_i) \mid \alpha_i \in \mathbb{N} \right\} \subseteq \mathbb{C}^{(\mathbb{R}^L)} \quad (5.40)$$

be the set of all 1PI integrands with L loops and m internal particles, such that $q_{i,0}^{(+)} \neq q_{j,0}^{(+)}$ for $i \neq j$, and let $G_{L,m}$ be the element of $\mathcal{F}_{L,m}$ with single poles only, namely

$$G_{L,m} = \prod_{i=1}^m G_F(q_i) \in \mathcal{F}_{L,m}. \quad (5.41)$$

Let us also define the bijection

$$\begin{aligned} \psi : \{G_{L,m}\} \times \mathbb{N}^m &\longrightarrow \mathcal{F}_{L,m} \\ (G_{L,m}, \alpha_1, \dots, \alpha_m) &\longmapsto \prod_{i=1}^m G_F^{\alpha_i}(q_i) \end{aligned} \quad (5.42)$$

with inverse ψ^{-1} . It is possible to iterate the nested residue to each function in $\mathcal{F}_{L,m}$. After the k -th iteration of the nested residues to every element of $\mathcal{F}_{L,m}$, a new set of

functions $\text{IRes}_k[\mathcal{F}_{L,m}] \subseteq \mathbb{C}^{(\mathbb{R}^{L-k})}$ is obtained. Defining the operator

$$\begin{aligned} \Phi_k : \text{IRes}_k[G_{L,m}] \times \mathbb{N}^m &\longrightarrow \text{IRes}_k[\mathcal{F}_{L,m}] \\ (G_{L,m}, \alpha_1, \dots, \alpha_m) &\longmapsto \left(\prod_{i=1}^m \frac{1}{(\alpha_i - 1)!} \frac{\partial^{\alpha_i - 1}}{\partial (q_{i,0}^{(+2)})^{\alpha_i - 1}} \right) G_{L,m} \end{aligned} \quad (5.43)$$

together with the identity map $id : \mathbb{N}^m \ni \vec{\alpha} \mapsto \vec{\alpha} \in \mathbb{N}^m$, the proof of Eq. (5.38) can be interpreted as commutative algebras. This is, for each $k \in \{1, \dots, L\}$, and in particular for $k = L - \rho$, the algebraic diagram presented in Fig. 5.5 commutes.

$$\begin{array}{ccccc} \mathcal{F}_{L,m} & \xrightarrow{(\text{Res} \circ i)^{L-\rho}} & \text{Res}_{L-\rho}[\mathcal{F}_{L,m}] & \xrightarrow{(\text{Res} \circ i)^\rho} & \text{Res}_L[\mathcal{F}_{L,m}] \\ \downarrow \psi^{-1} & & \uparrow \Phi_{L-\rho} & & \uparrow \Phi_L \\ \{G_{L,m}\} \times \mathbb{N}^m & \xrightarrow{(\text{Res} \circ i)^{L-\rho} \otimes id} & \text{Res}_{L-\rho}[\{G_{L,m}\}] \times \mathbb{N}^m & \xrightarrow{(\text{Res} \circ i)^\rho \otimes id} & \text{Res}_L[\{G_{L,m}\}] \times \mathbb{N}^m \end{array}$$

Figure 5.5: Algebraic diagram that shows the connection among expressions with simple and multiple poles, after computing the nested residues.

It is important to recall that derivatives do not introduce new divergences, although they increase their order. Thus, any cancellation taking place for simple poles should have a cancellation counterpart in the higher-order poles case. In this manner, any property of integrands with higher-order poles can be derived from properties of integrands with single poles only. For instance, Eq. (4.30) shows that for the scalar sunrise diagram,

$$\mathcal{I}_{\text{MLT}}^{(2)} \rightarrow \frac{1}{x_3} \left(\frac{1}{\lambda_1^+} + \frac{1}{\lambda_1^-} \right), \quad (5.44)$$

where $x_3 = 8q_{1,0}^{(+)} q_{2,0}^{(+)} q_{3,0}^{(+)}$ and $\lambda_1^\pm = q_{1,0}^{(+)} + q_{2,0}^{(+)} + q_{3,0}^{(+)} \pm p_0$. Then, for the integrand

$$\tilde{\mathcal{I}}_{\text{MLT}}^{(2)} = G_F(q_1) G_F(q_2) G_F^2(q_3), \quad (5.45)$$

the analogue of Eq. (4.30) is given by the derivative of Eq. (5.44) with respect to $q_{3,0}^{(+2)}$, this is,

$$\tilde{\mathcal{I}}_{\text{MLT}}^{(2)} \rightarrow -\frac{1}{2q_{3,0}^{(+)} x_3} \left(\frac{1}{(\lambda_1^+)^2} + \frac{1}{q_{3,0}^{(+)} \lambda_1^+} + \frac{1}{(\lambda_1^-)^2} + \frac{1}{q_{3,0}^{(+)} \lambda_1^-} \right). \quad (5.46)$$

The diagram of Fig. 5.5 happens to be important as its power is explicit in Eq. (5.44) and Eq. (5.46). This completes the proof of the sufficiency of the simple pole case to understand the analyticity of any Feynman integrand. Also, as it was mentioned before, external particles only introduce real shifts in Feynman propagators, and the imaginary parts remain untouched.

Chapter 6

Causal representation of multi-loop amplitudes within the loop-tree duality

Causal and non-causal singularities appear in a natural fashion in the multi-loop computations within perturbation theory of QFT. Regarding the non-causal singularities, as it was mentioned in Chapter 4 and formalized in Chapter 5, these divergences are not expected to appear in the final result of the calculations. An intuitive way of testing this cancellation of non-causal divergences is the numerical integration of loop integrals. As the LTD leads to a causal representation of scattering amplitudes, it is expected that a numerical implementation of the LTD approach would be more stable and faster than including non-causal divergences. This behaviour was firstly demonstrated for one-loop amplitudes [60, 62] and then to higher quantum orders [5, 69].

The LTD formalism has recently taken also a lot of attention from different working groups [63, 66, 67, 70] due to its advantages in the numerical implementations of loop integrals [61, 62, 64, 71, 72] as well as scattering amplitudes [73–79]. In particular, the computation of L -loop integrals within the LTD approach passes from a dL -dimensional integration space to a $(d - 1)L$ -dimensional integration space. As a matter of choice, this last integration space can be taken as the Euclidean space of the loop 3-momenta. Also, the hierarchies of scales are unambiguous within an Euclidean space, so that LTD has also been exploited as an alternative method [73, 80, 81] for asymptotic expansions [82]. Even more, extra external momenta or internal propagators do not change the number of integrations to be computed. In this manner, the CPU time necessary for numerical integrations does not increase drastically with the number of external momenta as in other numerical approaches.

In Chapter 4, the general ideas of the LTD formalism have been stated, and it was mentioned how the iterated application of the Cauchy’s residue theorem leads to the causal structure of a Feynman diagram. In Chapter 5, the computational algorithms needed to perform the LTD formalism have been formalised and the mathematical subtleties have been explained, so the factorization formulae can be developed for MLT, NMLT and N²MLT topological families. In this chapter, this idea is tested through numerical implementations for different topological classes at multi-loop level. Following this spirit, we test the causal structure of the MLT, NMLT and N²MLT multi-loop topologies. We start from their dual expansions presented in Chapter 4, which contain both causal and non-causal singularities. Then, we reconstruct the full analytical result from numerical evaluations over finite fields [83, 84]. This algorithm allows us to surpass the non-causal

propagators, since their cancellations are performed in an implicit manner. The algorithm here presented can be straightforwardly extended to any topology, N^k MLT with $k > 2$, and arbitrary internal configurations.

6.1 Finite fields and analytic reconstruction

The analytic reconstruction of the causal representation for multi-loop scalar diagrams is based on finite fields theory. This is due to the fact that, for an arbitrary prime number p , the equivalence classes of all integer numbers with the same remainder defined by

$$\forall a \in \{0, \dots, p-1\} ([a]_p = \{n \in \mathbb{Z} | n \equiv a \pmod{p}\}), \quad (6.1)$$

define the finite field

$$\mathbb{Z}_p = \{[a]_p | a \in \{0, \dots, p-1\}\}, \quad (6.2)$$

together with the operations

$$[a]_p + [b]_p = [a+b]_p \quad , \quad [a]_p [b]_p = [ab]_p. \quad (6.3)$$

From now on, elements in \mathbb{Z}_p are going to be written without square brackets nor sub-indices in order to have a better reading. In order to exploit the finite fields, it is worth mentioning that, given two integer numbers, a and b , with great common divisor $\text{GCD}(a, b)$, there exist two integers x and y such that

$$\text{GCD}(a, b) = ax + by. \quad (6.4)$$

The extended Euclidean algorithm, which starts with the vectors $(g_0, x_0, y_0) = (a, 1, 0)$ and $(g_1, x_1, y_1) = (b, 0, 1)$, for $|a| > |b|$, leads to $\text{GCD}(a, b)$ through the iterations

$$\begin{aligned} q_{i+1} &= \lfloor q_{i-1}/q_i \rfloor, \\ g_{i+1} &= g_{i-1} - q_i g_i, \\ x_{i+1} &= x_{i-1} - q_i x_i, \\ y_{i+1} &= y_{i-1} - q_i y_i, \end{aligned} \quad (6.5)$$

where $\lfloor \cdot \rfloor$ represents the floor function. At each step, $0 \leq |g_{i+1}| < |g_i|$, and eventually this algorithm leads to $g_{k+1} = 0$ for some step k . In this case, $g_k = \text{GCD}(a, b)$, $x_k = x$ and $y_k = y$. In the particular case where a and b are relatively prime numbers, $\text{GCD}(a, b) = 1$, in such a way that

$$1 = ax + by. \quad (6.6)$$

Then, $1 \equiv by \pmod{a}$, or equivalently,

$$\frac{1}{b} \equiv y \pmod{a}. \quad (6.7)$$

Let now m and u be two integers such that $u \equiv a/b \pmod{m}$, and we would like to reconstruct the rational number a/b . If we follow the Euclidean algorithm, Eq. (6.5), a set of equations of the form

$$g_i = x_i m + y_i u, \quad (6.8)$$

is obtained. If $\text{GCD}(m, y_i) = 1$, then $g_i/t_i \equiv u \pmod{m}$ step by step. As it was mentioned, for every i , $0 \leq |g_{i+1}| < |g_i|$. If $m > 2 \max\{a^2, b^2\}$, let j be the first step where $|g_j| \leq \lfloor m/2 \rfloor$ (which exists, as $|g_{i+1}| < |g_i|$ and for some k , $g_{k+1} = 0$). Then,

$$\frac{a}{b} = \frac{g_j}{t_j}. \quad (6.9)$$

Different approaches on the selection on m have been given. In Ref. [85], m is taken as different powers of a prime number p . In Ref. [83], the selection of m is given as a product of different prime numbers $m = p_1 \dots p_N$, so that the reconstruction algorithm is developed for each prime p_i , obtaining N sets of solutions, reaching the final solution through the Chinese remainder algorithm.

For the case of rational functions, in Ref. [85] the algorithm is developed in terms of the polynomial version of Eq. (6.4). In Ref. [83], the key idea is that the evaluation of any polynomial P in a given number α is equivalent to

$$P(x) \equiv P(\alpha) \pmod{(x - \alpha)}. \quad (6.10)$$

In this manner, if the evaluation is given in M different points $\{\alpha_1, \dots, \alpha_M\}$, then

$$m = (x - \alpha_1) \dots (x - \alpha_M). \quad (6.11)$$

Thus, the rational reconstruction algorithm is analogue to the reconstruction algorithm for rational numbers.

For the case of multivariate rational functions, in Ref. [84] the reconstruction of a rational function f of n different variables $\mathbf{z} = (z_1, \dots, z_n)$ introduces the function $h(t, \mathbf{z}) = f(tz_1, \dots, tz_n)$, and using the canonical representation of f , it is obtained

$$h(t, \mathbf{z}) = \frac{\sum_{r=0}^R p_r(\mathbf{z})t^r}{1 + \sum_{r'=1}^{R'} q_{r'}(\mathbf{z})t^{r'}}, \quad (6.12)$$

where p_r and $q_{r'}$ are homogeneous functions. A subtlety arises in Eq. (6.12) when the denominator has 0 as its constant term, yet this can be handled by shifting the function f from \mathbf{z} to $\mathbf{z} + \mathbf{s}$. Finally, the polynomials p_r and $q_{r'}$ are reconstructed variable by variable, and the limit $t \rightarrow 0$ is how the function f is reconstructed.

6.2 Causal representation of multi-loop integrals by analytic reconstruction

Starting from the LTD representations of the MLT, NMLT and N²MLT multi-loop topologies Eqs. (4.54), (4.62) and (4.66), that contain both causal and non-causal singularities, and motivated by their factorisation properties in terms of MLT subtopologies (for which we can obtain a causal representation, namely, free of non-causal singularities) we reconstruct in this section their full analytic expression in term of causal thresholds only. This is done applying numerical evaluation over finite fields [83, 84], in which we use the C++ implementation of the FINITEFLOW [86] algorithm together with its MATHEMATICA interface. In particular, we profit from the way how this algorithm solves linear systems.

After the reconstruction of analytical expressions with this numerical approach, we end up with rational functions, with on-shell loop momenta $q_{i,0}^{(+)}$ and the energy components of the external momenta, $p_{i,0}$ as variables. It turns out that this rational function is written only in terms of causal propagators [4], which always have the structure of sums of on-shell loop energies. The numerical evaluation of these functions is free of possible zeroes due to the absence of differences of $q_{i,0}^{(+)}$. A few comments on this pattern are given, and we interpret the result in terms of entangled causal thresholds.

Furthermore, a closed equation describing a pattern for the causal structure of an arbitrary topology with any number of loops is an important goal for this chapter. This gives a parametric expression at all orders and, hence, the iterated application of Cauchy's residue theorem is avoided.

6.2.1 The two-loop sunrise diagram

In order to fix the ideas, here we start with the scalar sunrise diagram. As it has been mentioned in Sec. 4.1.2, the iterated application of Cauchy's residue theorem to the energy components of the loop momenta in this diagram gives rise to the integrand

$$\begin{aligned}
G_F(1, 2, 3) \rightarrow & \frac{1}{4q_{1,0}^{(+)} q_{2,0}^{(+)}} \frac{1}{\left(q_{1,0}^{(+)} + q_{2,0}^{(+)} + p_0\right)^2 - q_{3,0}^{(+)^2}} \\
& + \frac{1}{4q_{1,0}^{(+)} q_{3,0}^{(+)}} \frac{1}{\left(q_{1,0}^{(+)} - q_{3,0}^{(+)} + p_0\right)^2 - q_{2,0}^{(+)^2}} \\
& \frac{1}{4q_{2,0}^{(+)} q_{3,0}^{(+)}} \frac{1}{\left(q_{2,0}^{(+)} + q_{3,0}^{(+)} - p_0\right)^2 - q_{1,0}^{(+)^2}},
\end{aligned} \tag{6.13}$$

which, after the application of partial fractions to each term, leads its causal structure given by

$$G_F(1, 2, 3) \rightarrow \frac{1}{8q_{1,0}^{(+)} q_{2,0}^{(+)} q_{3,0}^{(+)}} \left(\frac{1}{q_{1,0}^{(+)} + q_{2,0}^{(+)} + q_{3,0}^{(+)} + p_0} + \frac{1}{q_{1,0}^{(+)} + q_{2,0}^{(+)} + q_{3,0}^{(+)} - p_0} \right). \tag{6.14}$$

As mentioned before, Eq. (6.14) is free of non-causal thresholds, and the only explicit divergences are for $p_0 > 0$ in the second term, $p_0 < 0$ in the first term, and for $p_0 = 0$, both terms diverge simultaneously while integrating for $q_{i,0}^{(+)} \rightarrow 0$, for all $i \in \{1, 2, 3\}$.

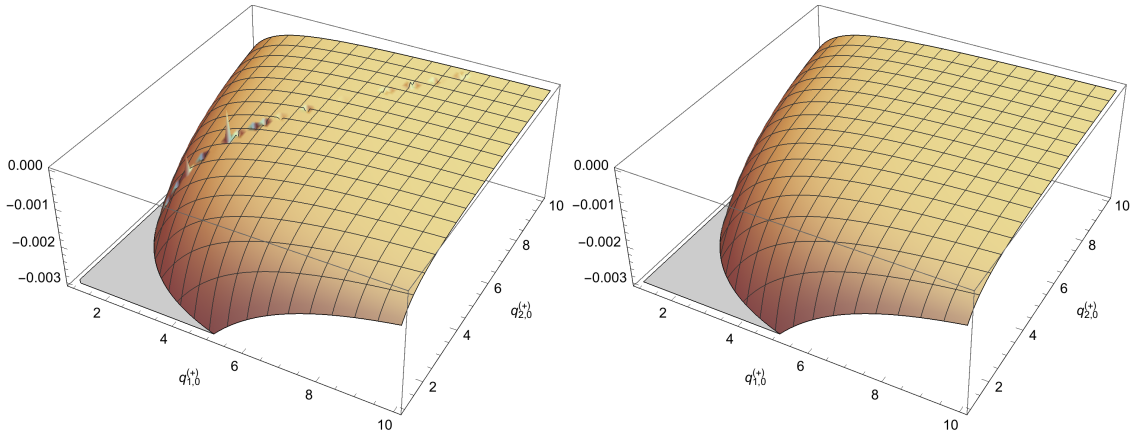


Figure 6.1: Three dimensional plots for the integrand of the two-loop sunrise diagram in terms of non-causal (left, Eq. (6.13)) and causal (right, Eq. (6.14)) propagators. The numerical fluctuations due to numerical cancellations of non-causal thresholds are visible on the left plot. The right plot is stable because the integrand expression is manifestly free of non-causal thresholds. The condition $p = 0$ is assumed.

A comment on the difference between both integrands, the one in Eq. (6.13) and the one in Eq. (6.14) is mandatory. The former includes some non-causal thresholds while the later does not, and they are physically equivalent. The relation obtained directly through the

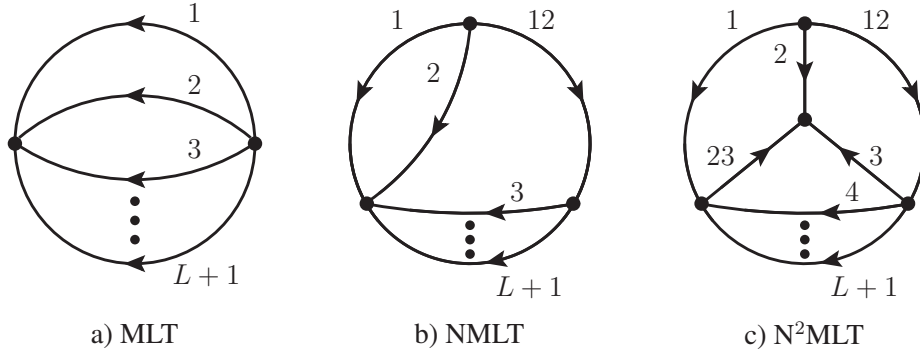


Figure 6.2: Maximal Loop Topology (MLT), Next-to-Maximal Loop Topology (NMLT) and Next-to-Next-to-Maximal Loop Topology (N^2 MLT) at L loops.

LTD formalism is not optimal for numerical implementations as the spurious singularities are present. This is depicted in Fig. 6.1, where the explicit fluctuations are associated to the non-physical singularities coming from the thresholds arising at $q_{1,0}^{(+)} \pm q_{2,0}^{(+)} \mp q_{3,0}^{(+)} = 0$, where $p_0 = 0$ is assumed.

6.2.2 Maximal Loop Topology

In Sec. 4.1, $MLT(L)$ diagram is defined as a Feynman diagram with L loops with $L + 1$ internal particles. This diagram is depicted in Fig 6.2a. This definition implies the integrand given in Eq. (4.53), namely

$$G_F(1, \dots, L, L+1) = G_F(1, \dots, L, 1 \dots L). \quad (6.15)$$

Naturally, as it was for the 1- and 2-loop case, partial fractions applied to the relation obtained from LTD to the $MLT(L)$ diagram leads to its causal representation, given by

$$G_F(1, \dots, L, L+1) \rightarrow -\frac{1}{x_{L+1}} \left(\frac{1}{\lambda_1^-} + \frac{1}{\lambda_1^+} \right), \quad (6.16)$$

where

$$x_{L+k} = \prod_{i=1}^{L+k} (2q_{i,0}^{(+)}) \quad , \quad \lambda_1^\pm = \sum_{i=1}^{L+1} q_{i,0}^{(+)} \pm p_0. \quad (6.17)$$

The simplicity of the causal representation of the $MLT(L)$ diagram makes it a well suited test for the reconstruction algorithm as will be presented below. By setting $L = 2$, we recover Eq. (6.14).

Although the causal structure of the $MLT(L)$ diagram presents two terms, each of which with one possible threshold, only one of them is active when integrating. Once the sign of the energy p_0 of the external particle is fixed, only one of the terms exhibits the singularity while the other term remains finite. The graphic interpretation of the causal structure is presented in Fig. 6.3.

6.2.3 NMLT vacuum integral

The MLT family of topological diagrams is the simplest one, which corresponds to Feynman diagrams with L loops and the corresponding $L + 1$ internal particles for a 2-point function. The simplest element of this family is the 2-point 1-loop function, sometimes

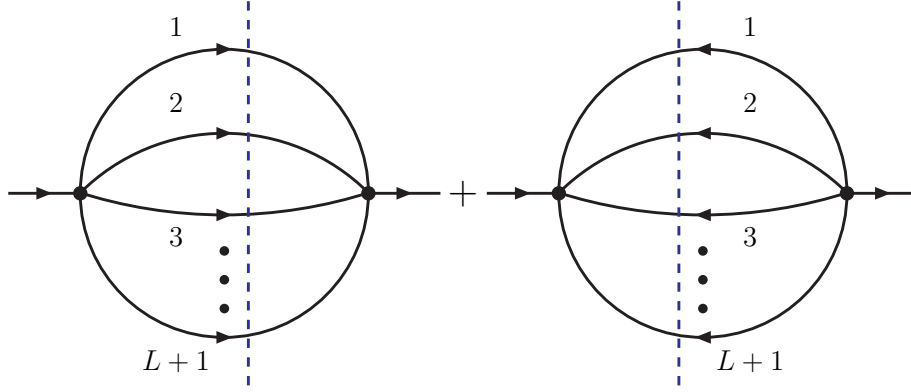


Figure 6.3: Causal thresholds of the MLT topology. The arrow on the external momentum represents the positive energy flow.

called *bubble function*. Also, the MLT(2) diagram is the well-known sunrise diagram. From a 3-loop level diagram, MLT family is not enough to understand all possible diagrams, so the NMLT and the N²MLT families are needed to characterize all 3-loop configurations of the internal particles. The relation obtained directly from the application of LTD formalism to each of these topological families leads to the factorization formulae given in Eqs. (4.62) and (4.66), containing both causal and non-causal thresholds. In order to simplify the computations, we start with the vacuum polarization diagram associated with the NMLT(3) diagram. This diagram is depicted in Fig. 6.2b.

The obtained causal representation is given by

$$\mathcal{A}_{\text{NMLT}}^{(L)}(1, 2, \dots, L+2) = \int_{\vec{e}_1, \dots, \vec{e}_L} \frac{2}{x_{L+2}} \frac{\sum_{i=1}^{L+2} q_{i,0}^{(+)}}{\lambda_1 \lambda_2 \lambda_3}. \quad (6.18)$$

where

$$\lambda_1 = \sum_{i=1}^{L+1} q_{i,0}^{(+)}, \quad \lambda_2 = q_{1,0}^{(+)} + q_{2,0}^{(+)} + q_{L+2,0}^{(+)}, \quad \lambda_3 = \sum_{i=3}^{L+2} q_{i,0}^{(+)}. \quad (6.19)$$

This causal structure can be written as a sum of fractions with numerator equal to 1 through partial fractions, obtaining

$$G_F(1, \dots, L, L+1, L+2) \rightarrow \frac{2}{x_{L+2}} \left(\frac{1}{\lambda_1 \lambda_2} + \frac{1}{\lambda_2 \lambda_3} + \frac{1}{\lambda_3 \lambda_1} \right). \quad (6.20)$$

Eq. (6.20) can also be reconstructed from numerical evaluations over finite fields. From the definition of the causal denominators (Eqs. (6.19)), it is possible to obtain the relations in the opposite direction. For the case where $L = 3$, we find

$$\begin{aligned} q_{1,0}^{(+)} &= \frac{1}{2} \left(\lambda_1 + \lambda_2 - \lambda_3 - 2q_{2,0}^{(+)} \right), & q_{5,0}^{(+)} &= \frac{1}{2} \left(-\lambda_1 + \lambda_2 + \lambda_3 \right). \\ q_{3,0}^{(+)} &= \frac{1}{2} \left(\lambda_1 - \lambda_2 + \lambda_3 - 2q_{4,0}^{(+)} \right), & & \end{aligned} \quad (6.21)$$

Substituting these relations in (6.18), we directly get (6.20). As the numerator of (6.18) is a linear function in $q_{i,0}^{(+)}$, both approaches are of the same difficulty. For more complex configurations, we will rely on analytic reconstruction.

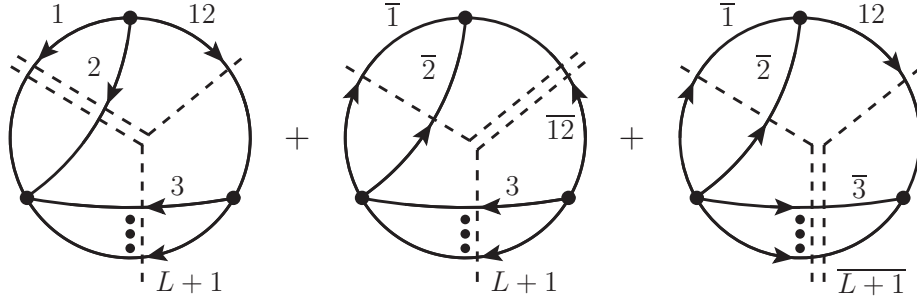


Figure 6.4: Entangled causal thresholds of the NMLT topology. External momenta not shown.

An interpretation of (6.20) in terms of what we call *entangled causal thresholds* can be given. Each of the λ_i represents a causal threshold singularity that requires that all the momentum flows are aligned in the same direction with respect to the isolated vertex. The product of two causal denominators can be understood as representing physical configurations where two propagators can simultaneously go on shell. For this to happen, the common propagators have to be in the same momentum flow orientation. This entanglement can also be understood from the factorisation identity that NMLT fulfils in terms of MLT subtopologies.

This entangled causal structure is pictorially presented in Fig. 6.4, where the dashed lines represent the internal lines that eventually go on-shell in a simultaneous manner; a subset of them is already on shell through LTD. Each diagram in Fig. 6.4 has two dashed lines that correspond to the two causal denominators λ_i and λ_j and are present in each term of Eq. (6.18). The causal thresholds are entangled due to the fact that momentum flow of the propagators that are common to both causal denominators are consistent. For instance, the first diagram of Fig. 6.4 represents the term $1/(\lambda_1\lambda_2)$, which corresponds to the causal thresholds $\{1, 2, \dots, L\}$ and $\{1, 2, L+1\}$ that share the entangled propagators $\{1, 2\}$.

6.2.4 N²MLT vacuum integral

The N²MLT is another topological family needed to describe all possible 3-loop 2-point functions. Actually, both MLT and NMLT families can be obtained from the N²MLT family if the topology is simplified, equivalently, if an internal particle is removed. The configuration of the internal momenta of this topological family is depicted in Fig. 6.2c. As mentioned in Sec. 4.1, an N²MLT(L) diagram is defined by its integrand, namely,

$$G_F(1, \dots, L, L+1, L+2, L+3) = G_F(1, \dots, L, 1 \dots L, 12, 23). \quad (6.22)$$

For the moment, we consider the vacuum polarization N²MLT(L) diagram. Together with the N²MLT topological family with the MLT and the NMLT families, every 3-loop level diagram can be understood, and hence any scattering amplitude.

From the LTD representation of N²MLT(L) integrand given in Eq. (4.66), we can obtain an integrand written as a rational function,

$$\mathcal{A}_{\text{N}^2\text{MLT}}^{(L)}(1, 2, \dots, L+3) = \int_{\vec{\ell}_1, \dots, \vec{\ell}_L} \frac{1}{x_{L+3}} \frac{N(\{q_{i,0}^{(+)}\})}{\prod_{i=1}^L \lambda_i}, \quad (6.23)$$

with λ_1 through λ_3 defined in Eq. (6.19),

$$\begin{aligned} \lambda_4 &= q_{2,0}^{(+)} + q_{3,0}^{(+)} + q_{L+3,0}^{(+)}, & \lambda_6 &= q_{1,0}^{(+)} + q_{3,0}^{(+)} + q_{L+2,0}^{(+)} + q_{L+3,0}^{(+)}, \\ \lambda_5 &= q_{1,0}^{(+)} + q_{L+3,0}^{(+)} + \sum_{i=4}^{L+1} q_{i,0}^{(+)}, & \lambda_7 &= q_{2,0}^{(+)} + \sum_{i=4}^{L+3} q_{i,0}^{(+)}, \end{aligned} \quad (6.24)$$

and $N(\{q_{i,0}^{(+)}\})$ a polynomial in $q_{i,0}^{(+)}$ of fourth degree. It is not straightforward to obtain a causal structure similar to those given in Eqs. (6.16) and (6.20) directly from Eq. (6.23). This is why we reconstruct the analytic expression through finite fields. In fact, it is seen that the causal denominators λ_i are not independent but a few relations among them hold. If we write $q_{i,0}^{(+)}$ and λ_1 in terms of the rest of the λ_i we obtain,

$$\begin{aligned} q_{1,0}^{(+)} &= \frac{1}{2}(\lambda_2 + \lambda_5 - \lambda_7), & q_{6,0}^{(+)} &= \frac{1}{2}(-\lambda_4 - \lambda_5 + \lambda_6 + \lambda_7), \\ q_{2,0}^{(+)} &= \frac{1}{2}(\lambda_2 + \lambda_4 - \lambda_6), & q_{7,0}^{(+)} &= \frac{1}{2}(-\lambda_2 - \lambda_3 + \lambda_6 + \lambda_7), \\ q_{3,0}^{(+)} &= \frac{1}{2}(\lambda_3 + \lambda_4 - \lambda_7), & \lambda_1 &= \lambda_2 + \lambda_3 + \lambda_4 + \lambda_5 - \lambda_6 - \lambda_7. \\ q_{4,0}^{(+)} &= \frac{1}{2}(\lambda_3 + \lambda_5 - \lambda_6 - 2q_{5,0}^{(+)}), \end{aligned} \quad (6.25)$$

Then, replacing $q_{i,0}^{(+)}$ and λ_i properly, according to their relations and performing a polynomial division, we get,

$$\begin{aligned} \mathcal{A}_{\text{N}^2\text{MLT}}^{(L)}(1, 2, \dots, L+3) &= - \int_{\vec{\ell}_1, \dots, \vec{\ell}_L} \frac{2}{x_{L+3}} \left[\frac{1}{\lambda_1} \left(\frac{1}{\lambda_2} + \frac{1}{\lambda_3} \right) \left(\frac{1}{\lambda_4} + \frac{1}{\lambda_5} \right) \right. \\ &\quad \left. + \frac{1}{\lambda_6} \left(\frac{1}{\lambda_2} + \frac{1}{\lambda_4} \right) \left(\frac{1}{\lambda_3} + \frac{1}{\lambda_5} \right) + \frac{1}{\lambda_7} \left(\frac{1}{\lambda_2} + \frac{1}{\lambda_5} \right) \left(\frac{1}{\lambda_3} + \frac{1}{\lambda_4} \right) \right]. \end{aligned} \quad (6.26)$$

Now we obtained for the N^2MLT family an expression for its causal structure analogous to the one obtained for the MLT and for the NMLT families. This causal structure is still valid to an arbitrary L -loop diagram within the N^2MLT topological family. An interpretation of Eq. (6.26) can be given following two approaches. One of them is together with the factorization formulae, so that each term represents a factorization of three different MLT diagram. The other interpretation can be given in terms of three entangled causal thresholds. A pictorial representation of this entanglement is presented in Fig. 6.5 for the first term in the right hand side of Eq. (6.26).

6.2.5 NMLT and N^2MLT topologies with external momenta

In this section, a generalization of the causal structure of the NMLT and N^2MLT vacuum diagrams presented in Sections 6.2.3 and 6.2.4 to the most general case that considers insertion of external momenta. Then, to obtain analytic and compact expressions for these topologies, we follow the same algorithm based on finite fields. The vacuum expressions obtained in Eqs. (6.20) and (6.26) give us insight to perform this computation. The insertion of these external momenta does not introduce any substantial difference from the causal physical behaviour of these integrals. The difference is that, as for the case of the causal structure of the $\text{MLT}(L)$ diagram given in Section 6.2.2, vacuum polarization diagrams have degenerate causal thresholds, as it can be seen from Eq. (4.58), where $\lambda_1^+ = \lambda_1^-$ as $p = 0$, while diagrams with external particles splits the degeneracy in an explicit form, as in can be seen in the structure of Eq. (6.16).

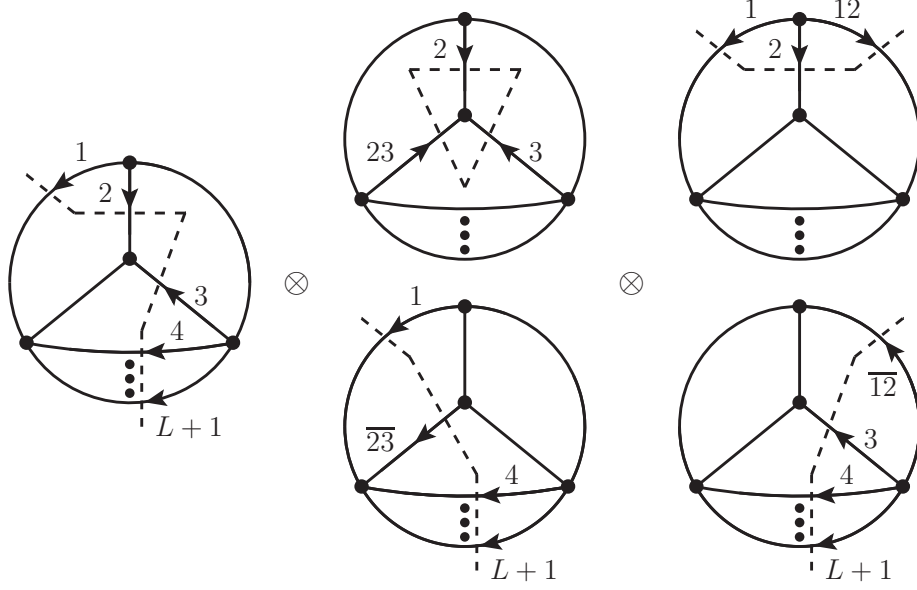


Figure 6.5: Entangled causal thresholds of the $N^2\text{MLT}$ topology. External momenta not shown.

Applying the same procedure for the insertion of the external momenta p_1 , p_2 and p_3 in the internal momenta $L+1$, $L+2$ and $L+3$ we obtain, respectively,

$$q_{L+1} = -\sum_{i=1}^{L+1} \ell_i - p_{13}, \quad q_{L+2} = -\ell_1 - \ell_2 + p_2, \quad q_{L+3} = -\ell_2 - \ell_3 - p_3. \quad (6.27)$$

The three external momenta p_i are considered to have positive energy when they are incoming. By momentum conservation, we have $p_{12} = p_1 + p_2$ for NMLT and $p_{123} = p_1 + p_2 + p_3$ for $N^2\text{MLT}$ as outgoing momentum in one of the vertices. It is important to notice that the causal propagators λ_i are shifted by the external momenta $\pm p_i$ or a linear combination of them, so that

$$\begin{aligned} \lambda_1^\pm &= \sum_{i=1}^{L+1} q_{i,0}^{(+)} \pm p_{13,0}, \\ \lambda_2^\pm &= q_{1,0}^{(+)} + q_{2,0}^{(+)} + q_{L+2,0}^{(+)} \pm p_{2,0}, & \lambda_3^\pm &= \sum_{i=3}^{L+2} q_{i,0}^{(+)} \mp p_{123,0}, \\ \lambda_4^\pm &= q_{2,0}^{(+)} + q_{3,0}^{(+)} + q_{L+3,0}^{(+)} \pm p_{3,0}, & \lambda_6^\pm &= q_{1,0}^{(+)} + q_{3,0}^{(+)} + q_{L+2,0}^{(+)} + q_{L+3,0}^{(+)} \pm p_{23,0}, \\ \lambda_5^\pm &= q_{1,0}^{(+)} + q_{L+3,0}^{(+)} + \sum_{i=4}^{L+1} q_{i,0}^{(+)} \pm p_{1,0}, & \lambda_7^\pm &= q_{2,0}^{(+)} + \sum_{i=4}^{L+3} q_{i,0}^{(+)} \pm p_{12,0}. \end{aligned} \quad (6.28)$$

With these causal denominators and the equations that we present next, we can describe, with a single representation, up to 3-point functions for NMLT and up to 4-point functions for $N^2\text{MLT}$.

The causal structure of the NMLT(L) diagram is a function of λ_1^\pm through λ_3^\pm , with

$p_3 = 0$, given by

$$\mathcal{A}_{\text{NMLT}}^{(L)}(1, 2, \dots, (L+1)_{-p_1}, (L+2)_{p_2}) = \int_{\vec{\ell}_1, \dots, \vec{\ell}_L} \frac{1}{x_{L+2}} \times \left[\frac{1}{\lambda_1^+ \lambda_2^-} + \frac{1}{\lambda_2^+ \lambda_3^-} + \frac{1}{\lambda_3^+ \lambda_1^-} + (\lambda_i^+ \leftrightarrow \lambda_i^-) \right]. \quad (6.29)$$

The insertion of the external momenta gives rise to the necessity of considering the entangled threshold configurations making a distinction between incoming and outgoing internal momenta, namely, if the momentum flow is positive or negative. With these conventions, positive energy flows correspond to incoming momenta. The exchange $\lambda_i^+ \leftrightarrow \lambda_i^-$ accounts for the configurations with opposite momentum flows and results in a splitting the terms obtained for the vacuum diagrams (recalling the overall factor 2 in each equation).

The causal N^2MLT representation also exhibits a very compact expression, namely,

$$\mathcal{A}_{\text{N}^2\text{MLT}}^{(L)}(1, 2, \dots, (L+1)_{-p_{13}}, (L+2)_{p_2}, (L+3)_{-p_3}) = - \int_{\vec{\ell}_1, \dots, \vec{\ell}_L} \frac{1}{x_{L+3}} \times \left[\frac{1}{\lambda_1^+} \left(\frac{1}{\lambda_2^-} + \frac{1}{\lambda_3^-} \right) \left(\frac{1}{\lambda_4^+} + \frac{1}{\lambda_5^+} \right) + \frac{1}{\lambda_6^+} \left(\frac{1}{\lambda_3^-} + \frac{1}{\lambda_5^-} \right) \left(\frac{1}{\lambda_2^+} + \frac{1}{\lambda_4^+} \right) + \frac{1}{\lambda_7^+} \left(\frac{1}{\lambda_3^-} + \frac{1}{\lambda_4^-} \right) \left(\frac{1}{\lambda_2^+} + \frac{1}{\lambda_5^+} \right) + (\lambda_i^+ \leftrightarrow \lambda_i^-) \right]. \quad (6.30)$$

Let us briefly summarise on the algorithm used to compute all these formulae. As mentioned before, we profit from the software `FINITEFLOW` and its built-in functions, `FFLinearFit` and `FFDenseSolve`, to analytically reconstruct the rational function of the causal structures and to find relations between $q_{i,0}^{(+)}$ and λ_i , respectively. We would like to remark that these expressions for $\text{MLT}(L)$, $\text{NMLT}(L)$ and $\text{N}^2\text{MLT}(L)$ have been analytically checked, with the application of the nested residues theorem, finding completely agreement. The pattern displayed by these topologies allows us to generalise and provide an all-order closed formula that has the mathematical support of the studies carried out in [1, 4]. This implies that only causal contributions remain in the final expressions, being all the non-causal or non-physical terms cancelled at intermediate steps. We also note that the causal structures of the topological families suggests a smooth numerical evaluation, which we profit in Sec. 6.4. Although we have presented explicit expressions only for scalar integrals, the algorithm is valid as well for non-scalar integrals.

6.3 Topologies with higher powers of the propagators

Up to this point, the discussion of the topological families has relied on the fact that they depend linearly on Feynman propagators. In practical applications, like UV local renormalisation [73, 75, 77] or multi-loop calculations, one also deals with higher-order poles when higher powers in the propagators appear [59, 87, 88]. In this section, we work on the compact formulae, Eqs. (6.20) and (6.26), and give a procedure for computing L -loop integrals with higher-order poles. Specifically, we expect the causal structure observed in these equations to hold in all cases, including higher powers of the propagators. Abusing of the notation, let us define,

$$\mathcal{A}_{\text{N}^{k-1}\text{MLT}}^{(L)}(1^{\alpha_1}, 2^{\alpha_2}, \dots, (L+k)^{\alpha_{L+k}}) = \int_{\ell_1, \dots, \ell_L} \mathcal{N} \times \prod_{i=1}^{L+k} (G_F(q_i))^{\alpha_i}, \quad (6.31)$$

with $k \in \{1, 2, 3\}$, for any L -loop integral within the MLT, NMLT and N^2 MLT topological families, where the superscript α_i are the power of the i -th propagator. In the following, for the sake of the simplicity, we restrict our study to the scalar case in which the numerator is $\mathcal{N} = 1$.

Recalling from Sec. 4.1.1, Eq. (4.11), that due to the quadratic structure of the Feynman propagator, it is straightforward to raise the power in the i -th propagator by simple performing $(\alpha_i - 1)$ derivatives with respect to $q_{i,0}^{(+)}$,

$$(G_F(q_i))^{\alpha_i} = \frac{1}{(\alpha_i - 1)!} \frac{\partial^{\alpha_i - 1}}{\partial \left((q_{i,0}^{(+)})^2 \right)^{\alpha_i - 1}} G_F(q_i). \quad (6.32)$$

Therefore, the results obtained in Sec. 6.2 can be used for is study. Furthermore, we stress that the expressions obtained in the present chapter are valid in any dimension, since the energy components of the loop momenta is the only one that has been integrated out. Hence, we can numerically evaluate these integrals in any integer dimensions. As mentioned before, the LTD formalism leads to the causal structures of N^{k-1} MLT diagrams considered in this work, and these representations do not change with the number of loops considered in each diagram and, also, the corresponding loop integrals with raised propagators will be causal. Now we will consider integrals that are ultraviolet and infrared finite, so that the numerical performance of the causal LTD representation can be tested.

Hence, if we were to evaluate finite integrals, considering the causal LTD representation with linear propagators and performing the derivatives in the on-shell energies $q_{i,0}^{(+)}$ is sufficient. For instance, the MLT configuration,

$$\mathcal{A}_{\text{MLT}}^{(L)}(1^2, 2^2, \dots, L^2, L+1) = \prod_{i=1}^L \frac{\partial}{\partial (q_{i,0}^{(+)})^2} \mathcal{A}_{\text{MLT}}^{(L)}(1, 2, \dots, L+1). \quad (6.33)$$

In order to elucidate the operation of raising powers, we consider the simplest case $\mathcal{A}_{\text{MLT}}^{(L)}(1^2, 2, \dots, L+1)$ with only one squared propagator. Since the causal denominators depend linearly on $q_{i,0}^{(+)}$, we can use the chain rule as follows,

$$\frac{\partial}{\partial (q_{i,0}^{(+)})^2} \bullet = \frac{1}{2q_{i,0}^{(+)}} \frac{\partial}{\partial (q_{i,0}^{(+)})} \bullet. \quad (6.34)$$

This leads to,

$$\begin{aligned} \mathcal{A}_{\text{MLT}}^{(L)}(1^2, 2, \dots, L+1) &= \frac{1}{2q_{1,0}^{(+)}} \frac{\partial}{\partial (q_{1,0}^{(+)})} \mathcal{A}_{\text{MLT}}^{(L)}(1, 2, \dots, L+1), \\ &= \int_{\vec{\ell}_1, \dots, \vec{\ell}_L} \frac{1}{x_{L+1} q_{1,0}^{(+)}} \left(\frac{1}{q_{1,0}^{(+)}} + \frac{1}{\lambda_1} \right) \frac{1}{\lambda_1}. \end{aligned} \quad (6.35)$$

In the following, we present the numerical evaluation of several MLT, NMLT and N^2 MLT internal configurations. We want to point out that the inclusion of internal masses does not stem any difficulty within LTD formalism. Thus, one needs to perform $(d - 1)$ integrations for each loop 3-momentum. The number of integrations turn out to be lower than in approaches based on Feynman parametrisation.

6.4 Numerical evaluation of N^{k-1} MLT

Given the results of Secs. 6.2 and 6.3, we now work on those expressions by numerically integrating in the $(d-1)$ -loop momenta, \mathbf{q}_i . This is done so that the stability of this set of formulae, written in terms of causal denominators, can be investigated. We evaluate multi-loop integrals in $d = 2, 3, 4$ space-time dimensions¹, and present results for topologies up to four loops.

The numerical results presented in this section are double checked with the softwares SECDEC 3.0 [89] and FIESTA 4.2 [90]. In the following, we present plots only with FIESTA 4.2 since the results do not present any difference with respect to SECDEC 3.0.

6.4.1 Two-dimensional integrals

The first non-trivial numerical application is for $d = 2$ space-time dimensions, where we perform L -loop integrations, this is, one numerical integration per loop. In order to perform these integrations, we embed the integration domain, \mathbb{R}^L , in the L -dimensional sphere. This integration variables have the property that only one variable goes to infinity,

$$r \in [0, \infty), \theta_1 \in [0, \pi], \dots, \theta_{L-2} \in [0, \pi], \theta_{L-1} \in [0, 2\pi], \quad (6.36)$$

which we can compactify, in order to have its domain mapped onto $[0, 1)$ through to the change of variable,

$$r \rightarrow \frac{x}{1-x}. \quad (6.37)$$

These operations are carried out in MATHEMATICA as well as the numerical integration, which was computed with the built-in function `NIntegrate`.

Then, we evaluate the multi-loop integrals in which the propagators of the lines $\{1, 2, \dots, L\}$, Eq. (6.15) have mass m_4^2 , while the other particles have mass m_5^2 . Likewise, we scan over $m_4^2 \in [1, 10]$ in order to test the smooth behaviour of these integrations. Here and in what follows, all kinematic invariants are implicitly given in GeV^2 . We integrate numerically up to four loops the MLT, NMLT and N^2 MLT topologies presented in Sec. 6.2. Nevertheless, the extension to higher loops does not give rise to any obstacle within our approach.

The numerical evaluation of the two-dimensional integrals is shown in Fig. 6.6, where the solid lines corresponds to the evaluation within LTD, and the dots represent the numerical evaluations performed by FIESTA 4.2 and SECDEC 3.0. The evaluation time per point was $\mathcal{O}(1'')$ in a desktop machine with an Intel i7 (3.4GHz) processor with 8 cores and 16 GB of RAM. Furthermore, we find that when more propagators or, equivalently, more external momenta are included, the number of integrals for the softwares based on sector decomposition increases with respect to the number of Feynman parameters, but within LTD, one always has to perform L integrations.

6.4.2 Three- and four-dimensional integrals

Naturally, the number of integrals to be computed depends on the momentum space dimension. Hence, we can use the same procedure of Sec. 6.4.1 to express all loop components in spherical coordinates. Thanks to the LTD theorem, we go from Minkowskian to Euclidean space, which corresponds to work in $\mathbb{R}^{(d-1)L}$. Then, the embedding in a $(d-1)L$ -dimensional sphere can be performed analogously as in the former section.

¹The case with $d = 1$ space-time dimensions [67] is trivial. One just replaces $q_{i,0}^{(+)} \rightarrow \sqrt{m_i^2}$.

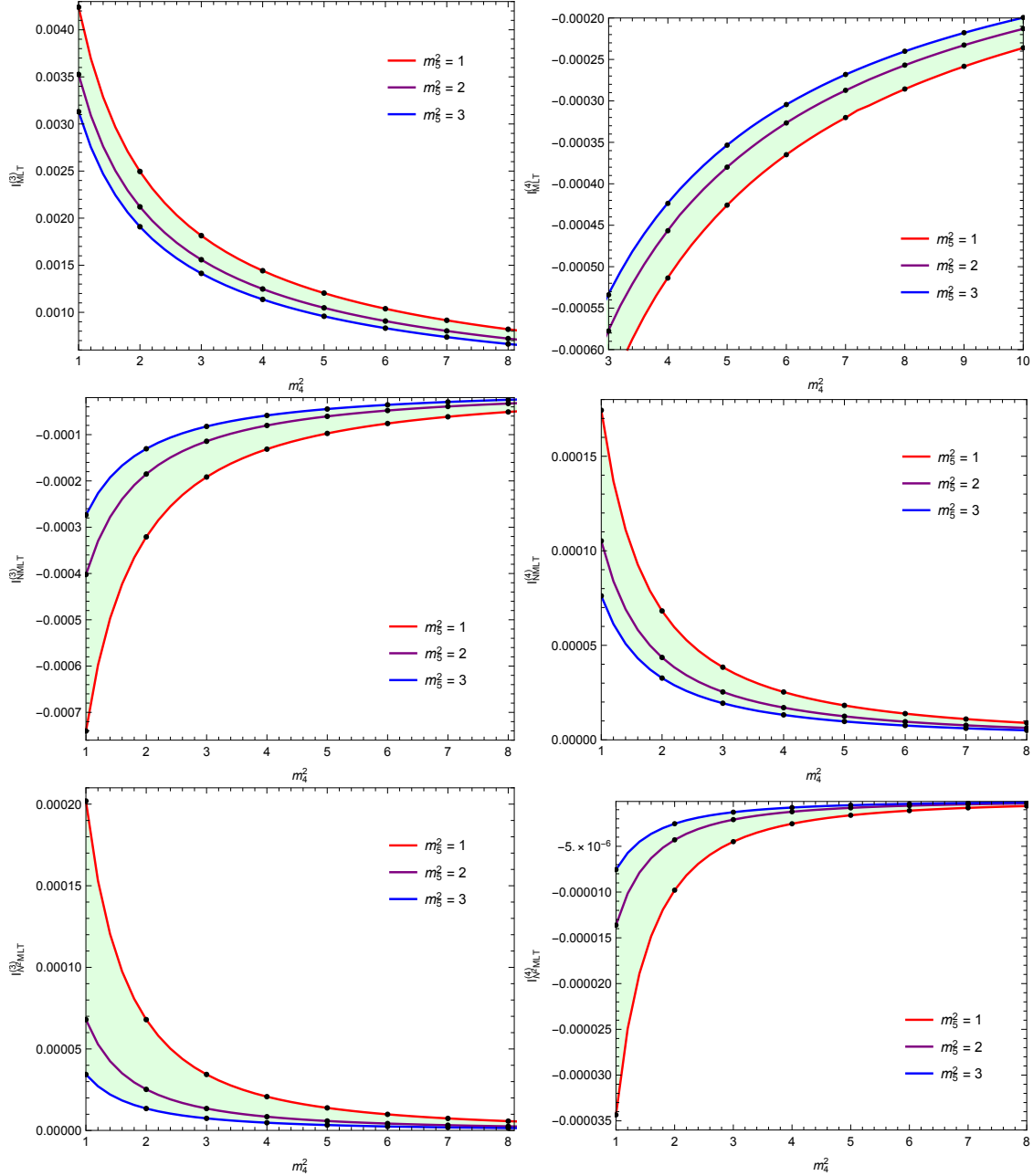


Figure 6.6: Two-dimensional MLT, NMLT and N^2 MLT at three and four loops, as a function of the internal masses m_4^2 and m_5^2 . Solid lines correspond to the analytic results of LTD and dots to the numerical results of FIESTA 4.2.

An equivalent approach where treating each loop momentum independently when doing the change of variables can be used. For instance, the integration domain can be separately expressed as follows,

$$\mathbb{R}^{(d-1)L} = \prod_{i=1}^L \mathbb{R}^{(d-1)}, \quad (6.38)$$

where each term in the product is the $(d-1)$ -dimensional space of each loop momentum. The main difference between this approach and the former one relies on how the behaviour of the integrand at infinity. On one hand, embedding the integrand in a $(d-1)L$ -dimensional sphere allows us to scan this behaviour with one single variable. On the other

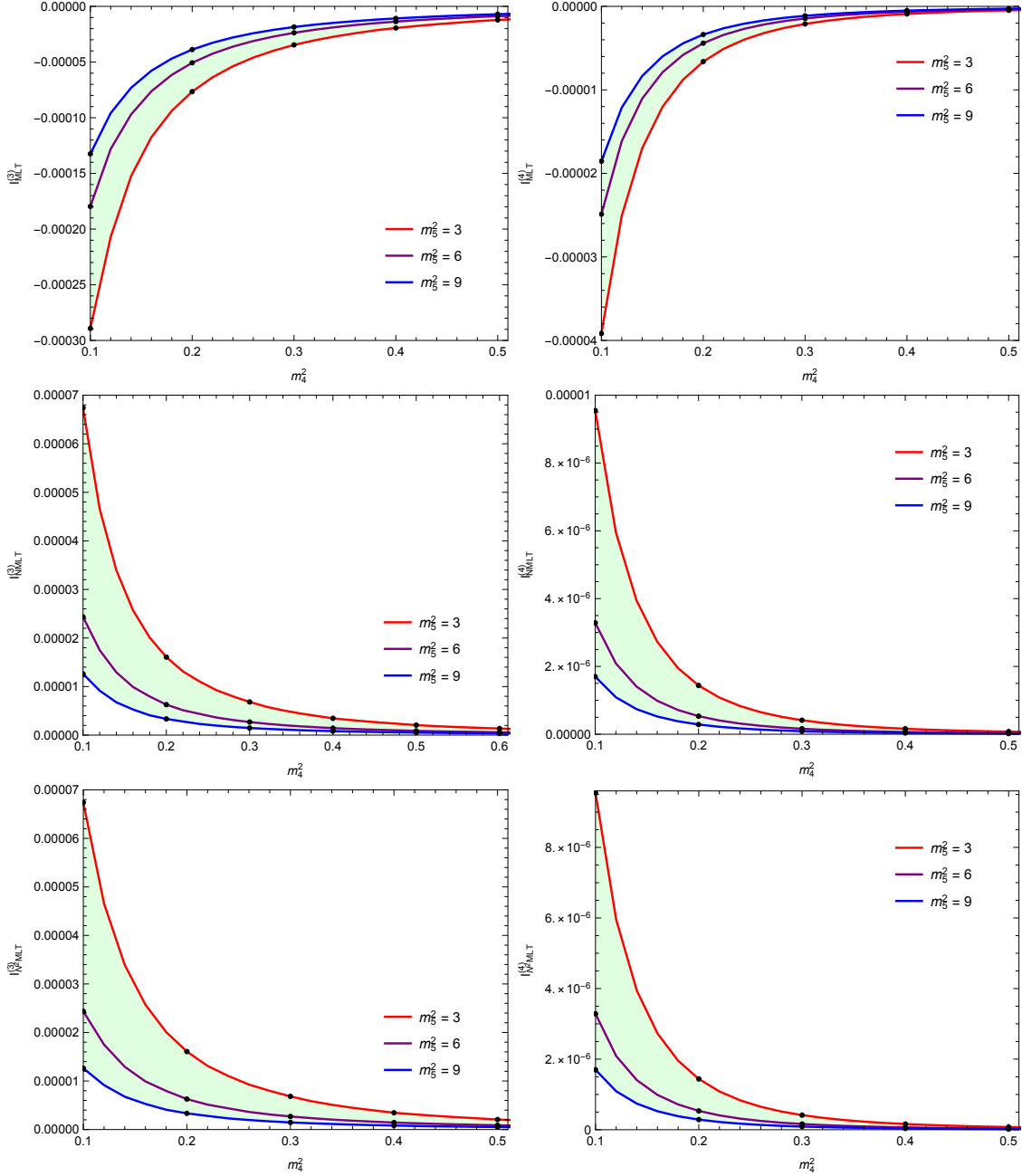


Figure 6.7: Three-dimensional MLT, NMLT and N^2 MLT at three and four loops, as a function of the internal masses m_4^2 and m_5^2 . Solid lines correspond to the analytic results of LTD and dots to the numerical results of FIESTA 4.2.

hand, in the product of $(d - 1)$ -dimensional spheres Eq.((6.38)), this behaviour is investigated with L variables. In the present discussion, both approaches are developed as a double check of our results.

The numerical integrations within LTD, in $d = 3$ and $d = 4$, for the MLT, NMLT and N^2 MLT configurations with higher powers in the propagators, obtained from the causal

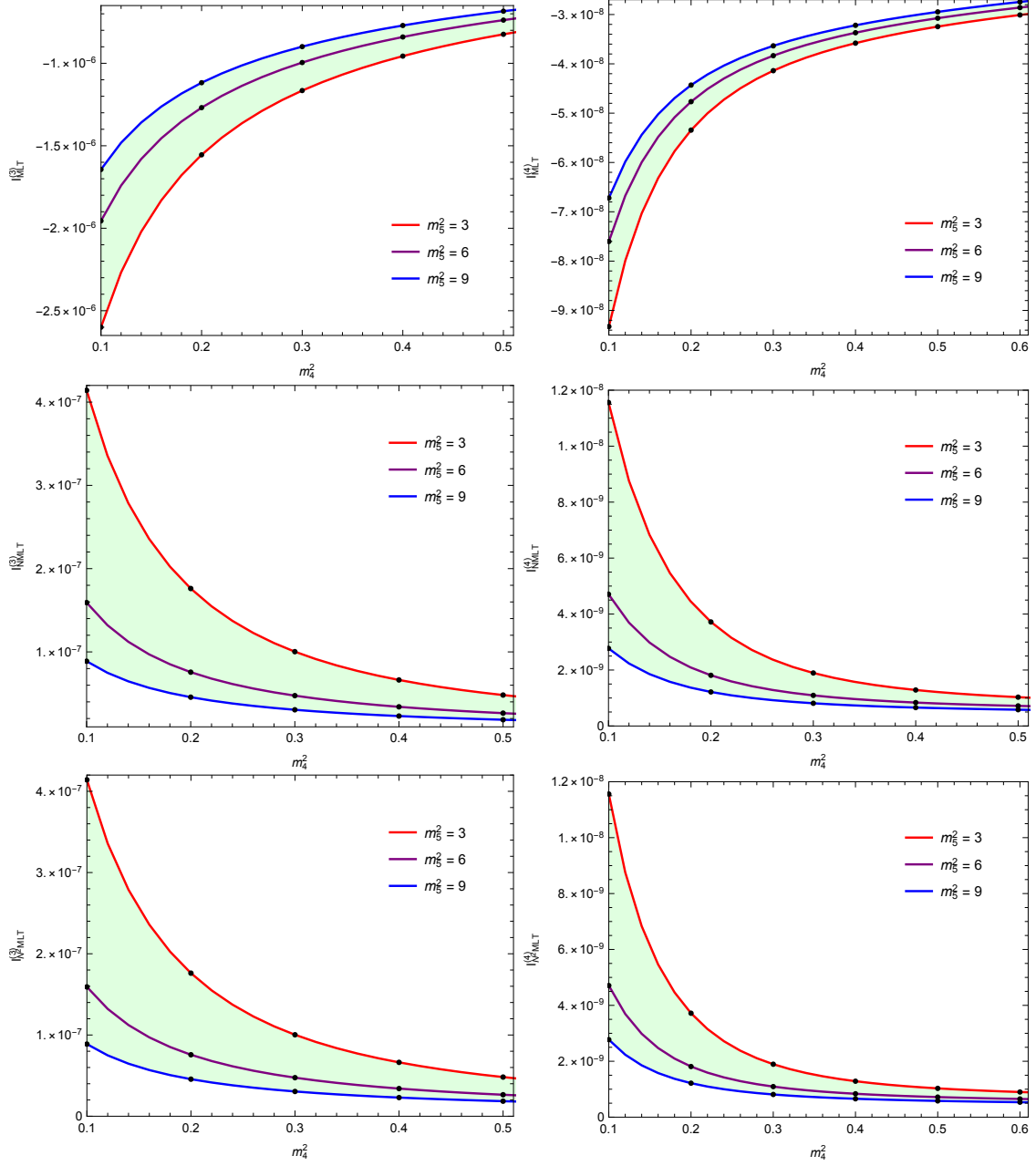


Figure 6.8: Four-dimensional MLT, NMLT and N^2 MLT at three and four loops, as a function of the internal masses m_4^2 and m_5^2 . Solid lines correspond to the analytic results of LTD and dots to the numerical results of FIESTA 4.2.

representations of Sec. 6.2,

$$\begin{aligned}
 \mathcal{A}_{N^{k-1}\text{MLT}}^{(L)}(1^2, 2^2, \dots, L^2, L+1, \dots, L+k) \\
 = \prod_{i=1}^L \frac{\partial}{\partial (q_{i,0}^{(+)})^2} \mathcal{A}_{N^{k-1}\text{MLT}}^{(L)}(1, 2, \dots, L+1, \dots, L+k), \quad (6.39)
 \end{aligned}$$

are shown in Fig. 6.7 and 6.8, respectively. In the same way as done in Sec. 6.4.1, we make a scan in m_4^2 , by fixing m_5^2 .

6.5 Geometrical interpretation of the causal thresholds

In terms of graph theory, a Feynman diagram can be understood as a multigraph, where an external particle can be regarded as an edge with one end having degree 1, while internal particles cannot satisfy this condition. Also, the auxiliary propagator, Eq. (5.29), allows us to interpret each MLT insertion as a single propagator. In this manner, a Feynman diagram of an arbitrary topological family can be studied by means of its minimal diagram regarding the number of loops. It is interesting that this minimal diagram coincides with the underlying simple graph of the Feynman diagram, as sketched in Fig. 5.4. Furthermore, the computation of the nested residues has the physical implication of orienting a subset of edges, as it can be seen in Fig. 4.6 for the $\text{MLT}(L)$ diagram.

Naturally, for an L -loop diagram, the computation of the nested residues will set on-shell L internal particles, as the energy component of the loop momentum is being integrated out, and thus evaluated on the corresponding negative-imaginary-part poles. Hence, nested residues carries an undirected graph into a partially directed graph. Moreover, the cancellation of non-causal thresholds leads to disjoint directed tree-level graphs, and the causal representation of a Feynman diagram can be interpreted as a sum of products of some elements of the cut space of the underlying simple graph. Furthermore, for the N^kMLT topological family, its causal representation includes a sum of terms, each of which having a product of $k + 1$ causal thresholds. It is important to recall that these k causal thresholds are entangled causal thresholds, which implies that not any k causal thresholds can appear in the same term of the causal representation. The conditions for causal thresholds to be entangled (and hence, to contribute together to the causal representation) is presented in Ref. [91]. In this section we just state these conditions.

For a Feynman diagram with L loops and n internal particles within the N^kMLT topological family, the causal thresholds become entangled if they satisfy:

- All internal particles become on-shell. In other words, all internal lines are cut by the union of the k causal thresholds.
- Causal thresholds do not intersect. This can be seen, for instance, in Figs. 6.4 and 6.5, where the causal cuts are represented by the dashed lines.
- Momentum flow of the internal lines associated to different causal thresholds are compatible. This is associated with the orientation of the directed graph obtained through the LTD formalism. In fact, this implies that this directed graph is acyclic.

With these three conditions, it is possible to reconstruct the causal representation of the N^kMLT topological family. Also, this implies a connection between complex analysis and graph theory.

Chapter 7

Summary and outlook

The study of theoretical physics in the high-energy regime has been developing in an astonishing manner over the last half century. This development has pushed the progress on high-precision computations to impressive results. Within these calculations, those studied by means of perturbative theory have increased considerably in complexity with each extra order of approximation.

Loop-Tree Duality (LTD) has proved its efficiency as a framework for high-precision computations through the last years, a new classification of Feynman diagrams which is independent on the number of loops but on the topology of the diagram, has been introduced. Using this classification, LTD has shown an amazing power to tackle scattering amplitudes for an arbitrary number of loops, leading to factorization formulae relating an arbitrary topological class to classes with lower topological complexity and, in turn, these factorization formulae lead to the causal structure of the scattering amplitude, showing an explicit agreement between analytical and numerical results. The application of the LTD formalism leads to a natural connection between integration over a d -dimensional Minkowski space and integration over a $(d - 1)$ -dimensional Euclidean space. A great amount of the work presented in this thesis has been developed in order to give solid mathematical foundations to the LTD formalism.

The first part of this work consisted in the establishment of the general ideas on the computational tools of LTD formalism to all perturbative orders in agreement with Cauchy's residue theorem. With these general ideas, the computational tools for the LTD formalism are presented, and some intuitive ideas are established. As a motivation, the 1-loop scalar diagram is presented and the LTD is developed for this case. It is highlighted that the complexity of the integrand obtained from the application of Cauchy's residue theorem abruptly increases with the number of external particles. Even more, for the simple case of 2 external particles, the simplification of the integrand to the causal representation is obtained, showing how the non-physical divergences cancel between each other. As a second example, the scalar 2-loop diagram is presented and some interesting features that were not presented in the 1-loop case appear. This includes the presence of displaced poles, and the cancellation of their contributions is sketched. It became impressive to notice that the scalar sunrise diagram and the scalar 1-loop 2-point diagram have the same functional structure of their causal representation.

After the study of the 1- and 2-loop scalar diagrams were completed, the next step was to present the full topological classification of Feynman diagrams. As the computations in this thesis were thought for an arbitrary number L of loops, a new notation is given in order to have not an overwhelming reading. With this notation, an algorithm to

identify the contributions to the iterated application of Cauchy's residue theorem is given, identifying positive- and negative-imaginary-part poles, as well as the displaced poles. An explicit explanation of the way the indices are evolving with each iteration of Cauchy's residue theorem is given, and the application of LTD formalism, together with this notation, is given to the general $\text{MLT}(L)$ diagram. The diagrammatic representation of the result of this computation in terms of the spanning trees of the underlying multi-graph of the MLT diagram is presented, and its causal representation is obtained after an algebraic simplification. We then interpret this causal representation of the scalar MLT topological family as a single propagator. Afterwards, the definition of the NMLT topological family is given, and the LTD formalism is applied in order to obtain the factorization formula of these diagrams. Then, the interpretation of this formula in terms of the spanning trees of the underlying graph is presented. This interpretation gave us some insight on what to expect for their causal representation. The same procedure is given for the $\text{N}^2\text{MLT}(L)$ diagram.

Once the computational tools of the LTD formalism were presented, together with a few of its applications (the MLT , NMLT and N^2MLT topological families), we have deepened on their mathematical foundations. The iterated residue is defined as the algorithm used in the LTD formalism, and after the proof of the cancellation of displaced poles for single poles is given, and the general case with higher-order poles is delayed to the Appendices, an analogue algorithm blind to the displaced poles called nested residues is defined. A geometrical interpretation of this cancellation is given and a direct proof of the cancellation of non-physical divergences in the $\text{MLT}(L)$ diagram is presented. Furthermore, we give a formal proof of the uniqueness of the causal structure of the MLT topological family independently on the order which the integrations are performed. Then we define the auxiliary propagator, which is the keystone of the topological classification of the Feynman diagrams, as it enable us to reduce the number of loops in each topological family. We finished the work with the study of higher order poles. We performed this study in detail in order to give a proof of the sufficiency of the simple poles case and how it is possible to obtain the causal structure of a diagram with higher-order poles once the one for a diagram with only simple poles is obtained.

Finally, we went on with the analytical reconstruction of the causal representations for the NMLT and N^2MLT topological families, identifying the entangled causal thresholds and associated the entanglement with a compatibility on the momentum flow of each causal threshold. We verified our results with numerical implementations, showing the smoothness of the causal structure compared with the function obtained directly from the iterated application of Cauchy's residue theorem. The non-physical divergences were naturally identified as the numerical fluctuations of these computations. Numerical integration of the $\text{NMLT}(3)$ and $\text{N}^2\text{MLT}(3)$ in 2, 3 and 4 dimensions is presented, showing a complete agreement with the analytic results, scanning the mass of a propagator. Also, a geometrical interpretation of the entangled causal thresholds is given.

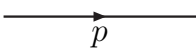
The LTD formalism has shown to be a quite powerful tool to reach high order computations in the perturbative expansion. Even when this thesis expects to provide solid foundations to analytic computations of scattering amplitudes to all orders within the perturbative theory, a huge amount of work still remains.


Appendix A

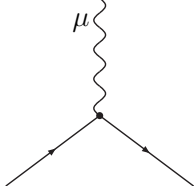
Feynman rules

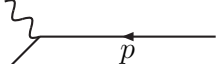
Here we present a list of Feynman rules that are extracted from the Lagrangian of the corresponding theory (the listed theories are QED, ϕ^4 and QCD). In this list, propagators are given in Feynman gauge.

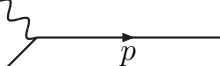
QED: $\mathcal{L} = \bar{\psi}(i\not{\partial} - m)\psi - \frac{1}{4}(F_{\mu\nu})^2 - e\bar{\psi}\gamma^\mu\psi A_\mu$

Fermion Propagator:  $= i(\not{p} + m)/(p^2 - m^2 + i0)$

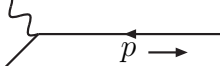
Boson propagator:  $= -ig_{\mu\nu}/(p^2 + i0)$

QED vertex:  $= iQe\gamma^\mu$ ($Q = -1$ for the electron)

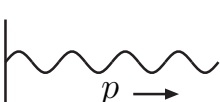
External fermion:  $= u_s(p)$ (incoming)

 $= \bar{u}_s(p)$ (outgoing)

External antifermion:  $= \bar{v}_s(p)$ (incoming)

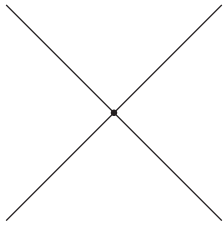
 $= v_s(p)$ (outgoing)

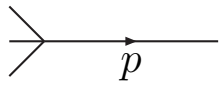
External boson:  $= \epsilon_\mu(p)$ (incoming)

 $= \epsilon_\mu^*(p)$ (outgoing)

ϕ^4 theory: $\mathcal{L} = \frac{1}{2}(\partial_\mu\phi)^2 - \frac{1}{2}m^2\phi^2 - \frac{\lambda^4}{4!}\phi^4$

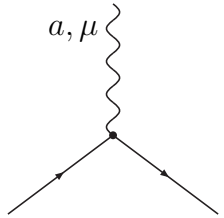
Scalar Propagator:  $= i/(p^2 - m^2 + i0)$

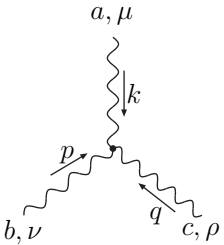
ϕ^4 vertex:  $= -i\lambda$

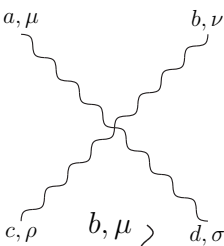
External scalar:  $= 1$


QCD:

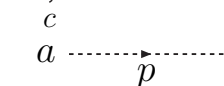
$$\mathcal{L} = \bar{\psi}(i\cancel{\partial} - m)\psi - \frac{1}{4}(\partial_\mu A_\nu^a - \partial_\nu A_\mu^a)^2 + gA_\mu^a \bar{\psi}\gamma^\mu\psi - g f^{abc}(\partial_\mu A_\nu^a)A^{\mu b}A^{\nu c} - g^2(f^{eab}A_\mu^a A_\nu^b)(f^{ecd}A^{\mu c}A^{\nu d})$$

Fermion vertex:  $= -ig\gamma^\mu t^a$

3-boson vertex:  $= g f^{abc}[g^{\mu\nu}(k-p)^\rho + g^{\nu\rho}(p-q)^\mu + g^{\rho\mu}(q-k)^\nu]$

4-boson vertex:  $= -ig^2[f^{abe}f^{cde}(g^{\mu\rho}g^{\nu\sigma} - g^{\mu\sigma}g^{\nu\rho}) + f^{ace}f^{bde}(g^{\mu\nu}g^{\rho\sigma} - g^{\mu\sigma}g^{\nu\rho}) + f^{ade}f^{bce}(g^{\mu\nu}g^{\rho\sigma} - g^{\nu\rho}g^{\mu\sigma})]$

Ghost vertex:  $= g f^{abc}p^\mu$

Ghost propagator:  $= i\delta^{ab}/(p^2 + i0)$

Appendix B

Code for the computation of the nested residues

In this Appendix, a code based on LTD formalism is given, to be used with MATHEMATICA. The purpose of this code is to compute the nested residues for the vacuum scalar N²MLT(L) diagram. The fundamental idea is that, iteration by iteration of the nested residues, the result depends only on the pole structure of the integrand, this is, on the location of the poles. Then, if the diagram has L loops and n internal particles, then each of the propagators can be written in the form

$$(G_F(q_i))^{-1} = (\vec{a} \cdot \vec{q}_0)^2 - \left(q_{i,0}^{(+)}\right)^2, \quad (\text{B.1})$$

where $\vec{q}_0 = (q_{1,0}, \dots, q_{L,0})$ and \vec{a} is a vector with 0 and 1 as entries. In the intermediate steps, some energies have been set on shell. In this manner, dual propagators can be written in the form

$$(G_D(q_i))^{-1} = \left(\vec{a}' \cdot \vec{q}_0 + \vec{b} \cdot \vec{q}_0^{(+)}\right)^2 - \left(q_{i,0}^{(+)}\right)^2, \quad (\text{B.2})$$

where $\vec{b} \in \{-1, 0, 1\}^n$.

So, the information needed to compute the nested residues is: 1) the vectors \vec{a} and \vec{b} in each step for each propagator, 2) the on-shell energies that are evaluated through the nested residues. In this manner, each propagator is represented by a list of two lists, the first representing the off-shell energy of the corresponding propagator and the second representing its on-shell energy. Regarding the first list, it contains two other lists, where the first one represents the vector \vec{a} , and the second list includes the indices of the on-shell energies to which the off-shell energy depends and the sign appearing in the linear combination of the off-shell energy (this is, from the term $\vec{b} \cdot \vec{q}_0^{(+)}$, we extract only the index of $q_{i,0}^{(+)}$ together with its sign, this is $b_i i$ for non-vanishing b_i). For instance, if in an intermediate step, the propagator $\left(\left(q_{1,0} + q_{2,0} - q_{3,0}^{(+)}\right)^2 - \left(q_{4,0}^{(+)}\right)^2\right)^{-1}$ appears, then it can be represented by the list $\{\{\{1, 1, 0, 0\}, \{-3\}\}, \{\{4\}\}\}$. As another example, the expression $\left(\left(q_{1,0} + q_{5,0}^{(+)} - q_{3,0}^{(+)}\right)^2 - \left(q_{4,0}^{(+)}\right)^2\right)^{-1}$ can be represented, in this code, as the list $\{\{\{1, 0, 0, 0\}, \{-3, 5\}\}, \{\{4\}\}\}$. With this in mind, this code computes the nested residues by looking at the elements of the lists and copying them in different positions. The displaced poles are not selected, and the final result is obtained, for the N²MLT(500) diagram, after 249 seconds, in a computer ASUS X555D.

```

(*n = 503; L = 500;*) q = Table[Table[0, {j, 1, L}], {i, 1, n}];
Do[
  q[[i, i]] = 1; q[[L + 1, i]] = 1;,
  {i, 1, L}];
q[[L + 2, 1]] = 1; q[[L + 2, 2]] = 1; q[[L + 3, 2]] = 1; q[[L + 3, 3]] = 1;
res = Table[{{q[[i]], {}}, {{i}}}, {i, 1, n}];
Do[ Do[
  g = res[[polos]]; m = Length[g]; factores = {};
  Do[
    If[g[[i,1,1,loop]] == 1,
      {factores = Append[factores, g[[i]]]; g = Drop[g, {i}];},
    {i,m,1,-1}];
m = Length[g]; lengthfactores = Length[factores];
residuos = Table[factores,{i,1,lengthfactores}];
Do[Do[
  If[Total[factores[[i,1,2]]] == -Total[Abs[factores[[i,1,2]]]], If[j != i,
    {residuos[[i,j,1,1]] = factores[[j,1,1]] - factores[[i,1,1]];
    residuos[[i,j,1,2]] = Union[factores[[j,1,2]], -factores[[i,1,2]], factores[[i,2,1]]];}],
  {j,1,lengthfactores}], {i,1,lengthfactores}];
Do[
  If[Total[factores[[i,1,2]]] == -Total[Abs[factores[[i,1,2]]]],
    {residuos[[i,i,1,2]] = {}}; Do[
      residuos[[i,i,1,1]] = 0,
    {1,1,L}]], {i,1,lengthfactores}];
lengthresiduos = Length[residuos];
Do[Do[
  If[loop > 1, If[residuos[[i,j,1,1,loop-1]] == -1,
    {residuos[[i,j,1]] = -residuos[[i,j,1]]}],
  {j,1,Length[residuos[[i]]}], {i,1,lengthresiduos}]; Do[
  If[loop > 1, If[g[[i,1,1,loop-1]] == -1,
    {g[[i, 1]] = -g[[i, 1]]}],
  {i, 1, m}];
Do[
  If[residuos[[i]] == factores,
    {residuos = Drop[residuos, {i}]}],
  {i, lengthresiduos, 1, -1}];
lengthresiduos = Length[residuos];
If[lengthresiduos == 0,
  {residuos = Append[residuos, g]},
  Do[
    residuos[[i]] = Union[g, residuos[[i]],
    {i,1,lengthresiduos}];
  res[[polos]] = residuos;
  Clear[g, m, factores, lengthfactores, lengthresiduos, residuos, q],
  {polos,1,Length[res}]];
res = Flatten[res, 1];,
{loop,L,1,-1}]; expression = Table[{}, {i,1,Length[res}]];
Do[Do[
  If[res[[i,j,1,2]] != {},
    expression[[i]] = Append[expression[[i]], res[[i,j,1,2]]],
  {j,1,Length[res[[i]]}], {i,1,Length[res}]];

```

```

universe = Flatten[Table[{-i,i}, {i,1,n}]];
repeated = Table[Table[{}, {j,1,Length[expression[[i]]]}, {i,1,Length[expression]}];
Do[Do[
  If[Length[Union[expression[[i,j]]] != Length[Union[Abs[expression[[i,j]]]]],
    Do[Do[
      If[expression[[i,j,k]] == -expression[[i,j,l]],
        repeated[[i, j]] = Append[repeated[[i, j]], expression[[i, j, k]]];
        repeated[[i, j]] = Append[repeated[[i, j]], expression[[i, j, l]]],
      {l,k,Length[expression[[i,j]]]}, {k,1,Length[expression[[i,j]]]}],
    {j,1,Length[expression[[i]]]}, {i,1,Length[expression]}];
Do[Do[
  If[repeated[[i,j]] != {},
    expression[[i,j]] = Intersection[expression[[i,j]],
      Complement[universe, repeated[[i,j]]]],
    {j,1,Length[repeated[[i]]]}, {i,1,Length[repeated]}];
Do[Do[
  expression[[i,j]][[0]] = G,
  {j,1,Length[expression[[i]]]}, {i,1,Length[expression]}]
Do[
  expression[[i]][[0]] = Times,
  {i,1,Length[expression]}]
expression[[0]] = Plus;
res = expression;
Clear[expression, universe, repeated];
res

```


Appendix C

Cancellation of displaced poles

The cancellation of the contribution to iterated residues from displaced poles, defined in Sec.5.1, is guaranteed by the following:

Lemma: Let $P(x_i, x_j)$ be a meromorphic function in both variables x_i and x_j whose poles are not located on $\{x_i, y_i + k_i\}$, $\{x_i, y_k - x_j + k_{ij}\}$ nor $\{x_j, y_k - y_i + k_{ij} - k_i\}$, with $k_i, k_{ij}, y_i, y_k \in \mathbb{C}$ where $y_i, y_k \in \{\text{Im}(z) < 0\}$, and let

$$F(x_i, x_j) = \frac{P(x_i, x_j)}{((x_i - k_i)^2 - y_i^2)^{\gamma_i} ((x_i + x_j - k_{ij})^2 - y_k^2)^{\gamma_k}}. \quad (\text{C.1})$$

Then, the iterated residue in each of the explicit poles satisfies

$$\begin{aligned} & \text{Res}(\text{Res}(F(x_i, x_j), \{x_i, y_i + k_i\}), \{x_j, y_k - y_i + k_{ij} - k_i\}) = \\ & -\text{Res}(\text{Res}(F(x_i, x_j), \{x_i, y_k - x_j + k_{ij}\}), \{x_j, y_k - y_i + k_{ij} - k_i\}). \end{aligned} \quad (\text{C.2})$$

Proof: If the shifts $x'_i = x_i - k_i$ and $x'_j = x_j - k_{ij} + k_i$ are performed, the function F can be rewritten in the form

$$F(x'_i, x'_j) = \frac{P(x'_i, x'_j)}{(x'^2_i - y_i^2)^{\gamma_i} ((x'_i + x'_j)^2 - y_k^2)^{\gamma_k}}. \quad (\text{C.3})$$

Without loss of generality, this is also equivalent to consider $k_i = k_{ij} = 0$.

The function in Eq. (C.3) has two explicit poles of order γ_i and γ_k within the half plane $\text{Im}(z) < 0$. Thus, the function F has an expansion of the form

$$F(x'_i, x'_j) = \sum_{r_i=-\gamma_i}^{\infty} \sum_{r_k=-\gamma_k}^{\infty} a_{r_i, r_k} (x'_i - y_i)^{\gamma_i} (x'_i + x'_j - y_k)^{r_k}. \quad (\text{C.4})$$

If the last factor of the right hand side of Eq. (C.4) is rewritten in the form $x'_i + x'_j - y_k = (x'_i - y_i) + (x'_j - y_k + y_i)$, and if the sum over r_k is split into negative and non-negative values, it is obtained

$$\begin{aligned} F(x'_i, x'_j) &= \sum_{r_i=-\gamma_i}^{\infty} \sum_{r_k=-\gamma_k}^{\infty} a_{r_i, r_k} (x'_i - y_i)^{\gamma_i} (x'_i + x'_j - y_k)^{r_k} \\ &= \sum_{r_i=-\gamma_i}^{\infty} \sum_{r_k=1}^{\gamma_k} \sum_{s=0}^{\infty} (-1)^{r_k+s} a_{r_i, -r_k} \frac{(x'_i - y_i)^{r_i+s}}{(r_k - 1)!} (x'_j - y_k + y_i)^{-r_k-s} \prod_{t=1}^{r_k-1} (s+t) \\ &+ \sum_{r_i=-\gamma_i}^{\infty} \sum_{r_k=0}^{\infty} \sum_{s=0}^{r_k} a_{r_i, r_k} \binom{r_k}{s} (x'_i - y_i)^{r_i+s} (x'_j - y_k + y_i)^{r_k-s}. \end{aligned} \quad (\text{C.5})$$

To compute the first residue of the function in Eq. (C.4), for $\{x'_i, y_i\}$, it is enough to take the coefficient of the term with the factor $(x'_i - y_i)^{-1}$ in the expansion of Eq. (C.5). Afterwards, to obtain the second residue, for $\{x'_j, y_k - y_i\}$, we select the coefficient of the term with the factor $(x'_j - y_k + y_i)^{-1}$. For the second sum, the second condition is never satisfied because $0 \leq s \leq r_k$ and such a factor demands the condition $s = r_k + 1$. For the first sum, the second condition is obtained for $r_k + s = 1$, and as $1 \leq r_k \leq \gamma_k$ and $0 \leq s < \infty$, there is just one term satisfying this condition, with $s = 0$ and $r_k = 1$. As $s = 0$, the first condition is satisfied for $r_i = -1$. Hence

$$\text{Res}(\text{Res}(F(x'_i, x'_j), \{x'_i, y_i\}), \{x'_j, y_k - y_i\}) = -a_{-1, -1}. \quad (\text{C.6})$$

If in the function in Eq. (C.4), we rewrite the second factor as $x'_i - y_i = (x'_i + x'_j - y_k) - (x'_j - y_k + y_i)$, and if the sum over r_i is split into negative and non-negative values, we obtain

$$\begin{aligned} F(x'_i, x'_j) &= \sum_{r_i=1}^{\gamma_i} \sum_{r_k=-\gamma_k}^{\infty} \sum_{s=0}^{\infty} a_{-r_i, r_k} \frac{(x'_i + x'_j - y_k)^{r_k+s}}{(r_i - 1)!} (x'_j - y_k + y_i)^{-r_i-s} \prod_{t=1}^{k_1-1} (s+t) \\ &+ \sum_{r_i=0}^{\infty} \sum_{r_k=-\gamma_k}^{\infty} \sum_{s=0}^{r_i} a_{r_i, r_k} \binom{r_i}{s} (x'_i + x'_j - y_k)^{r_k+s} (-x'_j + y_k - y_i)^{r_i-s}. \end{aligned} \quad (\text{C.7})$$

Again, the iterated residue of this expression is the coefficient of the terms proportional to $(x'_i + x'_j - y_k)^{-1}$ and $(x'_j - y_k + y_i)^{-1}$. For the first sum, this conditions are satisfied for $r_k + s = -1$ and $r_i + s = 1$. However, as $1 \leq r_i \leq \gamma_i$ and $0 \leq s$, the last condition is fulfilled only for $r_i = 1$ and $s = 0$. Thus, the first condition is expressed as $r_k = -1$. For the second sum, the first condition holds, but the second condition shall be expressed as $r_i - s = -1$ so that $s = r_i + 1$. However, it is given that $0 \leq s \leq r_i$ and then this sum does not contribute to the residue. Thus,

$$\text{Res}(\text{Res}(F(x'_i, x'_j), \{x'_i, y_k - x'_j\}), \{x'_j, y_k - y_i\}) = a_{-1, -1}. \quad (\text{C.8})$$

It is then concluded that

$$\begin{aligned} &\text{Res}(\text{Res}(F(x'_i, x'_j), \{x'_i, y_i\}), \{x'_j, y_k - y_i\}) = \\ &-\text{Res}(\text{Res}(F(x'_i, x'_j), \{x'_i, y_k - x'_j\}), \{x'_j, y_k - y_i\}). \end{aligned} \quad (\text{C.9})$$

If we then restore the original variables that are shifted by k_i and k_{ij} with respect to x'_i and x'_j , we arrive to the expression we wanted to demonstrate

$$\begin{aligned} &\text{Res}(\text{Res}(F(x_i, x_j), \{x_i, y_i + k_i\}), \{x_j, y_k - y_i + k_{ij} - k_i\}) = \\ &-\text{Res}(\text{Res}(F(x_i, x_j), \{x_i, y_k - x_j + k_{ij}\}), \{x_j, y_k - y_i + k_{ij} - k_i\}). \end{aligned} \quad (\text{C.10})$$

Appendix D

Proof by induction of the multi-loop MLT(L) representation

This Appendix presents a formal proof of the dual representation of MLT(L) in terms of nested residues (Eq. (4.54)). The proof is given by induction on the number of computed residues through the iterated residues algorithm.

Here, we start by analysing the dual representation of a scalar MLT(L) diagram with one propagator for each set. The original integrand in the Feynman representation is given by

$$\mathcal{I}_{\text{MLT}}^{(L)} = G_F(1, 2, \dots, L+1) = G_F(1, 2, \dots, L, 1 \dots L). \quad (\text{D.1})$$

After the computation of the first residue with respect to the variable x_L , we get

$$\begin{aligned} \text{Res}(\mathcal{I}_{\text{MLT}}^{(L)}, \{q_{L,0}, \text{Im}(q_{L,0}) < 0\}) &= G_D(1, 2, \dots, L-1, 0_{(L)}, 1 \dots (L-1)_L) \\ &+ G_D(1, \dots, n-2, 1 \dots (L-1)_{\overline{L+1}}, 0_{(L+1)}). \end{aligned} \quad (\text{D.2})$$

In order to prove the cancellation of the contributions of the displaced poles in each iteration of the iterated residues by mathematical induction, we assume that the function obtained after computing the first i iterated residues (for the last i variables) is given by

$$\begin{aligned} &G_F(1, \dots, L+1) \rightarrow G_F(1, \dots, L-i) \\ &\times \sum_{j=L-i+1}^{L+1} G_D(0_{(L-i+1)}, \dots, 0_{(j-1)}, 1 \dots (L-i)_{(L-i+1)\dots(j-1)\overline{(j+1)\dots(L+1)}, 0_{(j+1)}, \dots, 0_{(L+1)}), \end{aligned} \quad (\text{D.3})$$

where it has been factorized out the Feynman propagator $G_F(1, \dots, L-i)$ as it depends on independent primitive variables. Then, the set of poles of the function given in Eq. (D.3) with respect to the variable $q_{L-i,0}$ is given by

$$\begin{aligned} &\text{Poles}[G_F(1, \dots, L+1), q_{L+1,0}, \dots, q_{L-i-1,0}; q_{L-i,0}] \\ &= \{\pm q_{L-i,0}^{(+)}\} \cup \left(\bigcup_{j=L-i+1}^L \left\{ - \sum_{j=1}^{L-i-1} q_{j,0} \pm q_{j,0}^{(+)} - \sum_{k=L-i+1}^{j-1} q_{k,0}^{(+)} + \sum_{k=j+1}^{L+1} q_{k,0}^{(+)} \right\} \right) \\ &\cup \left\{ k_{L+1,0} - \sum_{n=1}^{L-i-1} q_{n,0} - \sum_{n=L-i+1}^L q_{n,0}^{(+)} \pm q_{L+1,0}^{(+)} \right\}. \end{aligned} \quad (\text{D.4})$$

Although the first component in Eq. (D.4) has a single negative-imaginary-part pole, namely $q_{L-i,0}^{(+)}$, the second component contains one negative-imaginary-part pole and the

third component has one positive-imaginary-part pole, because,

$$\text{Im} \left(\sum_{k=L-i+1}^{L+1} q_{k,0}^{(+)} \right) < 0, \quad (\text{D.5})$$

while all other poles are displaced poles, we should select only the residues of the non-displaced poles with negative imaginary part.

Following with the next nested residue, we get,

$$\begin{aligned} & G_F(1, \dots, L+1) \rightarrow G_F(1, \dots, L-i-1) \\ & \times \left(\sum_{j=L-i}^{L+1} G_D(0_{(L-i)}, \dots, 0_{(j-1)}, 1 \dots (L-i-1)_{(L-i)\dots(j-1)\overline{(j+1)\dots(L+1)}, 0_{(j+1)}, \dots, 0_{(L+1)}} \right. \\ & \left. + G_D(1 \dots (L-i-1)_{(L-i)\dots(L+1)}, 0_{(L-i)} \dots, 0_{(L+1)}) \right) \\ & = G_F(1, \dots, L-i-1) \\ & \times \sum_{j=L-i}^{L+1} G_D(0_{(L-i)}, \dots, 0_{(j-1)}, 1 \dots (L-i-1)_{(L-i)\dots(j-1)\overline{(j+1)\dots(L+1)}, 0_{(j+1)}, \dots, 0_{(L+1)}}. \end{aligned} \quad (\text{D.6})$$

Hence, this proves by induction that the computation of the first i iterated residues, results into the expression in Eq. (D.3).

In particular, after computing all the residues, it is obtained

$$G_F(1, \dots, L+1) \rightarrow \sum_{j=1}^{L+1} G_D(0_{(1)}, \dots, 0_{(j-1)}, 0_{1\dots(j-1)\overline{(j+1)\dots(L+1)}, 0_{(j+1)}, \dots, 0_{(L+1)}}). \quad (\text{D.7})$$

It is worth to say that the proof of Eq. (D.3) is general enough to cover the case involving an arbitrary topological complexity. This is because we can isolate the higher-topology structure inside the factor $G_F(1, \dots, L-i-1)$, and proceed as described. Thus, Eq. (D.3) can be applied to Feynman diagrams with higher topological complexity and any number of loops.

Bibliography

- [1] J. Jesús Aguilera-Verdugo, F. Driencourt-Mangin, R. J. Hernández-Pinto, J. Plenter, R. M. Prisco, N. S. Ramírez-Uribe, A. E. Rentería-Olivo, G. Rodrigo, G. F. R. Sborlini, W. J. Torres Bobadilla and F. Tramontano, *A Stroll through the Loop-Tree Duality*, *Symmetry* **13** (2021) 6, 1029 [[2104.14621](#)].
- [2] J. Jesús Aguilera-Verdugo, R. J. Hernández-Pinto, G. Rodrigo, G. F. R. Sborlini and W. J. Torres Bobadilla, *Mathematical properties of nested residues and their application to multi-loop scattering amplitudes*, *JHEP* **02** (2021) 112 [[2010.12971](#)].
- [3] J. J. Aguilera-Verdugo, R. J. Hernandez-Pinto, G. Rodrigo, G. F. R. Sborlini and W. J. Torres Bobadilla, *Causal representation of multi-loop Feynman integrands within the loop-tree duality*, *JHEP* **01** (2021) 069 [[2006.11217](#)].
- [4] J. J. Aguilera-Verdugo, F. Driencourt-Mangin, R. J. Hernández-Pinto, J. Plenter, S. Ramirez-Uribe, A. E. Renteria Olivo, G. Rodrigo, G. F. R. Sborlini, W. J. Torres Bobadilla and S. Tracz, *Open Loop Amplitudes and Causality to All Orders and Powers from the Loop-Tree Duality*, *Phys. Rev. Lett.* **124** (2020) 21, 211602 [[2001.03564](#)].
- [5] J. J. Aguilera-Verdugo, F. Driencourt-Mangin, J. Plenter, S. Ramírez-Uribe, G. Rodrigo, G. F. R. Sborlini, W. J. Torres Bobadilla and S. Tracz, *Causality, unitarity thresholds, anomalous thresholds and infrared singularities from the loop-tree duality at higher orders*, *JHEP* **12** (2019) 163 [[1904.08389](#)].
- [6] J. J. Aguilera-Verdugo, F. Driencourt-Mangin, J. Plenter, S. Ramírez-Uribe, G. Rodrigo, G. F. R. Sborlini, W. J. Torres Bobadilla and S. Tracz, *Unsubtractions at NNLO*, *CERN Yellow Reports: Monographs* **3** (2020) 169-176.
- [7] J. J. Thomson, *Cathode rays*, *Phil. Mag. Ser. 5* **44** (1897) 293-316.
- [8] M. Planck, *On the Law of Distribution of Energy in the Normal Spectrum*, *Annalen Phys.* **4** (1901) 553.
- [9] A. Einstein, *Concerning an heuristic point of view toward the emission and transformation of light*, *Annalen Phys.* **17** (1905) 132-148.
- [10] A. Einstein, *On the electrodynamics of moving bodies*, *Annalen Phys.* **17** (1905) 891-921.
- [11] E. Rutherford, *The scattering of alpha and beta particles by matter and the structure of the atom*, *Phil. Mag. Ser. 6* **21** (1911) 669-688.
- [12] L. V. P. R. de Broglie, *Recherches sur la théorie des quanta*, *Annals Phys.* **2** (1925) 22-128.
- [13] E. Schrödinger, *Quantisierung als Eigenwertproblem*, *Annalen Phys.* **384** (1926) 4, 361-376.

- [14] O. Klein, *Quantum Theory and Five-Dimensional Theory of Relativity*. (In German and English), *Z. Phys.* **37** (1926) 895-906.
- [15] P. A. M. Dirac, *The quantum theory of the electron*, *Proc. Roy. Soc. Lond. A* **117** (1928) 610-624.
- [16] P. Jordan, *On the Quantum mechanics of the gas degeneracy*, *Z. Phys.* **44** (1927) 473-480.
- [17] P. Jordan and E. P. Wigner, *About the Pauli exclusion principle*, *Z. Phys.* **47** (1928) 631-651.
- [18] J. S. Schwinger, *Quantum electrodynamics. I A covariant formulation*, *Phys. Rev.* **74** (1948) 1439.
- [19] J. S. Schwinger, *On Quantum electrodynamics and the magnetic moment of the electron*, *Phys. Rev.* **73** (1948) 416-417.
- [20] J. S. Schwinger, *Quantum electrodynamics. 2. Vacuum polarization and selfenergy*, *Phys. Rev.* **75** (1948) 651.
- [21] J. Schwinger, *On the Polarization of Fast Neutrons*, *Phys. Rev.* **73** (1948) 407-409.
- [22] J. S. Schwinger, *Quantum electrodynamics. III: The electromagnetic properties of the electron: Radiative corrections to scattering*, *Phys. Rev.* **76** (1949) 790-817.
- [23] J. Schwinger, *On Radiative Corrections to Electron Scattering*, *Phys. Rev.* **75** (1949) 898-899.
- [24] S. i. Tomonaga, *On the Effect of the Field Reactions on the Interaction of Mesotrons and Nuclear Particles. III*, *Prog. Theor. Phys.* **2** (1949) 1, 6-24.
- [25] S. i. Tomonaga, *On the Effect of the Field Reactions on the Interaction of Mesotrons and Nuclear Particles. IV*, *Prog. Theor. Phys.* **2** (1949) 2, 63-70.
- [26] Z. Koba, T. Tati and S. i. Tomonaga, *On a Relativistically Invariant Formulation of the Quantum Theory of Wave Fields. II: Case of Interacting Electromagnetic and Electron Fields*, *Prog. Theor. Phys.* **2** (1947) 3, 101-116.
- [27] S. I. Tomonaga and J. R. Oppenheimer, *On Infinite Field Reactions in Quantum Field Theory*, *Phys. Rev.* **74** (1948) 224-225.
- [28] R. P. Feynman, *The Theory of positrons*, *Phys. Rev.* **76**, 749-759 (1949).
- [29] A. Salam and J. C. Ward, *Weak and electromagnetic interactions*, *Nuovo Cim.* **11** (1959) 568-577.
- [30] C. N. Yang and R. L. Mills, *Conservation of Isotopic Spin and Isotopic Gauge Invariance*, *Phys. Rev.* **96** (1954) 191-195.
- [31] M. Gell-Mann, *A Schematic Model of Baryons and Mesons*, *Phys. Lett.* **8**, 214-215 (1964).
- [32] G. Zweig, *An $SU(3)$ model for strong interaction symmetry and its breaking. Version 1*, CERN-TH-401.
- [33] G. Zweig, *An $SU(3)$ model for strong interaction symmetry and its breaking. Version 2*, CERN-TH-412.

- [34] O. W. Greenberg, *Spin and Unitary Spin Independence in a Paraquark Model of Baryons and Mesons*, *Phys. Rev. Lett.* **13** (1964) 598-602.
- [35] M. Y. Han and Y. Nambu, *Three Triplet Model with Double $SU(3)$ Symmetry*, *Phys. Rev.* **139** (1965) B1006-B1010.
- [36] H. Fritzsch, M. Gell-Mann and H. Leutwyler, *Advantages of the Color Octet Gluon Picture*, *Phys. Lett. B* **47** (1973) 365-368.
- [37] D. J. Gross and F. Wilczek, *Asymptotically free gauge theories. 2*, *Phys. Rev. D* **9** (1974) 980-993.
- [38] H. D. Politzer, *Reliable Perturbative Results for Strong Interactions?*, *Phys. Rev. Lett.* **30** (1973) 1346-1349.
- [39] L. D. Faddeev and V. N. Popov, *Feynman Diagrams for the Yang-Mills Field*, *Phys. Lett. B* **25** (1967) 29-30.
- [40] M. E. Peskin and D. V. Schroeder, 1995, *An Introduction to quantum field theory*, Addison-Wesley. Reading, USA. ISBN:978-0-201-50397-5.
- [41] S. Weinberg, 2005, *The Quantum theory of fields. Vol. 1: Foundations*, Cambridge University Press. ISBN:978-0-521-67053-1.
- [42] S. Weinberg, 2013, *The quantum theory of fields. Vol. 2: Modern applications*, Cambridge University Press. ISBN:978-1-139-63247-8.
- [43] R. Ticciati, 1999, *Quantum field theory for mathematicians*, *Encyclopedia of Mathematics and its Applications*. Cambridge University Press.
- [44] S. L. Glashow and S. Weinberg, *Breaking chiral symmetry*, *Phys. Rev. Lett.* **20** (1968) 224-227.
- [45] A. Salam, *Weak and Electromagnetic Interactions*, *Conf. Proc. C* **680519** (1968) 367-377.
- [46] N. Cabibbo, *Unitary Symmetry and Leptonic Decays*, *Phys. Rev. Lett.* **10** (1963) 531-533.
- [47] M. Kobayashi and T. Maskawa, *CP Violation in the Renormalizable Theory of Weak Interaction*, *Prog. Theor. Phys.* **49** (1973) 652-657.
- [48] D. J. Gross and F. Wilczek, *Ultraviolet Behavior of Nonabelian Gauge Theories*, *Phys. Rev. Lett.* **30** (1973) 1343-1346.
- [49] V. Khachatryan *et al.* [CMS], *Measurement and QCD analysis of double-differential inclusive jet cross sections in pp collisions at $\sqrt{s} = 8$ TeV and cross section ratios to 2.76 and 7 TeV*, *JHEP* **03** (2017) 156 [[1609.05331](#)].
- [50] C. G. Bollini and J. J. Giambiagi, *Dimensional Renormalization: The Number of Dimensions as a Regularizing Parameter*, *Nuovo Cim. B* **12** (1972) 20-26.
- [51] G. 't Hooft and M. J. G. Veltman, *Regularization and Renormalization of Gauge Fields*, *Nucl. Phys. B* **44** (1972) 189-213.
- [52] W. Pauli and F. Villars, *On the Invariant regularization in relativistic quantum theory*, *Rev. Mod. Phys.* **21** (1949) 434-444.

- [53] K. G. Wilson, *Confinement of Quarks*, *Phys. Rev. D* **10** (1974) 2445-2459.
- [54] S. Catani, L. Cieri, D. de Florian, G. Ferrera and M. Grazzini, *Universality of transverse-momentum resummation and hard factors at the NNLO*, *Nucl. Phys. B* **881** (2014) 414-443 [[1311.1654](#)].
- [55] R. E. Cutkosky, *Singularities and discontinuities of Feynman amplitudes*, *J. Math. Phys.* **1** (1960) 429-433.
- [56] S. Catani, T. Gleisberg, F. Krauss, G. Rodrigo and J. C. Winter, *From loops to trees by-passing Feynman's theorem*, *JHEP* **09** (2008) 065 [[0804.3170](#)].
- [57] G. Rodrigo, S. Catani, T. Gleisberg, F. Krauss and J. C. Winter, *From multileg loops to trees (by-passing Feynman's Tree Theorem)*, *Nucl. Phys. B Proc. Suppl.* **183** (2008) 262-267 [[0807.0531](#)].
- [58] I. Bierenbaum, S. Catani, P. Draggiotis and G. Rodrigo, *A Tree-Loop Duality Relation at Two Loops and Beyond*, *JHEP* **10** (2010) 073 [[1007.0194](#)].
- [59] I. Bierenbaum, S. Buchta, P. Draggiotis, I. Malamos and G. Rodrigo, *Tree-Loop Duality Relation beyond simple poles*, *JHEP* **03** (2013) 025 [[1211.5048](#)].
- [60] S. Buchta, G. Chachamis, P. Draggiotis, I. Malamos and G. Rodrigo, *On the singular behaviour of scattering amplitudes in quantum field theory*, *JHEP* **11** (2014) 014 [[1405.7850](#)].
- [61] S. Buchta, *Theoretical foundations and applications of the Loop-Tree Duality in Quantum Field Theories*, Valencia U., IFIC, 2015. [[1509.07167](#)].
- [62] S. Buchta, G. Chachamis, P. Draggiotis and G. Rodrigo, *Numerical implementation of the loop-tree duality method*, *Eur. Phys. J. C* **77** (2017) 5, 274 [[1510.00187](#)].
- [63] Z. Capatti, V. Hirschi, D. Kermanschah and B. Ruijl, *Loop-Tree Duality for Multi-loop Numerical Integration*, *Phys. Rev. Lett.* **123** (2019) 15, 151602 [[1906.06138](#)].
- [64] Z. Capatti, V. Hirschi, D. Kermanschah, A. Pelloni and B. Ruijl, *Numerical Loop-Tree Duality: contour deformation and subtraction*, *JHEP* **04** (2020) 096 [[1912.09291](#)].
- [65] Z. Capatti, V. Hirschi, D. Kermanschah, A. Pelloni and B. Ruijl, *Manifestly Causal Loop-Tree Duality*, [[2009.05509](#)].
- [66] R. Runkel, Z. Ször, J. P. Vesga and S. Weinzierl, *Causality and loop-tree duality at higher loops*, [erratum: *Phys. Rev. Lett.* **123**, no.5, 059902 (2019)] *Phys. Rev. Lett.* **122** (2019) 11, 111603 [[1902.02135](#)].
- [67] R. Runkel, Z. Ször, J. P. Vesga and S. Weinzierl, *Integrands of loop amplitudes within loop-tree duality*, *Phys. Rev. D* **101** (2020) 11, 116014 [[1906.02218](#)].
- [68] R. Runkel, Z. Ször, J. P. Vesga and S. Weinzierl, *A new formulation of the loop-tree duality at higher loops*, *14th International Symposium on Radiative Corrections: Application of Quantum Field Theory to Phenomenology*. [[1911.09610](#)].
- [69] J. J. Aguilera-Verdugo, R. J. Hernández-Pinto, S. Ramírez-Uribe, G. Rodrigo, G. F. R. Sborlini, W. J. Torres Bobadilla, *Manifestly Causal Scattering Amplitudes*, Snowmass 2021 - Letter of Intention.

- [70] E. T. Tomboulis, *Causality and Unitarity via the Tree-Loop Duality Relation*, *JHEP* **05** (2017) 148 [[1701.07052](#)].
- [71] W. J. Torres Bobadilla, *Loop-tree duality from vertices and edges*, *JHEP* **04** (2021) 183 [[2102.05048](#)].
- [72] W. J. T. Bobadilla, *Lotty – The loop-tree duality automation*, *Eur. Phys. J. C* **81** (2021) 6, 514 [[2103.09237](#)].
- [73] F. Driencourt-Mangin, G. Rodrigo and G. F. R. Sborlini, *Universal dual amplitudes and asymptotic expansions for $gg \rightarrow H$ and $H \rightarrow \gamma\gamma$ in four dimensions*, *Eur. Phys. J. C* **78** (2018) 3, 231 [[1702.07581](#)].
- [74] J. L. Jurado, G. Rodrigo and W. J. Torres Bobadilla, *From Jacobi off-shell currents to integral relations*, *JHEP* **12** (2017) 122 [[1710.11010](#)].
- [75] F. Driencourt-Mangin, G. Rodrigo, G. F. R. Sborlini and W. J. Torres Bobadilla, *Universal four-dimensional representation of $H \rightarrow \gamma\gamma$ at two loops through the Loop-Tree Duality*, *JHEP* **02** (2019) 143 [[1901.09853](#)].
- [76] F. Driencourt-Mangin, *Four-dimensional representation of scattering amplitudes and physical observables through the application of the Loop-Tree Duality theorem*, Valencia U., IFIC. [[1907.12450](#)].
- [77] F. Driencourt-Mangin, G. Rodrigo, G. F. R. Sborlini and W. J. Torres Bobadilla, *On the interplay between the loop-tree duality and helicity amplitudes*, [[1911.11125](#)].
- [78] G. F. R. Sborlini, F. Driencourt-Mangin, R. Hernandez-Pinto and G. Rodrigo, *Four-dimensional unsubtraction from the loop-tree duality*, *JHEP* **08** (2016) 160 [[1604.06699](#)].
- [79] G. F. R. Sborlini, F. Driencourt-Mangin and G. Rodrigo, *Four-dimensional unsubtraction with massive particles*, *JHEP* **10** (2016) 162 [[1608.01584](#)].
- [80] J. Plenter, *Asymptotic Expansions Through the Loop-Tree Duality*, *Acta Phys. Polon. B* **50** (2019) 1983-1992.
- [81] J. Plenter and G. Rodrigo, *Asymptotic expansions through the loop-tree duality*, *Eur. Phys. J. C* **81** (2021) 4, 320 [[2005.02119](#)].
- [82] M. Beneke and V. A. Smirnov, *Asymptotic expansion of Feynman integrals near threshold*, *Nucl. Phys. B* **522** (1998) 321-344 [[hep-ph/9711391](#)].
- [83] A. von Manteuffel and R. M. Schabinger, *A novel approach to integration by parts reduction*, *Phys. Lett. B* **744** (2015) 101-104 [[1406.4513](#)].
- [84] T. Peraro, *Scattering amplitudes over finite fields and multivariate functional reconstruction*, *JHEP* **12** (2016) 030 [[1608.01902](#)].
- [85] P. S. Wang, *A P -Adic Algorithm for Univariate Partial Fractions*, *Proceedings of the Fourth ACM Symposium on Symbolic and Algebraic Computation*, Association for Computing Machinery. New York, NY, USA.
- [86] T. Peraro, *FiniteFlow: multivariate functional reconstruction using finite fields and dataflow graphs*, *JHEP* **07** (2019) 031 [[1905.08019](#)].
- [87] K. G. Chetyrkin and F. V. Tkachov, *Integration by Parts: The Algorithm to Calculate beta Functions in 4 Loops*, *Nucl. Phys. B* **192** (1981) 159-204.

-
- [88] S. Laporta, *High precision calculation of multiloop Feynman integrals by difference equations*, *Int. J. Mod. Phys. A* **15** (2000) 5087-5159 [[hep-ph/0102033](#)].
- [89] S. Borowka, G. Heinrich, S. P. Jones, M. Kerner, J. Schlenk and T. Zirke, *SecDec-3.0: numerical evaluation of multi-scale integrals beyond one loop*, *Comput. Phys. Commun.* **196** (2015) 470-491 [[1502.06595](#)].
- [90] A. V. Smirnov, *FIESTA4: Optimized Feynman integral calculations with GPU support*, *Comput. Phys. Commun.* **204** (2016) 189-199 [[1511.03614](#)].
- [91] G. F. R. Sborlini, *Geometrical approach to causality in multiloop amplitudes*, *Phys. Rev. D* **104** (2021) 3, 036014 [[2102.05062](#)].